DISCRETE NON-ABELIAN SYMMETRIES BEYOND THE STANDARD MODEL

by

Ariel Rock

A dissertation submitted in partial fulfillment of
the requirements for the degree of

Doctor of Philosophy

(Physics)

at the

UNIVERSITY OF WISCONSIN–MADISON

2021

Date of final oral examination: June 03, 2021

The dissertation is approved by the following members of the Final Oral Committee:

Lisa Everett, Professor, Physics

Vernon Barger, Vilas Professor and Van Vleck Professor, Physics

Yang Bai, Associate Professor, Physics

Ellen Zweibel, William L Kraushaar Professor, Astronomy

For my parents

It was a hard thing to undo this knot.
The rainbow shines, but only in the thought
Of him that looks. Yet not in that alone,
For who makes rainbows by invention?
And many standing round a waterfall
See one bow each, yet not the same to all,
But each a hand's breadth further than the next.
The sun on falling waters writes the text
Which yet is in the eye or in the thought.
It was a hard thing to undo this knot.

— Gerard Manley Hopkins,

"It was a hard thing to undo this knot"

Abstract

The use of symmetry has been fundamental in the development of the Standard Model, and we continue to be guided by symmetric considerations in building BSM theories of supersymmetry breaking and flavor. In this thesis, we analyze a minimal flavored gauge mediation model of supersymmetry breaking in which the electroweak Higgs and messenger doublets mix as multiplets of a discrete non-Abelian symmetry given by the group S3.

We show that in a specific limit, sizable stop mixing and flavor diagonal soft supersymmetry breaking parameters are achieved. In most of the parameter space, the masses of the colored superpartners are at most in the 5–6 TeV range. We show that couplings at the renormalizable level do not lead to viable quark mixing parameters, requiring the inclusion of higher-dimensional operators. As a concrete exploration of this idea, we show that the Cabibbo angle can be generated within this framework via such couplings and explore the scenario's phenomenological implications.

In a separate direction, we also explore the effects of correlations among observable parameters of neutrino mixing on predictions for the leptonic Dirac CP-violating phase. Focusing on a standard class of theoretical models of neutrino mixing governed by discrete non-Abelian symmetries corrected by a single charged lepton rotation, we show that we can guarantee a physically meaningful prediction for the most likely value of the leptonic Dirac CP-violating phase.

ACKNOWLEDGMENTS

Completing a PhD in particle theory is – with apologies to Gerard Manley Hopkins – a hard knot to undo. I am most definitely not Alexander the Great, and without the fortune of having a wonderful group of mentors, confidantes, colleagues and friends to guide me, the knot would still be tied tight.

Firstly, I want to thank my advisor Lisa Everett, whose encyclopedic knowledge of physics and steadfast commitment to her students is remarkable. I can confidently state that without her guidance I would not have completed this PhD. The standards of incisiveness, meticulousness and care with which she approaches high energy physics is an inspiration, and I can only hope to rise to such levels as I move forward. It is rare to meet people who are as brilliant as they are dedicated to the success of the next generation of physicists, and it has been a privilege to work with her.

I would also like to thank the other mentors I have been lucky to have as I have moved through my physics career. I want to thank the other members of my defense committee, Ellen Zweibel, Yang Bai and, in particular, Vernon Barger for his guidance this past year. I also want to thank Jeff Schmidt for his kindness and humor. I thank my collaborators with whom I had the pleasure of working on the projects in this thesis: Todd Garon, Ray Ramos and Alexander Stuart. Additionally, I would like to thank Tristan Smith, whose support, friendship and relentless positivity continued well after I graduated from Swarthmore. I also want thank Ben Taylor for being both the paragon physics teacher and for being the reason I had enough courage to pursue physics in the first place.

I also want to acknowledge the absolute joy and support I have received from my relationships with my colleagues and friends both in and out of Chamberlin. I thank my (official and unofficial) office mates Alex, Greg, Eddie, Sida and Shu Tian for our vibrant discussions about physics and life. I also want to thank Innes, whose commiseration spanning 14 time zones is testament to the wonders of modern telecommunications. Beyond

the theory world, I would like to thank: Harry and Miranda, for their cheerleading, hospitality and assorted neighborly actions; Michael, for who, despite having a sleep schedule as extreme as mine, is a font of neutrino-based optimism; Adam, for being at least slightly more level-headed than I am about the PhD process; Wren, for an infinite sense of humor; Kit and Juliette, for forgiving me for calling Juliette "Stella" for two years; and Ilyas, for his unwavering wit and guidance throughout the pandemic.

I want to express my gratitude to Ken, Emily, Jason, Lauren, Joe, Holly and Doug for adopting me as a child into such a warm, caring friend group that makes Madison feel like home. Outside of Madison, I want to commend Sam, Annie, Yumi, Holden, Azucena, Jorin, Quinn, Dan, Peter, Molly, Tessa and Muriel for listening to me ramble about the trials and tribulations of graduate school for a much longer time than I had any right to expect. I also am grateful for my friendships with Nat, Noah and Katherine – despite our paths crossing less than once, on average. I finally want to express my appreciation for Lucian, Emma, Alex and Maggie for their continued loyalty and support for almost 15 years; likewise for Emilia, who continuously inspires me to be a better scientist.

But most of all, I would like to thank my family, who from the beginning of my life have been dedicated to my well-being and success: from their sacrifice to leave friends and family to immigrate to the US so as to give my brother and me access to better education and opportunities, to the support and care they gave during the pandemic. I would not have, in any imagining, been able to do this without them.

DISCARD THIS PAGE

TABLE OF CONTENTS

Page

Page

DISCARD THIS PAGE

LIST OF TABLES

DISCARD THIS PAGE

LIST OF FIGURES

Figure Page

Figure Page

Part 1: Introduction and Theoretical Overview

Thesis Outline

This dissertation is structured into three parts. In Part 1 we summarize the history and development of the Standard Model. We then summarize the mathematical structure of the Standard Model, after which we introduce the particle content and notation of the Standard Model. We then cover electroweak symmetry breaking and the generation of fermion masses and their mixings. This brings us to a discussion of the free parameters of the Standard Model which is the first of three issues with the Standard Model that will be addressed: the aesthetics of the Standard Model, naturalness in the Standard Model, and the contextualization of the Standard Model within cosmology.

Part 2 begins with a background section on supersymmetry and the minimal supersymmetric Standard Model, especially emphasizing the topic of supersymmetry breaking. The remainder of Part 2 is devoted to the development and phenomenological consequences of a new model of non-Abelian flavored gauge-mediated supersymmetry breaking. We first build a model in which a phenomenologically acceptable Standard Model Higgs mass is achieved with relatively light superpartners. We then extend this model with a nonrenormalizable operator that allows us to obtain Cabibbo-sized quark mixing in the first two generations.

Part 3 starts with the standard beyond-the-Standard Model framework needed to account for neutrino masses, specifically the Maki–Nakagawa–Sakata-Pontecorvo neutrino mixing matrix and the type-I seesaw mechanism of neutrino mass generation. As an example of a prototypical procedure of the use of discrete non-Abelian symmetries in neutrino model building, we explain obtaining tribimaximal mixing via tetrahedral symmetry. We then detail a new self-consistent method of predicting the leptonic Dirac CP-violating phase based on the correlations among observable parameters of neutrino mixing in a specific class of models based on discrete non-Abelian symmetries.

Chapter 1

The Standard Model

1.1 The Historical Development of the Standard Model Since the Twentieth Century

The Standard Model [1–3] is the quantum field theory that for the past forty years has successfully described the strong, weak and electromagnetic interactions of fundamental particles to an extremely high level of accuracy; as of now, the Standard Model is the most experimentally-corroborated theory of physics ever formulated. Its current success and elegance, however, belie the inordinate efforts of thousands of particle theorists and experimentalists over the past near-century. Furthermore, we must recognize the oftentimes decades-long gaps between theory and observation in the history of Standard Model. With this cognizance, and in order to properly contextualize this thesis' work beyond the Standard Model, we now provide a brief (and necessarily simplistic) history of the development and verification of the Standard Model.

Dirac's construction of relativistic quantum mechanics in 1928 [4] in many ways marks the beginning of accelerated development of modern particle physics through the twentieth century. Only five years later, Anderson discovered the positron [5], substantiating the prediction of antimatter from the Dirac equation. Almost simultaneously, Chadwick observed the neutron[6] – the precursor the the mid-century flurry of baryon (and meson) discoveries. This discovery led Heisenberg [7] and Wigner [8] to introduce the concept

of isotopic spin (isospin), a symmetry that was proven invaluable in accommodating the "particle zoo" of mesons soon to be discovered.

Fermi then introduced his eponymous theory of the weak force [9], which introduced to the world the neutrino, a particle initially theorized by Pauli to rescue conservation of energy in beta decays[10]. While Fermi's theory was initially rejected by *Nature* for containing "speculations too remote from reality to be of interest to the reader," it was finally validated twenty-two years later with Cowan and Reines' discovery of the electron neutrino in 1956[11].

Shortly after the introduction of Fermi theory and nuclear isospin, Yukawa posited that the residual nuclear strong force is mediated by a neutral scalar [12]. A particle with mass aligning with Yukawa's prediction was discovered in 1937 [13, 14] – the muon. The muon was not Yukawa's required particle, which was the pion, (discovered in 1947 [15]), but the muon's existence further expanded the elementary particle inventory by establishing a new generation. It was around this time that Tomonaga[16] and Feynman[17] introduced the first quantum field theory, quantum electrodynamics, which would eventually be incorporated entirely into the Standard Model.

It was in the 1950s and 1960s that our current formulation of the Standard Model began to take shape. Our understanding of the weak force was further refined in 1957 with the observation of parity-violation in weak processes [18, 19], and the chiral formulation of the weak force and its unification with quantum electrodynamics proceeded in a series of papers by Glashow [1], Salam[3, 20] and Weinberg [2]. It was only twenty years later when this electroweak theory was confirmed with the observation of the $W^{\pm}$ and Z^0 bosons at the UA1 [21, 22] and UA2 [23] experiments at CERN.

At the same time, the proliferation of observed mesons and baryons led Gell-Mann [24] and Ne'eman [25] to independently introduce the eightfold way in 1961, taxonomizing baryons and mesons via an extension of isospin symmetry that includes strangeness. This was extended in 1964 by Gell-Mann[26] (and by Zweig[27]) in the quark (aces) model. The theory of quarks was promoted from being a purely placeholding construction to a

dynamical theory with the introduction of $SU(3)$ color charge by Greenberg, Han and Nambu [28, 29] in 1964 and culminating in the formulation of quantum chromodynamics as a Yang-Mills gauge theory in 1973 by Fritzsch, Gell-Mann and Leutwyler[30].

The quark model also played a role in the completing our understanding of the weak sector, as in 1970 Glashow, Iliopoulos, and Maiani extended the work of Cabibbo [31], proposing the GIM mechanism to explain the suppression of flavor-changing neutral currents in the Standard Model[32]. The GIM mechanism required the existence of a fourth at-that-time unobserved quark, the charm – which was confirmed by the discovery of the J/Ψ particle in 1974 by concurrent teams at SLAC[33] and Brookhaven [34]. Meanwhile, in 1973, Kobayashi and Maskawa [35] extended the GIM mechanism to accommodate the existence of CP-violation in the weak sector (seen by Christenson in 1964[36]). They did so by postulating the existence of two additional quarks, the b and the t. The bottom quark was found in 1977 at Fermilab [37], and the top eighteen years later again at Fermilab, by the CDF [38] and D0 [39] collaborations.

By 1995, the Standard Model was almost complete, and all that remained was the verification of the Higgs mechanism. The Higgs mechanism was introduced in a 1964 series of four papers on symmetry breaking in PRL by Higgs, Englert, Brout, Guralnik, Hagen and Kibble [40–43]. Without it, the theory of electroweak interactions as developed by Glashow, Weinberg and Salam would not be gauge-invariant, nor would quarks and leptons be able to acquire mass. Nevertheless, it was only in 2012 that the ATLAS [44] and CMS [45] experiments at the LHC finally corroborated the Higgs mechanism via the observation of a 125 GeV scalar particle consistent with the Higgs Boson. See Figure 1.1 for the results for Higgs mass searches over different channels for ATLAS as of March 2021.

Now, with the confirmation of the Higgs boson, almost all collider data agree with the Standard Model. For instance, as can be seen in Figure 1.2, there is robust agreement between Standard Model predicted production cross sections for various particles and observations.

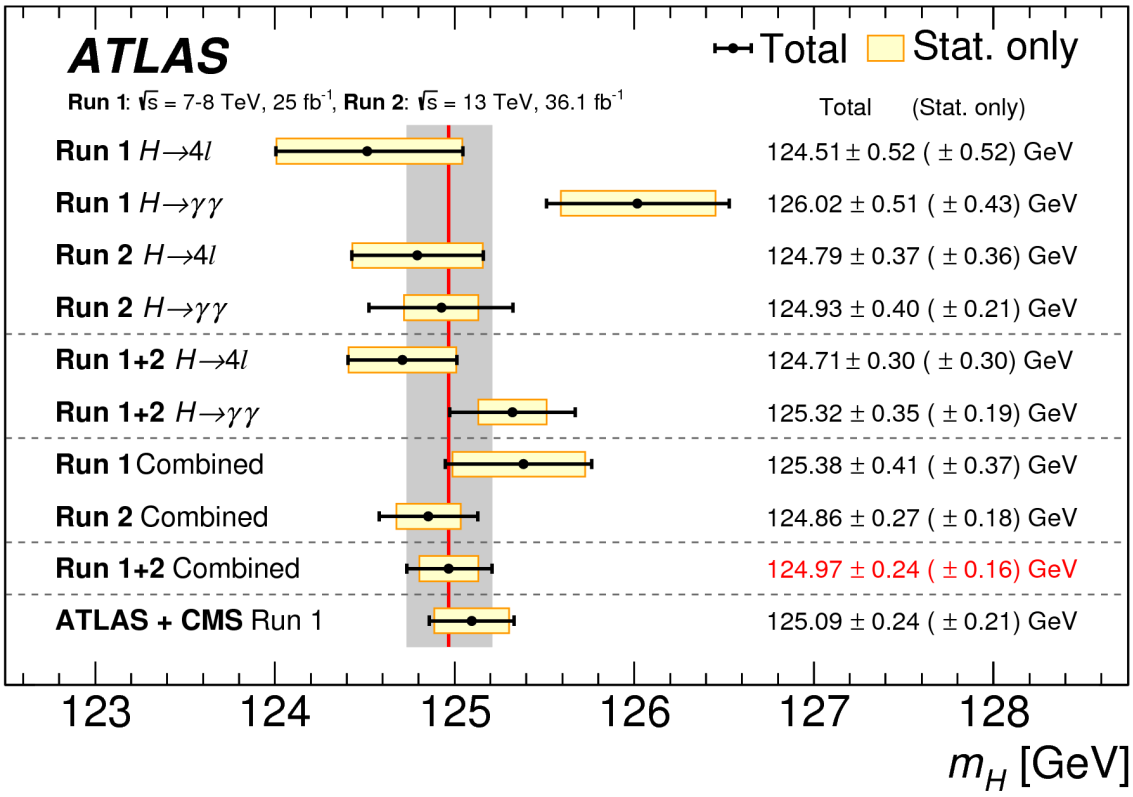

Figure 1.1: A summary of the Higgs boson mass searches done at the ATLAS experiment. Image from [46].

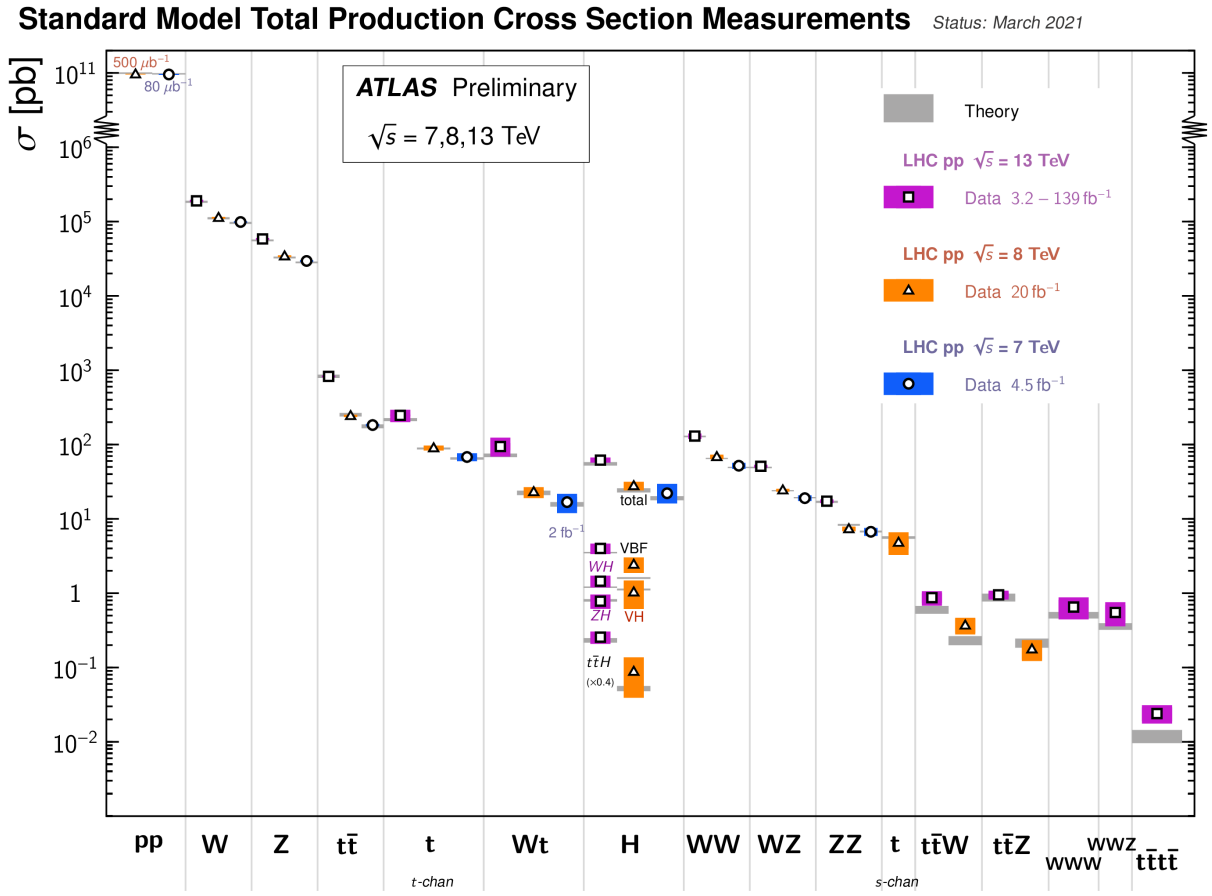

Figure 1.2: A comparison between total production cross sections for Standard Model particles with their theoretical predictions. From [47]

Nevertheless, the Standard Model is not yet complete as a framework for all of particle physics. There are multiple issues with it as a theory; among others, some of these problems are: the proliferation of free parameters and the flavor problem, the unnaturalness of the weak scale, and the absence of a source of neutrino masses and mixing. In this thesis, we will build phenomenological models beyond the Standard Model to address these issues, with a focus on the flavor problem. Specifically, we will embed the Standard Model fields into representations of non-Abelian discrete groups and use their rich structure to build models of flavor. It is this author's hope that the scenarios present in this thesis are one day able to be confirmed by experiment, mirroring the history that lead to the development of the Standard Model.

1.2 The Mathematical Framework of the Standard Model

We now move on from the history of the Standard Model in order to detail its mathematical structure.

1.2.1 Spacetime, Particles and Symmetry

We state that a particle is an irreducible representation of the algebra of spacetime transformations[48]. The transformations of spacetime are translations, rotations and boosts, and together form a Lie group, called the Poincaré group[49]. If translations are excluded, this is the Lorentz Group.

The algebra of the Poincaré group is generated by the operators P_μ and $M_{\mu\nu}$, with

$$[P^\mu, P^\nu] = 0 \tag{1.1}$$

$$[M^{\mu\nu}, P^\sigma] = i\left(g^{\sigma\nu}P^\mu - g^{\sigma\mu}P^\nu\right) \tag{1.2}$$

$$[M^{\mu\nu}, M^{\rho\sigma}] = i\left(g^{\mu\rho}M^{\nu\sigma} - g^{\nu\rho}M^{\mu\sigma} - g^{\mu\sigma}M^{\mu\rho} + g^{\nu\sigma}M^{\mu\rho}\right). \tag{1.3}$$

Spacetime translations are generated by the momentum operator P_μ, rotations by operators $J_i = 1/2\epsilon_{ijk}M^{ij}$ and boosts by operators $K_i = M^{i0}$.

Defining the Pauli-Lubański vector $W_\mu = \frac{1}{2}\epsilon_{\mu\nu\rho\sigma}M^{\nu\rho}P^\sigma$, a particle can be defined as an object that is an eigenstate of both $P^\mu P_\mu$ and $W^\mu W_\mu$, as these two operators commute with every element of the Poincaré algebra. A massive particle will have eigenvalues under these operators $-m^2$ and $m^2 s(s+1)$, respectively, and therefore one can label massive particles as states with definite mass m and definite spin s. We identify massless particles as a massless states with fixed helicity[1].

One should note that this is a classification with respect to the symmetries of four-dimensional spacetime, and therefore cannot account for other distinguishing characteristics of particles, namely their charges.

1.2.2 Charges, Internal Symmetries and the Standard Model

As per Noether's theorem [51], any continuous symmetry of a classical Lagrangian results in a conserved current. This correspondence between continuous symmetry and conservation carries over to quantum theories. In a relativistic, quantum theory, the conserved charges associated with a force must be due to a local, continuous gauge symmetry.

The standard formulation of theories with gauge symmetries, or gauge theories, utilizes the framework of Yang and Mills[52]. The symmetry group for a Yang-Mills theory is $SU(N)$ for $N \geq 2$. An element of the gauge group is given by $U(x) = \exp(i\alpha^a(x)T^a)$, where T^a are the generators of the group algebra. These generators are normalized in such a way that $2\,\mathrm{Tr}(T^aT^b) = \delta^{ab}$, and we may express the Lie algebra as

$$[T^a, T^b] = if^{abc}T^c, \tag{1.4}$$

where f^{abc} are the structure constants of the algebra. The gauge fields, A^a_μ, occupy the adjoint representation of the Lie algebra, they transform as

$$A^a_\mu T^a \to U(x)A^a_\mu T^a U^\dagger(x) + \frac{i}{g}U(x)\partial_\mu U^\dagger(x), \tag{1.5}$$

under an action of the gauge group. g is the coupling strength for the theory.

[1] For a much more detailed explanation of this process using the mathematical structure of the group generated by W^μ, Wigner's little group, see Section 2.5 in [50].

Matter that is charged under the gauge symmetry exists in the fundamental representation of the group, and transform as

$$\psi \to U(x)\psi. \tag{1.6}$$

In order to maintain gauge invariance, in a gauge theory all derivatives ∂_μ must be promoted to covariant derivatives

$$D_\mu = \partial_\mu - igA^a_\mu T^a. \tag{1.7}$$

It is through this derivative that charged matter will couple to the gauge vectors.

Defining the field strength tensor $F^c_{\mu\nu}$ by

$$F^c_{\mu\nu} = \partial_\mu A^c_\nu - \partial_\nu A^c_\mu + g f^{abc} A^a_\mu A^b_\nu, \tag{1.8}$$

the kinetic Lagrangian for the gauge fields is then given by

$$\mathcal{L}_{\text{gauge}} = -\frac{1}{4} F^{c\mu\nu} F_{c\mu\nu}, \tag{1.9}$$

whereas the kinetic operators for charged matter is given by

$$\mathcal{L}_{\text{kinetic}} = i\overline{\psi}\gamma^\mu D_\mu \psi. \tag{1.10}$$

We briefly note that in the Standard Model, left and right-handed fermions exist in different representations of the gauge group, so further refinement of the above is needed. This will also require the introduction of a Higgs mechanism to generate fermionic matter. As for the Standard Model itself, it is a chiral Yang-Mills theory, with gauge group $G_{\text{SM}} = SU(3)_c \times SU(2)_L \times U(1)_Y$. In addition to its gauge structure, the Standard Model contains three generations of matter and a scalar sector comprised of a single Higgs doublet that spontaneously breaks electroweak symmetry.

1.3 The Physical Structure of the Standard Model

1.3.1 Particle Content of the Standard Model

We now introduce the particle (field) content of the Standard Model. A table indicating the fields' representations, spins and notations is given in Table 1.1. There are four broad categories of field: the quarks, the leptons, the gauge bosons, and the Higgs field.

The quarks and leptons comprise the matter content of the Standard Model and are spin $1/2$ fermions. There are three generations of these fermions. The combined numbers of leptons and fermions in each generation is fixed by their individual $U(1)$ charges to be such that all gauge anomalies vanish. Generations are often referred to as families, and within individual types of particle, flavors.

The Flavor Problem

The underlying reason as to why there are (at least) three families is an open question in particle physics. Each of the three generations exists in the exact same representation of G_{SM}, and if they were massless, each would be completely identical. This is not the case, as can be seen in Table 1.2. Each successive generation is more massive than the last and, as we will see, families can mix. In the massless limit, the Standard Model gains an $SU(3)^5 \times U(1)^5$ global flavor symmetry.

The Yukawa sector breaks this symmetry. The exact way in which this symmetry is broken, or why the Yukawa couplings assume their observed values, remains an open problem in particle physics.

Gauge Structure

Each quark comes in three colors, which are the charges for $SU(3)_c$. Leptons are uncharged under $SU(3)_c$. The left-handed fermions all carry $SU(2)_L$ charge, which is weak isospin, whereas the right-handed fermions do not. Lastly, all fermions carry $U(1)_Y$ hypercharge.

The Standard Model		
Field		Representation $(SU(3)_c, SU(2)_L)_{U(1)_Y}$
Spin $1/2$		
Quarks	$Q_i \equiv (u_L, d_L)_i = \{(u_L, d_L), (c_L, s_L), (t_L, b_L)\}$	$(\mathbf{3}, \mathbf{2})_{1/6}$
	$(u_R)_i = \{u_R, c_R, t_R\}$	$(\mathbf{3}, \mathbf{1})_{2/3}$
	$(d_R)_i = \{d_R, s_R, b_R\}$	$(\mathbf{3}, \mathbf{1})_{-1/3}$
Leptons	$L_i \equiv (\nu_L, e_L)_i = \{(\nu_e, e_L), (\nu_\mu, \mu_L), (\nu_\tau, \tau_L)\}$	$(\mathbf{1}, \mathbf{2})_{-1/2}$
	$(e_R)_i = \{e_R, \mu_R, \tau_R\}$	$(\mathbf{1}, \mathbf{1})_{-1}$
Spin 1		
Gauge Bosons	$W_\mu \equiv (W_\mu^+, W_\mu^0, W_\mu^-)$	$(\mathbf{1}, \mathbf{3})_0$
	B_μ^0	$(\mathbf{1}, \mathbf{1})_0$
	g_μ	$(\mathbf{8}, \mathbf{1})_0$
Spin 0		
Higgs	$H = (\phi^+, \phi^0)$	$(\mathbf{1}, \mathbf{2})_{1/2}$

Table 1.1: The fields of the Standard Model and their representations. The subscript $i = \{1, 2, 3\}$ indicates the generation. Parentheses indicate $SU(2)_L$ representations, and brackets display the generations explicitly. Note that the $SU(3)_c$ color indices are suppressed on the quark and gluon fields.

The gauge bosons are spin 1 vector fields. They are the "force carriers" of the Standard Model. The gluons, g, correspond to the $SU(3)_c$ gauge subgroup of G_{SM}. This is the group that governs the strong force. There are eight gluons, which can carry three types of $SU(3)_c$ color charge.

The fields W and B correspond to the $SU(2)_L \times U(1)_Y$ subgroup of G_{SM}, which together comprise the electroweak force. They carry weak isospin and hypercharge respectively.

One of the defining features of the Standard Model is that right-handed fermions do not carry any weak isospin charge and therefore do not interact with the $SU(2)_L$ bosons. Right-handed fermions exist in the trivial, or singlet, representation of $SU(2)_L$. Additionally, right and left handed fermions carry different $U(1)_Y$ charges, It is for this reason that u_L and u_R, for example, are listed as different fields.

Additionally, the massive nature of the $W^{\pm}$ and Z^0 bosons and the existence of Dirac masses necessitate a Higgs mechanism and electroweak symmetry breaking (EWSB), which we now discuss.

Electroweak Symmetry Breaking

In addition to the $\mathcal{L}_{\text{gauge}}$ and $\mathcal{L}_{\text{kinetic}}$ Lagrangians in Eqs. 1.9 and 1.10, the Standard Model also contains a Higgs sector Lagrangian and a Yukawa sector Lagrangian. The Higgs Lagrangian is

$$\mathcal{L}_{\text{Higgs}} = (D^{\mu}H)^{\dagger}(D_{\mu}H) - V(H) \tag{1.11}$$

$$V(H) = \mu^2 H^{\dagger}H + \lambda(H^{\dagger}H)^2. \tag{1.12}$$

If $\mu^2 < 0,$ the Higgs field will acquire a VEV, which we can take to be real and neutral by an $SU(2)_L \times U(1)_Y$ gauge transformation. Its VEV is then

$$v = \langle H \rangle = \sqrt{\frac{-\mu^2}{\lambda}}. \tag{1.13}$$

This VEV is not invariant under the group $SU(2)_L \times U(1)_Y$, so the electroweak gauge symmetry is broken into a $U(1)_{EM}$ symmetry, where $U(1)_{EM}$ is the gauge group of electromagnetism. The real degree of freedom of the ϕ^0 component of H acquires a mass, and

this particle is the Higgs boson h^0, with mass $m_{h^0}^2 = -\mu^2$ This process is called electroweak symmetry breaking (EWSB).

Of the three T^i generators of $SU(2)_L$ and the Y generator of $U(1)_Y$, the only remaining generator that keeps the vacuum invariant is the linear combination $Q = T^3 + Y$, which is the electromagnetic charge operator that generates $U(1)_{EM}$.

Through the $(D^\mu H)^\dagger (D_\mu H)$ interaction of the Higgs Lagrangian, the electroweak gauge fields $W_\mu^\pm$ gain masses, along with a linear combination of B_μ^0 and W_μ^0. This linear combination is the weak Z_μ^0 boson. There is a massless, orthogonal linear combination as well, which is the photon, A_μ. After electroweak symmetry breaking, the $(D^\mu H)^\dagger (D_\mu H)$ operator creates a term

$$\left(\frac{vg}{2}\right)^2 W_\mu^+ W^{\mu -}, \tag{1.14}$$

indicating the $W^\pm$ have acquired a mass

$$M_W = \frac{1}{2} vg. \tag{1.15}$$

Additionally, the neutral bosons B_μ^0 and W_μ^0 mix, with their mixing governed by the matrix

$$M_{WB} = \frac{v^2}{8} \begin{pmatrix} g^2 & -gg' \\ -gg' & g'^2 \end{pmatrix}. \tag{1.16}$$

The eigenvectors of this matrix are the A_μ and Z_μ^0 gauge bosons, which can be expressed as the linear combinations

$$\begin{pmatrix} Z_\mu^0 \\ A_\mu \end{pmatrix} = \begin{pmatrix} \cos\theta_W & -\sin\theta_W \\ \sin\theta_W & \cos\theta_W \end{pmatrix} \begin{pmatrix} W_\mu^0 \\ B_\mu^0 \end{pmatrix}, \tag{1.17}$$

where θ_W is the Weinberg angle, defined as

$$g \tan\theta_W = g'. \tag{1.18}$$

The eigenvalue corresponding to the A_μ eigenvector is zero, indicating the photon stays massless, whereas the Z_μ^0 acquires a mass

$$M_Z = \sec\theta_W M_W. \tag{1.19}$$

1.3.2 Fermion Masses and Mixings

Along with $\mathcal{L}_{\text{Higgs}}$, there is also a $\mathcal{L}_{\text{Yukawa}}$ that couples fermions to the Higgs field to generate their masses[2] . It is given by (suppressing gauge indices for clarity)

$$-\mathcal{L}_{\text{Yukawa}} = Y^d_{ij}\overline{Q}_{Li}d_{Rj}H + Y^L_{ij}\overline{L}_{Li}e_{Rj}H + Y^u_{ij}\overline{Q}_{Li}u_{Rj}\tilde{H} + \text{h.c}, \tag{1.20}$$

where $\tilde{H} = i\sigma_2 H^*$. After EWSB, the Higgs field becomes

$$H \to \frac{1}{\sqrt{2}}\begin{pmatrix} 0 \\ v + h^0 \end{pmatrix}. \tag{1.21}$$

This generates mass terms for the fermions, with

$$-\mathcal{L}_{\text{Yukawa}} \supset -\mathcal{L}_{\text{mass}} = \frac{vY^d_{ij}}{\sqrt{2}}\overline{d}_{Li}d_{Rj} + \frac{vY^L_{ij}}{\sqrt{2}}\overline{e}_{Li}e_{Rj} + \frac{vY^u_{ij}}{\sqrt{2}}\overline{u}_{Li}u_{Rj} + \text{h.c} \tag{1.22}$$

$$\equiv m^d_{ij}\overline{d}_{Li}d_{Rj} + m^L_{ij}\overline{e}_{Li}e_{Rj} + m^u_{ij}\overline{u}_{Li}u_{Rj} + \text{h.c}. \tag{1.23}$$

Fermions that acquire mass via a term of the form $m\bar{\psi}\psi$ are referred to as Dirac fermions.

Note that these m_{ij} are not necessarily diagonal, and therefore each must be diagonalized biunitarily in the following way:

$$m^{\text{diag}} = U_L m U_R^\dagger. \tag{1.24}$$

The entries on the diagonal of m^{diag} are the mass eigenvalues of the quarks and charged leptons. These values are not the invariant masses of the particles; they are only Lagrangian parameters that are related to the physical masses via renormalization group flow. For experimentally determined physical masses of particles in the Standard Model, see Table 1.2. The range of quark and charged lepton masses spans many orders of magnitude. The addition confirmation of sub-eV massive neutrino widens this range. It is the construction of these mass hierarchies that will inform our model building in this dissertation.

[2]N.B. While neutrinos are fermions with mass, their mass generation is wholly outside the Standard Model. We will come back to this topic in Part 3.

The diagonalization process given in Eq. 1.24 can also be thought of as a rotation on the fermion fields, with U_L acting on the left-handed fields and U_R on the right-handed. This rotation brings the fields into the mass basis[3].

Particle Masses			
Fermions			
Generation	1	2	3
Up-Type Quarks	$m_u = 2.16^{+0.49}_{-0.26}$ MeV	$m_c = 1.27 \pm 0.02$ GeV	$m_t = 172.76 \pm 0.30$ GeV
Down-Type Quarks	$m_d = 4.67^{+0.48}_{-0.16}$ MeV	$m_s = 93^{+11}_{-5}$ MeV	$m_b = 4.18^{+0.03}_{-0.02}$ GeV
Charged Leptons	$m_e = 0.51109 \pm 3.1 \times 10^{-9}$ MeV	$m_\mu = 105.66 \pm 2.4 \times 10^{-6}$ MeV	$m_\mu = 1776.9 \pm 0.12$ MeV
Combined Neutrino Masses	$\sum_\nu m_\nu < 0.15$ eV		
Gauge Bosons			
Photon	Gluon	W Bosons	Z Boson
$m_\gamma = 0$	$m_g = 0$	$m_W = 80.379 \pm 0.012$ GeV	$m_Z = 91.188 \pm 0.0021$ GeV
Higgs Boson			
$m_h = 125.1 \pm .14$ GeV			

Table 1.2: Experimentally determined particle masses as listed in [53]. The masses for the u, d and s quarks are quoted with their current masses using $\overline{\text{MS}}$ at $\mu = 2$ GeV. The c and b quarks are quoted as their running masses in the $\overline{\text{MS}}$ scheme, and the top quark is quoted at its directly-measured value.

This has deep ramifications on the phenomenology of the Standard Model. After EWSB, the charged-current interactions mediated by $W^\pm_\mu$ couple to quarks via terms of the form

$$\mathcal{L}_{cc} \sim W^+_\mu \bar{u}_{Li} \gamma^\mu d_{Li} + \text{h.c.} \tag{1.25}$$

Note that this is diagonal, since by definition u_L and d_L form a single doublet representation of $SU(2)_L$. However, this is not the mass basis, and by rotating the quarks into the mass basis we introducing mixing. To wit:

$$\mathcal{L}_{cc} \rightsquigarrow W^+_\mu \bar{u}_{Li} \left(U_{uL} U^\dagger_{dL} \right)_{ij} \gamma^\mu d_{Lj} + \text{h.c}, \tag{1.26}$$

where the quarks are in the mass basis.

[3]Unless there is ambiguity, we will denote the mass basis with the same notation as the interaction basis.

We see that there is now a matrix $U_{uL}U_{dL}^{\dagger}$ that mixes generations. This matrix is known as the Cabibbo-Kobayashi-Maskawa matrix, or V_{CKM}[31, 35][4]. An example charged-current interaction that would mix an up and strange quark is given in Figure 1.3. The entries of V_{CKM} appear in these diagrams and affect their amplitudes.

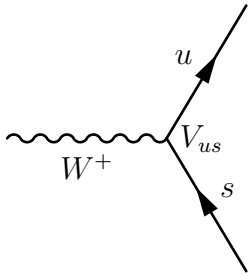

Figure 1.3: A typical weak vertex that mixes up and strange quarks. Note the appearance of an entry of V_{CKM}.

V_{CKM} is a general unitary 3×3 matrix, meaning it has nine free parameters: three real mixing angles and six complex phases. Five of the complex phases may be absorbed by redefinitions of the quark fields, leaving V_{CKM} to be parameterized by three angles θ_{12}, θ_{23} and θ_{13}, and one CP-violating phase δ. Denoting $\sin\theta_{ij} = s_{ij}$ and $\cos\theta_{ij} = c_{ij}$, the canonical parameterization for V_{CKM} is given by the PDG as [53]:

$$V_{\text{CKM}} = \begin{pmatrix} 1 & 0 & 0 \\ 0 & c_{23} & s_{23} \\ 0 & -s_{23} & c_{23} \end{pmatrix} \begin{pmatrix} c_{13} & 0 & s_{13}e^{-i\delta} \\ 0 & 1 & 0 \\ -s_{13}e^{i\delta} & 0 & c_{13} \end{pmatrix} \begin{pmatrix} c_{12} & s_{12} & 0 \\ -s_{12} & c_{12} & 0 \\ 0 & 0 & 0 \end{pmatrix}. \tag{1.27}$$

The current global fits for these parameters as given by the PDG are listen in Table 1.3,

Canonically, the angle θ_{12} is known as the Cabibbo angle. It controls mixing between the first and second generations and is the largest mixing angle. The relative magnitudes of the entries in V_{CKM} is given diagrammatically on the left of Figure 1.4. Note that V_{CKM} is highly structured, with the diagonal elements being the largest and the off diagonals being

[4]Note that it is often convention to define the up quark interaction in 1.20 as initially diagonal and then define the weak eigenbasis for the down quarks in terms of the mass states via $d_i^{\text{weak}} = V_{\text{CKM}} d_i^{\text{mass}}$.

CKM Parameter	Value
s_{12}	$0.22650 \pm .000048$
s_{23}	$0.04053^{+0.00083}_{-0.00061}$
s_{13}	$0.00361^{+0.00011}_{-0.00009}$
δ	$1.196^{+0.045}_{-0.043}$

Table 1.3: The current global fit values of the CKM mixing and phase angles, as reported in the PDG [53].

supressed. Furthermore, note that $|V_{ub}| < |V_{cb}| < |V_{us}|$, indicating that mixing between distant generations is suppressed.

We should contrast the highly-structured, mostly-diagonal nature of V_{CKM} with mixing in the neutrino sector, which will be discussed further in Chapter 5. It is now known that neutrinos have mass, and therefore weak eigenstates mix [54–60]. Analogously to V_{CKM}, there exists the Maki-Nakagawa-Sakata-Pontecorvo mixing matrix, U_{MNSP}, such that

$$\begin{pmatrix} \nu_e \\ \nu_\mu \\ \nu_\tau \end{pmatrix} = \underbrace{\begin{pmatrix} U_{e1} & U_{e2} & U_{e3} \\ U_{\mu 1} & U_{\mu 2} & U_{\mu 3} \\ U_{\tau 1} & U_{\tau 2} & U_{\tau 3} \end{pmatrix}}_{U_{\text{MNSP}}} \begin{pmatrix} \nu_1 \\ \nu_2 \\ \nu_3 \end{pmatrix}. \tag{1.28}$$

The fields $\nu_{e,\mu,\tau}$ are neutrinos in the weak interaction basis, and $\nu_{1,2,3}$ are the mass eigenstates. However, the qualitative behavior of U_{MNSP} is significantly different than that of V_{CKM}. As can be seen on the right of Figure 1.4, U_{MNSP} has large off-diagonal entries, which is markedly different from the off-diagonal suppression in V_{CKM}.

This parametric behavior has significant ramifications for model-building. The structure of V_{CKM} makes it clear that one may describe it as a diagonal matrix with off-diagonal perturbations. Using the standard notation where $s_{12} = \lambda$, one may roughly consider V_{CKM} via the following expansion

$$V_{\text{CKM}} \sim \mathbb{1}_{3\times 3} + \lambda V_{1-2\text{ mixing}} + \lambda^2 V_{2-3\text{ mixing}} + \lambda^3 V_{1-3\text{ mixing}} + \mathcal{O}(\lambda^4). \tag{1.29}$$

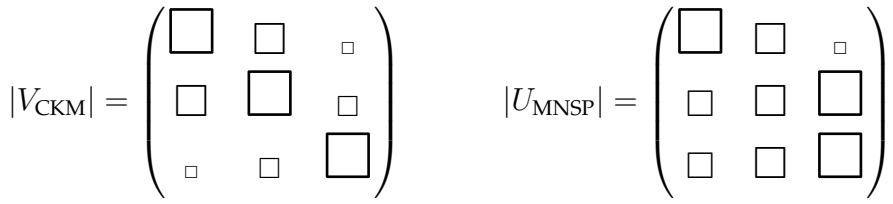

Figure 1.4: Relative magnitudes of the entries of V_{CKM}, (left), and U_{MNSP}, (right). Larger boxes indicate larger magnitudes. Note that the boxes are not to scale between V_{CKM} and U_{MNSP}.

This expansion is the Wolfenstein parameterization [61]:

$$V_{\text{CKM}} = \begin{pmatrix} 1-\lambda^2/2 & \lambda & A\lambda^3(\rho - i\eta) \\ -\lambda & 1-\lambda^2/2 & A\lambda^2 \\ A\lambda^3(1-\rho-i\eta) & -A\lambda^2 & 1 \end{pmatrix} + \mathcal{O}(\lambda^4), \tag{1.30}$$

where $\lambda = s_{13}$, $A\lambda^2 = s_{23}$ and $A\lambda^3(\rho + i\eta) = s_{13}e^{i\delta}$.

The model-building implication of the ability to perturbatively expand V_{CKM} in small λ is that the use of a $U(1)$ Froggatt-Nielsen mechanism is appropriate[62]. While nothing actively precludes constructing U_{MNSP} in such a way, the existence of large mixing angles indicates that the use of finite, non-Abelian discrete symmetries is warranted. We will see an explicit construction of such a model in Chapter 5.

In the absence of such models, however, the parameters of V_{CKM} and U_{MNSP} are completely free, with no reason to assume the values that they take. This is only one aspect of lack of *a priori* principles for the values of the parameters in the theory, which hints a much broader question about the writ large incompleteness of the Standard Model.

1.4 Issues with the SM

1.4.1 Aesthetics

We would like a fundamental theory to take as few inputs as possible, both numerically and structurally. This is not the case in the Standard Model. Among the aspects of the Standard Model that require explicit choices in its construction are: the numerical values of the 19 free parameters in the theory, the existence of three identical generations of matter and their representations, and the choice of the gauge group G_{SM}.

Let us first briefly list the 19 parameters of the Standard Model in Table 1.4. The gauge sector of the Standard Model has three free gauge couplings: g, the $SU(2)_L$ gauge coupling, g', the $U(1)_Y$ gauge coupling, g_s, the $SU(3)_c$ gauge coupling. Note that it is often preferable to work with the quantities $\alpha_i = g_i^2/(4\pi)$. Also in the gauge sector is θ_{QCD}, the strong CP-violating angle [5]. There are two parameters from the scalar Higgs sector, m_h^2 and v.

Parameters of the Standard Model		
Sector	Parameters	Number
Gauge	g, g', g_s	3
	θ_{QCD}	1
Higgs	m_h^2, v	2
Quarks	m_u, m_d, m_c, m_s, m_t, m_b	6
	θ_{12}, θ_{23}, θ_{13}, δ	4
Leptons	m_u, m_d, m_c	3
	Total	19

Table 1.4: Parameters of the Standard Model

The Yukawa sector has 13 parameters, more than double the number of parameters in the gauge and Higgs sectors combined. As we have seen, there is an observed hierarchy in

[5] The question of the existence and value of θ_{QCD} is known as the strong CP problem. Experimentally, $|\theta_{\text{QCD}}| < 10^{-11}$, and the mechanism that keeps it so small is not yet fully known [53].

the Yukawa sector; quarks and leptons display a mass hierarchy and V_{CKM} is structured as a diagonal matrix with systematic perturbations off the diagonal. These parameters comprise what is known as the flavor sector of the Standard Model. The question of a full understanding of sector is known as the flavor problem.

The absence of an underlying reason for the values of the gauge couplings is *a fortiori* a question of the origin of the entire gauge structure of the Standard Model. Formally, a single generation of Standard Model fermions is defined as the completely reducible

$$(\mathbf{3},\mathbf{2})_{1/6} \oplus (\mathbf{3},\mathbf{1})_{2/3} \oplus (\mathbf{3},\mathbf{1})_{-1/3} \oplus (\mathbf{1},\mathbf{2})_{-1/2} \oplus (\mathbf{1},\mathbf{1})_{-1} \tag{1.31}$$

representation of the gauge group $G_{SM} = SU(3)_c \times SU(2)_L \times U(1)_Y$. It would be preferable to have a formulation of the Standard Model that is less reducible. These formulations are known as grand unified theories (GUTs), wherein G_{SM} is a subgroup of a simple group at a high scale, G_{GUT}. In these theories, a generation of fermions may exist as a less-reducible representation of G_{GUT}, such as the $\mathbf{10} \oplus \mathbf{5}$ of $SU(5)$, or the $\mathbf{16}$ of $SO(10)$[63, 64]. There are also GUTs that attempt to combine all three generations of fermions into one representation, such as in models of $SO(18)$ comprehensive unification[65].

Furthermore, the running of the gauge couplings in the Standard Model display slightly convergent behavior at a high scale $\mu_{\text{GUT}} \sim 10^{16}$ GeV, but do not actually converge, as shown in Figure 1.5 in the case of $SU(5)$ unification. Note that in Figure 1.5 $\alpha_2 \equiv \alpha$, $\alpha_3 \equiv \alpha_s$ and α' is normalized such that $\alpha_1 \equiv (5/3)\alpha'$, as is required for $SU(5)$ GUTs.

This lack of convergence indicates that additional physics must be added between M_Z and μ_{GUT}. As we shall see, supersymmetry can provide the necessary modifications to the renormalization group equations needed to achieve quantitative gauge coupling unification.

1.4.2 Naturalness

Another question about the parameters of the Standard Model is the reason as to why all physical parameters are at or below the weak scale[6]. The naturalness problem shows

[6]Much of this analysis follows argumentation in [66, 67].

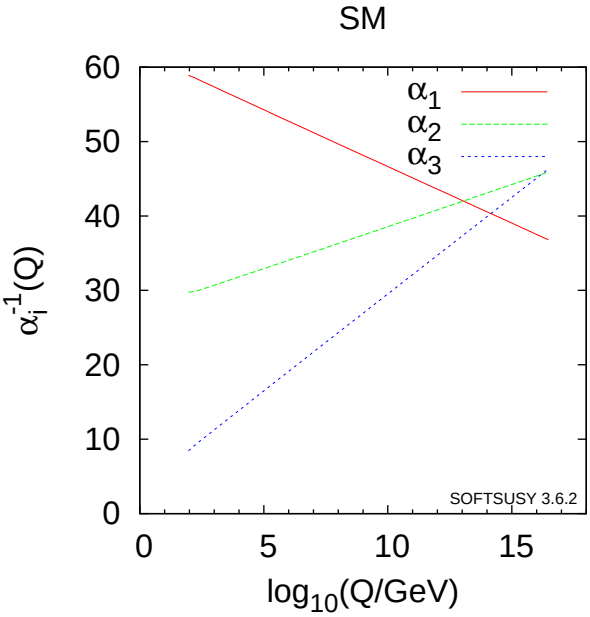

Figure 1.5: The two-loop RG-evolution of the Standard Model gauge couplings, displaying the lack of marked convergence at $\mu_{\mathrm{GUT}} \sim 10^{16}$ GeV. From [53].

that the Standard Model – which is an effective field theory – can be substantially affected by physics at a much higher scale. More specifically, there is no mechanism for maintaining the separation of the weak scale of the Standard Model and higher scales. This can be seen in the Higgs sector in the following way.

Consider the diagram in Figure 1.6. This contributes to the self-energy correction to the Higgs mass, giving

$$\delta\mu^2 = -\frac{3|y_t|^2}{8\pi^2}\left[\Lambda_{UV}^2 - 3m_t^2 \ln\left(\frac{\Lambda_{UV}^2 + m_t^2}{m_t^2}\right) + \dots\right], \tag{1.32}$$

where y_t is the top quark Yukawa coupling. The form of Eq. 1.32 is interesting and problematic for two reasons. The first is that δm_h^2 is quadratic in Λ_{UV}. The quadratic divergence is often taken to be a statement of the hierarchy problem: the Higgs mass has a tendency to be corrected to the UV scale.

As the Standard Model is an effective field theory, one may interpret Λ_{UV} as the scale at which the Standard Model is no longer valid. If there is no new physics between the

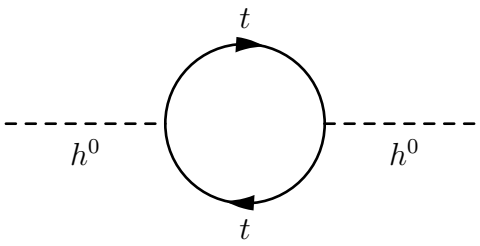

Figure 1.6: The top-quark contribution to the Higgs' self-energy.

weak scale of the Standard Model and the Λ_{UV} scale of its ascended theory, then the Higgs mass will get pushed up to Λ_{UV}. This demonstrates one aspect of the hierarchy problem; the Higgs mass is unprotected within the EFT of the Standard Model.

An additional aspect of the hierarchy problem is apparent from the logarithmically divergent term in Eq. 1.32. Specifically, we see that $\delta\mu^2$ is dependent on m_t^2, indicating that the Higgs is sensitive to the masses of particles it couples to.

Assume, for example, the existence of a colorless scalar ϕ of mass $m_t < m_\phi \ll \Lambda_{UV}$, and that it couples to the Higgs via $-\lambda_\phi |H|^2|\phi|^2$. It will therefore introduce a correction similar to Eq. 1.32,

$$\delta_\phi \mu^2 = \frac{\lambda_\phi}{16\pi^2}\left[\Lambda_{UV}^2 - m_\phi^2 \ln\left(\frac{\Lambda_{UV}^2 + m_\phi^2}{m_\phi^2}\right) + \dots\right]. \tag{1.33}$$

If λ_ϕ were generic, this new physics would not cancel the quadratic divergence in m_h^2. If, however, we were to have $\lambda_\phi = 6|y_t|^2$, we see that the quadratic divergences in Eq. 1.32 and in Eq. 1.33 cancel, i.e

$$\delta\mu^2 + \delta_\phi\mu^2 = -\frac{3|y_t|^2}{8\pi^2}\left[m_\phi^2 \ln\left(\frac{\Lambda_{UV}^2 + m_\phi^2}{m_\phi^2}\right) - 3m_t^2 \ln\left(\frac{\Lambda_{UV}^2 + m_t^2}{m_t^2}\right) + \dots\right]. \tag{1.34}$$

The hierarchy problem is still present, however. The scale of the new physics we have introduced is m_ϕ. The role of m_ϕ is to cancel the large corrections due to physics at Λ_{UV}. However, since $m_t < m_\phi$, the overall correction to $\delta\mu^2$ will still go as m_ϕ^2, and the Higgs will once again be driven towards a high scale

Therefore with the introduction of new physics, the weak scale will generically approach the next highest scale in the theory. In Part 2, we will see how supersymmetry keeps these scales separated without the need to fine-tune.

1.4.3 Cosmology

While the Standard Model is predictive at the micro-scale, it does not answer many of the outstanding questions in astrophysics and cosmology. It is well known that there is a significant imbalance of matter and antimatter[68–71]. While it is theoretically possible to explain baryon asymmetry using Standard Model processes [72], the magnitude of the observed asymmetry is much too large to be feasibly generated. If one extends the Standard Model to contain heavy right-handed sterile neutrinos, this asymmetry may generated dynamically via the process of leptogenesis[73]. Baryogenesis may also come from sphalerons during the electroweak phase transition, although this still requires extending the Standard Model [74].

It is also well-established that the universe is expanding [75] at a rate that indicates the presence of dark energy [76, 77]. Again, the Standard Model provides lacks a mechanism for explanation. There are many BSM theories that are amenable to models of dark energy[7]; as one example, in theories where supersymmetry breaks softly via mediation, the cosmological constant can receive a contribution of order $\sim M_X^4$ arising from the hidden sector supersymmetry breaking scale, M_X [80–82] – a specific implementation of quintessence theories[83].

Another contribution to the energy density of the universe is dark matter[70, 71, 84, 85, 85], which massively outnumbers baryonic matter. The Standard Model does not contain any particles that could feasibly be dark matter candidates. However, if R-parity is conserved in supersymmetry, it may be that the lightest supersymmetric partner is a candidate for dark matter [86]. Another interesting supersymmetric dark matter source could be the messengers in theories of gauge-mediated supersymmetry breaking[87]. Nevertheless, supersymmetry is only one of the myriad dark matter models under considering, for a review see [88].

[7] See the reviews [78, 79] for overviews of the vast range of dark energy models.

1.5 The Next Steps

The Standard Model, while an historic achievement in its scope, accuracy and predictivity, is not a complete theory of particle physics. This is where beyond the Standard Model (BSM) physics begins. Moving forward, Part 2 of this thesis will focus on addressing the problems of naturalness and flavor using the framework of supersymmetry and discrete non-Abelian family symmetries. This is in no way the unique path forward, nor – as we have seen– are those the only open problems, but we have chosen to do so for concrete reasons. Namely, the LHC and other experiments continue to provide interesting data on flavor effects, and supersymmetry continues to be the most well-tested and robust BSM theory in use. Much of its parameter space has been, and continues to be probed by experiment. As an example, see Figure 1.7 for a summary plot of ATLAS supersymmetry searches and their current bounds. As searches for supersymmetry are still ongoing, and supersymmetry has not yet been ruled it, now is a good to time build supersymmetric models that may be testable in the near future.

More specifically, we will build a model of supersymmetry breaking in which a finite non-Abelian discrete symmetry plays a paramount role. This model of supersymmetry breaking will allow us approach the flavor problem in a nonstandard way – through supersymmetry breaking itself. As both flavor and supersymmetry are broken at the collider scale, we will detail a model wherein the origin of both descend from a single symmetry.

Looking forward to Part 3, we will discuss the issue of neutrino masses and mixings. Again, we will use the paradigm of discrete non-Abelian symmetries to analyze models of neutrino flavor and the associated predictions for CP-violating parameters in that sector.

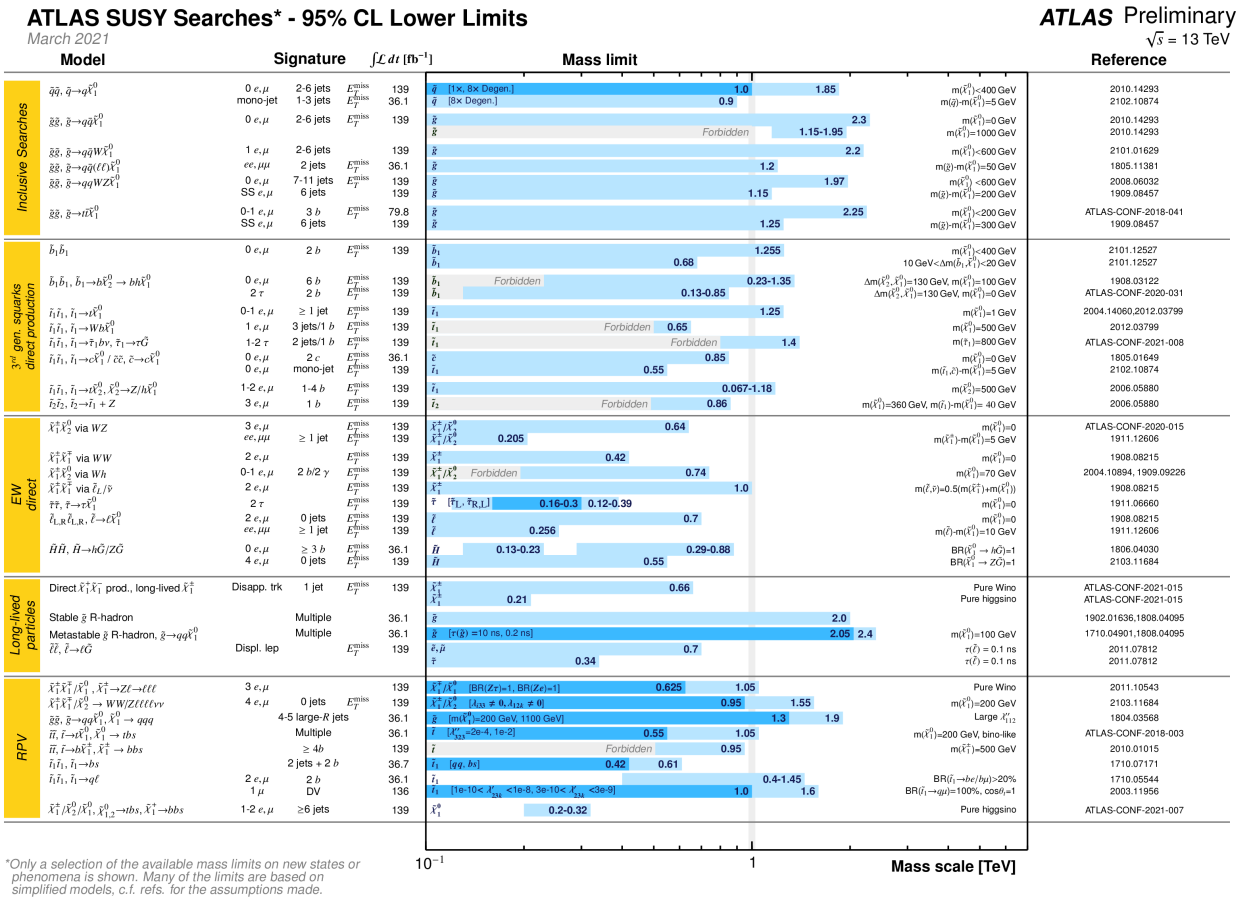

Figure 1.7: Current mass reach for supersymmetry searches by ATLAS. From [89]

Part 2: Family and Supersymmetry Breaking

Chapter 2

Supersymmetry

We have established that the Standard Model – while an enormous success – is incomplete. Furthermore, the hierarchy problem indicates that the Standard model is quadratically sensitive to any additional physics at higher scales. The pessimist may take these statements together to mean that there is no chance of incorporating new physics beyond the Standard Model without making it unnatural, but the pragmatist concludes the following: a viable BSM theory should keep the Standard Model down at the weak scale. One theory that extends that Standard Model while *enforcing* the stability of electroweak scale is supersymmetry.

In this chapter, we summarize the machinery of supersymmetry in order to introduce supersymmetry breaking. We then discuss previous work done in a specific iteration of supersymmetry breaking – called flavored gauge mediation – as background for the author's work as detailed in Chapters 3 and 4.

2.1 Intro to Supersymmetry

Supersymmetry is an additional symmetry imposed on the Standard Model wherein there is a supersymmetry transformation that maps every particle in the Standard Model to a superpartner with spin that differs by $1/2$. This transformation, generated by Q, schematically operates as

$$Q\,|\text{Boson}\rangle \to |\text{Fermion}\rangle\,, \qquad Q\,|\text{Fermion}\rangle \to |\text{Boson}\rangle\,. \tag{2.1}$$

For this operation to make mathematical sense, we see that Q must be spinorial, so it should carry a spinor index, α. Additionally, since Q_α is a spinor, its Dirac adjoint must also be an operator, denoted by $\overline{Q}_{\dot{\alpha}}$. The exact form and algebraic properties of this operator[1] Q_α are strongly constrained by various theorems [90, 91]. Specifically, the *supersymmetry algebra* must satisfy

$$\{Q_\alpha, \overline{Q}_{\dot{\alpha}}\} = 2\sigma^\mu_{\alpha\dot{\alpha}} P_\mu, \tag{2.2}$$

$$\{Q_\alpha, Q_\alpha\} = \{\overline{Q}_{\dot{\alpha}}, \overline{Q}_{\dot{\alpha}}\} = 0 \tag{2.3}$$

$$[Q_\alpha, P^\mu] = [\overline{Q}_{\dot{\alpha}}, P^\mu] = 0. \tag{2.4}$$

What we can see from the supersymmetry algebra is that the Poincaré algebra which generates spacetime is contained within the supersymmetry algebra. As we have seen, particles are defined as irreducible representations of the Poincaré algebra; the analogous statement for supersymmetry is that the irreducible representations of the supersymmetry algebra are *supermultiplets*. Supermultiplets contain both bosonic and fermionic degrees of freedom, which are connected via transformations generated by Q, making Eq. 2.1 a more rigorous statement. It can also be shown that Q commutes with internal symmetry generators, indicating that supermultiplets can be well-defined representations of gauge groups.

For a theory with $N = 1$ supersymmetry generators in $D = 4$ spacetime dimensions, there two categories of supermultiplets: *chiral* and *vector* supermultiplets. A chiral supermultiplet contains the physical fields ϕ (a complex scalar) and ϕ (a two-component Weyl fermion). Analogously, the vector supermultiplet contains the physical fields A_{mu} (a spin-1 gauge boson) and λ (a spin 1/2 spinor called the *gaugino*[2]). However, one can show that supersymmetry algebra only closes if the physical fields remain on-shell, which would preclude its quantization. The solution is to introduce non-propagating degrees of

[1] We have been eliding the fact that there can be $N \leq 8$ pairs of supersymmetry generators, but in this work we will only consider situations where $N = 1$.

[2] See Table 2.1 for superpartner naming conventions.

freedom into the supermultiplets–a complex scalar F in the chiral supermultiplet, and a real scalar D in the vector supermultiplet.

Since the supersymmetry algebra is an extension of the Poincaré algebra, we can think of supersymmetry as extending the geometry of spacetime. Rigorously, the four spacetime coordinates x^μ that label a field $\phi(x^\mu)$ are extended to include additional non-commuting fermionic coordinates, $x^\nu \rightarrow (x^\mu, \theta_\alpha, \overline{\theta}^{\dot{\alpha}})$. In superspace, the supermultiplets operate as unified *superfields*, and supersymmetry transformations become infinitesimal translations and rotations in superspace. We will denote the superfield corresponding to a chiral supermultiplet as $\mathbf{\Phi}$, that of a vector supermultiplet by $\mathbf{V}$ and drop the distinction between superfield and supermultiplet.

The Lagrangian in a supersymmetric theory can be constructed from three functions of the superfields (along with specifying particle and gauge content). The first is the superpotential, a holomorphic function of the superfields. In the case of renormalizable supersymmetric theories, it is of the form

$$W = L^i \mathbf{\Phi}_i + M^{ij} \mathbf{\Phi}_i \mathbf{\Phi}_j + Y^{ijk} \mathbf{\Phi}_i \mathbf{\Phi}_j \mathbf{\Phi}_k. \tag{2.5}$$

The L term is forbidden if there are no gauge-singlet superfields in the theory, which is true in the cases we shall consider.

The second is the Kähler potential, a real-valued function of the superfields which in renormalizable theories is just $K = \mathbf{\Phi}^i \mathbf{\Phi}_i^*$ at tree level. The last is the gauge kinetic function f, which in theories with less than two $U(1)$ gauge groups is just a complex number. Additionally, the scalar potential is a function of the F and D terms of the theory, which in globally supersymmetric theories is given by

$$V = \sum_i |F_i|^2 + \frac{1}{2} D_a^2. \tag{2.6}$$

We are now at a point where we can make precise the statement that supersymmetry solves the hierarchy problem.

2.1.1 Supersymmetry and the Hierarchy Problem

All non-gauge interactions in a supersymmetric theory descend from the superpotential W via

$$\mathcal{L} = \int \mathrm{d}^2\theta\, W + \int \mathrm{d}^2\bar{\theta}\, W^*. \tag{2.7}$$

Since the same parameter in Y applies to every member of a supermultiplet, supersymmetry enforces very strict relationships between different operators. Let us consider specifically all vertices between Higgs and top supermultiplets. In Figure 2.1, the Standard Model top Yukawa interaction on the left requires the existence of the supersymmetrized vertex on the right. Since F_{tL} is non-propagating, it must be intergrated out, leading to the four-point vertex in Figure 2.2.

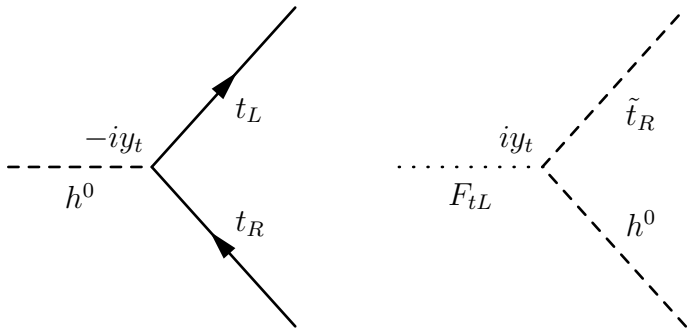

Figure 2.1: The top Yukawa term and its supersymmetrization.

Note that this is exactly the vertex detailed above Eq. 1.33. Note that there is an equivalent diagram coupling $\tilde{t}_L$ and h_0, with the same vertex. Additionally, $\tilde{t}_{L,R}$ come in three colors, so there is a total contribution from vertices of this form with value $g|y_t|^2$. Note that this is precisely the relationship we desired in Section 1.4.2. There are additional three-point diagrams between $\tilde{t}_{L,R}$, and h^0, which will exactly cancel the $m_t^2 \ln\left(\frac{\Lambda_{UV}^2+m_t^2}{m_t^2}\right)$ term in Eq. 1.32.

It can be shown that this cancellation persists at all order for all corrections to the Higgs' self-energy. In fact, the holomorphicity of the superpotential guarantees that all perturbative corrections to any of its parameters vanish[92–97]. This is not the case for broken

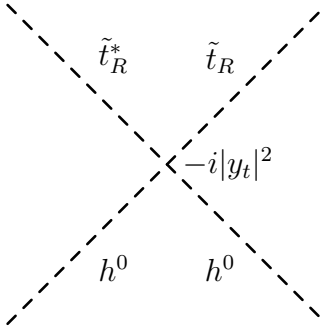

Figure 2.2: The effect four-point Higgs-stop vertex.

supersymmetry, but if supersymmetry is broken "softly," the divergences are at most logarithmic [98].

2.1.2 The Soft Lagrangian

If $\langle V \rangle \neq 0$, the vacuum state will not be supersymmetrically invariant, and supersymmetry will be spontaneously broken. Therefore if either a D or F term acquires a VEV, then supersymmetry will break.

Phenomenologically, supersymmetry must indeed be broken. As seen in Eq. 2.2, Q commutes with P, so all fields in the same supermultiplet have the same mass – which is obviously ruled out by current collider data. The exact mechanism of supersymmetry breaking can take myriad forms (see Section 2.3), but our ignorance can by parameterized by the following effective *soft*[3] Lagrangian. The following set of couplings have been shown to be the complete set of possible terms that are always soft[98–101]:

$$\mathcal{L}_{\text{soft}} = -\left(\overbrace{M^a \lambda_a \lambda_a}^{\text{gaugino masses}} + \underbrace{\frac{1}{2} b^{ij} \phi_i \phi_j}_{\text{bilinear operators}} + \overbrace{\frac{1}{6} a^{ijk} \phi_i \phi_j \phi_k}^{\text{trilinear operators}} \right) + \text{h.c.} - \overbrace{\tilde{m}_{ij}^2 \phi_i^* \phi_j}^{\text{scalar mass}^2} . \tag{2.8}$$

In coming sections, we will see how various models of supersymmetry breaking will generate these terms.

[3] Soft in that it breaks supersymmetry but does not lead to the usual scalar-induced quadratic divergences.

With these objects, (W, $\mathcal{L}_{\text{soft}}$, K, and f), we are now ready to build the supersymmetrized version of the Standard Model.

2.2 The Minimal Supersymmetric Standard Model

We now turn to the task of supersymmetrizing the Standard Model. We will keep the gauge structure the same, and so our first step is to determine the field content of this theory. To this end, we will embed every Standard Model field into a supermultiplet in a straightforward manner. We also extend the Higgs sector of the Standard Model. One reason for doing so is that the Yukawa sector descends from the superpotential, which is holomorphic. Therefore, any appearance of the usual $\overline{\mathbf{2}}$ field $\tilde{H} = i\sigma_2 H$ is inadmissible at the level of the superpotential. Furthermore, two Higgs fields are required for anomaly cancellation. We therefore introduce the field H_d, which is responsible for the down-quark and lepton Yukawa terms. The field field content and their represention are given in Table 2.1.

The superpotential of this theory is given by

$$W_{\text{MSSM}} = y_u Q\overline{u}H_u + y_d Q\overline{d}H_d + y_e L\overline{e}Hd + \mu H_u H_d. \tag{2.9}$$

For clarity, gauge and flavor indices are supressed and contracted in the usual way. Of course, this superpotential is not inclusive of all possible couplings without the imposition of further symmetries. We additionally impose a global conservation of *R-parity*. R-parity is a $\mathbb{Z}_2$ symmetry, were the R-parity of a field is defined as

$$P_R = (-1)^{3(B-L)+2s} \tag{2.10}$$

, where B is the baryon number, L is the lepton number and s the spin of the particle. Practically, R-parity assigns a value of $+1$ to all Standard Model particles, and -1 to all superpartners. R-parity has significant phenomenological consequences, as it forbids interactions with an odd number of superpartners with the result that:

- Rapid proton decay via superpartner exchange is forbidden and

The Minimal Supersymmetric Standard Model				
Superfield		Spin 1/2	Spin 0	Representation
(S)Quarks	Q_i	(u_{Li}, d_{Li})	$(\tilde{u}_{Li}, \tilde{d}_{Li}) \equiv \tilde{Q}_i$	$(\mathbf{3}, \mathbf{2})_{1/6}$
	$\overline{u}_i$	$\left(u_L^c\right)_i$	$\tilde{u}_{Ri}^*$	$(\overline{\mathbf{3}}, \mathbf{1})_{-2/3}$
	$\overline{d}_i$	$\left(d_L^c\right)_i$	$\tilde{d}_{Ri}^*$	$(\overline{\mathbf{3}}, \mathbf{1})_{1/3}$
(S)Leptons	L_i	(ν_{Li}, e_{Li})	$(\tilde{\nu}_{Li}, \tilde{e}_{Li}) \equiv \tilde{L}_i$	$(\mathbf{1}, \mathbf{2})_{-1/2}$
	$\overline{e}_i$	$\left(e_L^c\right)_i$	$\tilde{e}_{Ri}^*$	$(\mathbf{1}, \mathbf{1})_1$
Higgs(inos)	H_u	$(\tilde{H}_u^+, \tilde{H}_u^0) \equiv \tilde{H}_u$	$(H_u^+, H_u^0) \equiv H_u$	$(\mathbf{1}, \mathbf{2})_{1/2}$
	H_d	$(\tilde{H}_d^0, \tilde{H}_d^-) \equiv \tilde{H}_d$	$(H_d^0, H_d^-) \equiv H_d$	$(\mathbf{1}, \mathbf{2})_{-1/2}$
		Spin 1	Spin 1/2	
Gauge(inos)	$W^{\pm,0}$	$W^{\pm,0}$	$\tilde{W}^{\pm,0}$	$(\mathbf{1}, \mathbf{3})_0$
	B^0	B^0	$\tilde{B}^0$	$(\mathbf{1}, \mathbf{1})_0$
	g	g	$\tilde{g}$	$(\mathbf{8}, \mathbf{1})_0$

Table 2.1: The field content of the MSSM field and their representations. Note that it is convention to define the $SU(2)$-singlet fields in terms of the conjugate of a left-handed Weyl fermion. Within a supermultiplet, the un-tilded field corresponds to the usual SM field, and the tilded labels its superpartner. The naming convention for the tilded fields are to append an "s" to the beginning of the name for a scalar partner, and add "ino" to the end of a fermionic superpartner.

- The lightest supersymmetric partner (LSP) is stable.

This superpotential (and the imposition of R-parity) defines what we will call the Minimal Supersymmetric Standard Model (MSSM).

One feature of the MSSM worth commenting on is that the gauge couplings unify at a high scale to a much stronger degree than in the Standard Model alone, as can seen by comparing the two plots in Figure 2.3. Maintaining this behavior will be an important requirement for building models of supersymmetry breaking.

As we have seen, the Standard Model has – excluding neutrino masses – 19 parameters. The superpotential in Eq. 2.9 has only introduced one additional complex parameter, μ, so one might believe that the MSSM is indeed a minimal theory. Unfortunately, we know that supersymmetry must be broken, and as such we must include $\mathcal{L}_{\text{soft}}$ as part of the MSSM Lagrangian. With the field content specified in Table 2.1,

$$\begin{aligned}
\mathcal{L}_{\text{soft}} = &-\frac{1}{2}\left(M_3\tilde{g}\tilde{g} + M_2\tilde{W}\tilde{W} + M_1\tilde{B}\tilde{B} + \text{h.c.}\right) \\
&- \epsilon_{\alpha\beta}\left(\tilde{u}^*_{Ri}\, A_{uij}\, \tilde{Q}^\alpha_j H^\beta_u - \tilde{d}^*_{Ri}\, A_{dij}\, \tilde{Q}^\alpha_j H^\beta_d - \tilde{e}^*_{Ri}\, A_{eij}\, \tilde{L}^\alpha_j H^\beta_d + \text{h.c.}\right) \\
&- \left(\tilde{Q}^*_i\, m^2_{Qij}\, \tilde{Q}_j + \tilde{L}^*_i\, m^2_{Lij}\, \tilde{L}_j + \tilde{u}^*_{Ri}\, m^2_{\tilde{u}ij}\, \tilde{u}_{Rj} + \tilde{d}^*_{Ri}\, m^2_{\tilde{d}ij}\, \tilde{d}_{Rj} + \tilde{e}^*_{Ri}\, m^2_{\tilde{e}ij}\, \tilde{e}_{Rj}\right) \\
&- \left\{ m^2_{H_u}|H_u|^2 + m^2_{H_d}|H_d|^2 + \left(b\epsilon_{\alpha\beta}H^\alpha_u H^\beta_d + \text{h.c.}\right)\right\}. \qquad (2.11)
\end{aligned}$$

With this inclusion, the MSSM contains a massive 124 free parameters[102]. Of course, an overwhelming number of these parameters are already excluded by existing data on FCNCs and CP violation. In order to get a better understanding of the behavior and importance of the parameters contained within $\mathcal{L}_{\text{soft}}$, we now explore electroweak symmetry breaking in the context of the MSSM.

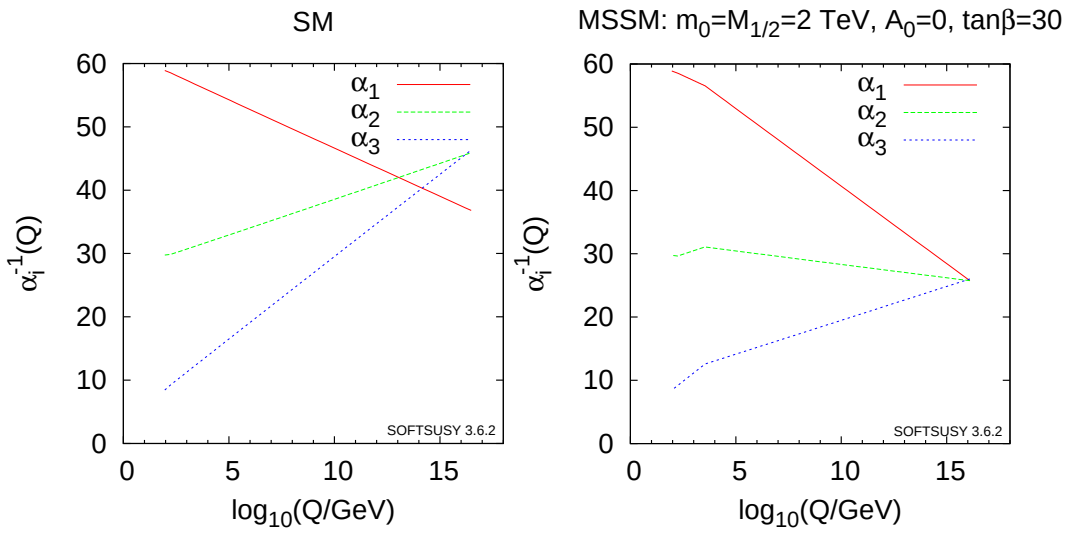

Figure 2.3: The two loop running of gauge couplings in the Standard Model (left) and MSSM (right) in the instance of $SU(5)$ unification. The supersymmetry threshold is taken to be 2 TeV. Note the lack of convergence of the running gauge couplings in the Standard Model, as compared with the much closer convergence of the running couplings in the MSSM. Image from [53].

2.2.1 Electroweak Symmetry Breaking

The Higgs sector potential has contributions from F and D_a fields, as in Eq. 2.6, as well as contributions coming from $\mathcal{L}_{soft}$. Explicitly, we have

$$\begin{aligned} V_{\text{Higgs}} = &\left(|\mu|^2 + m_{Hu}^2\right)\left(\left|H_u^+\right|^2 + \left|H_u^0\right|^2\right) + \left(|\mu|^2 + m_{Hud}^2\right)\left(\left|H_d^0\right|^2 + \left|H_d^-\right|^2\right) \\ &+ \left(\epsilon_{\alpha\beta} b H_u^\alpha H_d^\beta + \text{c.c}\right) + \frac{1}{8}\left(g^2 + g'^2\right)\left(\left|H_u^+\right|^2 + \left|H_u^0\right|^2 - \left|H_d^0\right|^2 - \left|H_d^-\right|^2\right)^2 \\ &+ \frac{1}{2}\left|H_u^+ H_d^{0*} + H_u^0 H_d^{-*}\right|^2 . \end{aligned} \tag{2.12}$$

In order to find the minimum of this potential, we use the allowed $SU(2)_L$ gauge freedom to rotate away H_u^+ and H_d^- at the minimum. Additionally, b may be made real and positive by a redefinition of the phases of $H_{u,d}$. Therefore, the potential around the minimum becomes

$$\begin{aligned} V_{\text{Higgs}} = &\left(|\mu|^2 + m_{Hu}^2\right)\left|H_u^0\right|^2 + \left(|\mu|^2 + m_{Hud}^2\right)\left|H_d^0\right|^2 \\ &- \left(b H_u^0 H_d^0 + \text{c.c}\right) + \frac{1}{8}\left(g^2 + g'^2\right)\left(\left|H_u^0\right|^2 - \left|H_d^0\right|^2\right)^2 . \end{aligned} \tag{2.13}$$

In order for this potential to caused electroweak symmetry breaking, it must be that: 1) the point $\left\langle H_u^0\right\rangle = \left\langle H_d^0\right\rangle = 0$ is not a stable minimum; and 2) that the potential is bounded from below – a possibility if $H_u^0 = H_d^0$. These two conditions put constraints on the parameter space, with

$$b^2 > \left(|\mu|^2 + m_{Hu}^2\right)\left(|\mu|^2 + m_{Hd}^2\right) \tag{2.14}$$

$$2b < |\mu|^2 + m_{Hu}^2 + m_{Hud}^2. \tag{2.15}$$

Now, denoting $\left\langle H_u^0\right\rangle = v_u$ and $\left\langle H_d^0\right\rangle = v_d$, electroweak symmetry breaking can continue *mutatis mutandis*, where

$$m_Z^2 = \frac{1}{2}\left(g^2 + g'^2\right)\left(v_u^2 + v_d^2\right) \tag{2.16}$$

$$m_W^2 = \frac{1}{2} g^2 \left(v_u^2 + v_d^2\right) . \tag{2.17}$$

With foresight, define $\left(v_u^2 + v_d^2\right) = v^2$ and $\tan\beta = v_u/v_d$. Thus, the potential in Eq. 2.13 subject to the constraints Eqs. 2.14 and 2.15, we find that the potential is minimized when

$$|\mu|^2 + m_{Hu}^2 = b\tan\beta + \frac{1}{2}m_Z^2\cos 2\beta \tag{2.18}$$

$$|\mu|^2 + m_{Hd}^2 = b\cot\beta - \frac{1}{2}m_Z^2\cos 2\beta. \tag{2.19}$$

It is worth pausing to consider the implications of relations Eqs. 2.14–2.18. Most obviously, they begin to demonstrate the promised winnowing down of parameters in the MSSM. We do, however, have the first hint of a rather important issue in model building within the MSSM. Note that the parameters m_{Hu}^2, m_{Hd}^2 and b come directly from $\mathcal{L}_{\text{soft}}$, which mean that they should be of the weak scale, and m_Z^2 is obviously of the weak scale. This indicates that, barring large cancellations, $|\mu|^2$ should also be weak scale. This should make us uncomfortable in that μ is a supersymmetry-*preserving* parameter in the superpotential, which should live at the high scale were supersymmetry is unbroken. This tension is referred to as the μ-problem[103]; we will see this show up quite often.

With the confirmation of the existence of a Higgs-like scalar particle at 125 GeV [44, 45], should make sure that this Higgs potential also produces a Standard Model-like light Higgs boson at $m_h = 125$ GeV. Before electroweak symmetry breaking, there are four complex scalar fields with eight total degrees of freedom in the Higgs sector, viz.: H_u^+, H_u^0, H_d^0, and H_d^-. Of course, three degrees of freedom are absorbed by the longitudinal modes of the Z and $W^\pm$ bosons, so there remain five degrees of freedom running around after electroweak symmetry breaking. The potential in Eq. 2.12 can be diagonalized after symmetry breaking to give five real scalar eigenstates: the neutral, CP even h_0 and H_0; the neutral, CP odd A^0; and the charged $H^\pm$. The lightest CP even field h_0 is our Standard Model Higgs.

This causes an immediate issue. It is well known that the tree-level upper bound for $m_{h^0}^2$ is far too low, and large loop corrections are needed to get to a phenomenologically

accepted value[99–101, 104]. As the parameters determining the dominant radiative correction will come up later, we write the one loop correction explicitly

$$m_{h^0}^2 \leq m_Z^2 + \frac{3g^2 m_t^4}{8\pi^2 m_W^2}\left\{\ln\left(\frac{M_s^2}{m_t^2}\right) + \frac{X_t^2}{M_s^2}\left(1 - \frac{X_t^2}{12M_s^2}\right)\right\}, \tag{2.20}$$

where m_t is the top quark mass, $M_s^2 = (m_{\tilde{t}_1}^2 + m_{\tilde{t}_1}^2)/2$ is the average mass-squared of the top squarks, and $X_t = A_t - \mu\cot\beta$ is the stop mixing parameter[4]. This correction can bring up the $m_{h^0}^2$ bound by either taking M_s^2 larger or $|X_t|/M_s$ near $\sqrt{6}$ [105–108]. The former is relatively unpalatable, as very high scale for stop masses does not make for a testable theory, whereas mechanisms for the latter sometimes (not always!) run the risk of introducing unacceptable FCNCs. We will take these issues into account as we build a model of supersymmetry breaking.

2.3 Supersymmetry Breaking

Supersymmetry is a restrictive theory, and as such one must be careful in breaking it. For instance, in non-anomalous, renormalizable theories with tree-level spontaneous supersymmetry breaking, the following identity must hold

$$\mathrm{STr}(m^2) \equiv \sum_J (-1)^{(2J)}(2J+1)m_J^2 = 0, \tag{2.21}$$

where the sum runs over the spins of fields in the same supermultiplet[109]. This is untenable, as this identity would require that superpartners for already observed Standard Model particles be much too light [110]. We therefore must move away from tree-level renormalizable supersymmetry breaking. The paradigmatic solution is to break supersymmetry in a sector that only couples to the observable sector via higher order mediation [111–114]. A cartoon of this scenario is given in Figure 2.4. There are myriad specific implementations of this procedure[5], but we shall focus on a family of models called *gauge mediation*.

[4] $A_t = A_{u33}$ where $(A_u)_{ij}$ is the trilinear operator from $\mathcal{L}_{\text{soft}}$ that couples H_u, $\tilde{Q}$ and $\tilde{u}_R^*$.
[5] See [115] for a broad overview of the different possibilities.

Figure 2.4: The general outline of mediated supersymmetry breaking. Note that *mediation* refers to mechanism whose couplings are parametrically suppressed.

2.3.1 Gauge Mediation

In gauge mediation (GMSB) [110, 116–125], the mediation mechanism is expanded to include an intermediate sector of *messengers*. These messengers interact directly with supersymmetry breaking sector via non-gauged couplings, but coupling to the observable sector with Standard Model gauge interactions. This is shown diagrammatically in Figure 2.5. The messengers communicate the supersymmetry breaking to the observable sector via loop-interactions, which when integrated generate $\mathcal{L}_{\text{soft}}$. To be much more explicit, we detail the minimal implementation of GMSB (mGMSB) and its consequences following the reviews of [125, 126].

Denote the field that breaks supersymmetry in the hidden sector by X. Through a dynamic mechanism about which we are agnostic, it acquires a VEV $\langle X \rangle = M + \theta^2 F$. Note that the appearance of VEV for its F-term break supersymmetry. This field couples to the messengers, N pairs of chiral fields Φ_i and $\overline{\Phi_i}$. It is often the case that these messenger pairs exist as vector-like representations of the full GUT group in which the Standard Model gauge group is embedded – most often $\mathbf{5}$ and $\overline{\mathbf{5}}$ of $SU(5)$. The superpotential governing this coupling, after choosing an appropriate diagonal basis, is

$$W_{X\Phi} = \sum_{i}^{N} \lambda_i X \Phi_i \overline{\Phi_i}. \tag{2.22}$$

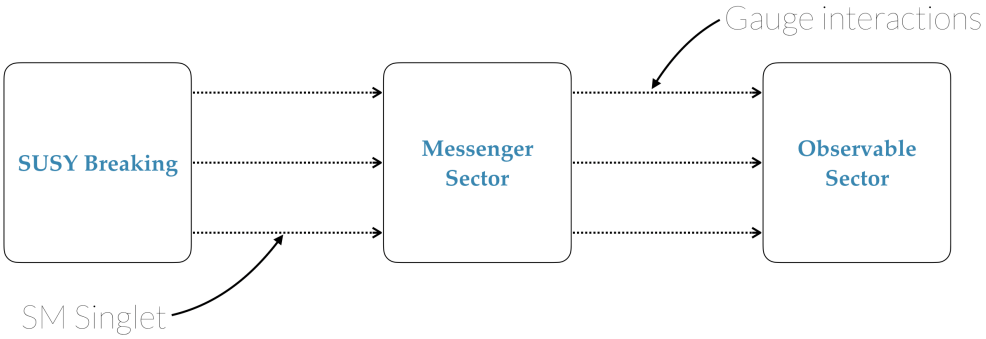

Figure 2.5: The general outline of gauge mediated supersymmetry breaking

Once X acquires a VEV, the messenger fields acquire a mass, which after being integrated out lead to the following effective $\mathcal{L}_{\text{soft}}$ terms at the scale M

$$M_a = \frac{g_a^2}{16\pi^2}\Lambda \sum_i^N 2T_a(\mathbf{r_i})g(x_i) \tag{2.23}$$

$$m_{\tilde{f}}^2 = 2\Lambda^2 \sum_a \left(\frac{g_a^2}{16\pi^2}\right)^2 C_a(\mathbf{r}) \sum_i^N 2T_a(\mathbf{r}_i)f(x_i) \tag{2.24}$$

$$A_{ijk} = 0 + \mathcal{O}\left(\frac{g_a^2}{16\pi^2}\right)^2, \tag{2.25}$$

where $\Lambda = |\lambda_i F/M|$, $x_i = \Lambda/(M)$, $T_a(\mathbf{r}_i)$ is the Dynkin index of the ith messenger pair, $C_a(\mathbf{r}_{\tilde{f}})$ is the quadratic Casimir invariant for the field $\tilde{f}$, and the a runs over the gauge groups. Note that $g(x_i)$ and $f(x_i)$ are loop functions that are approximately equal to unity for $x_i \ll 1$. Additionally, for our choice of the messenger pairs existing as $\mathbf{5}$, $\overline{\mathbf{5}}$ representations of $SU(5)$, $T_a(\mathbf{r}_i) = 1/2$. Example diagrams contributing to the terms in Eq. 2.23 and Eq. 2.24 is given in Figure 2.6. In a theory of gauge mediated supersymmetry breaking, there are a total of five parameters. They are: N, the number of messenger pairs; M_{mess}, the messenger masses; Λ, the messenger scale; $\tan\beta$; and the sign of μ.

There are several illuminating consequences of the structure of these terms. Firstly, it is clear that scalar and gaugino masses are of the same magnitude, as $m_{\tilde{f}}^2 \sim (g_a^2/16\pi^2)^2\Lambda^2$ and $M_a \sim g_a^2/16\pi^2\Lambda$. Secondly, mGMSB introduces minimal flavor violation, since the A_{ijk}

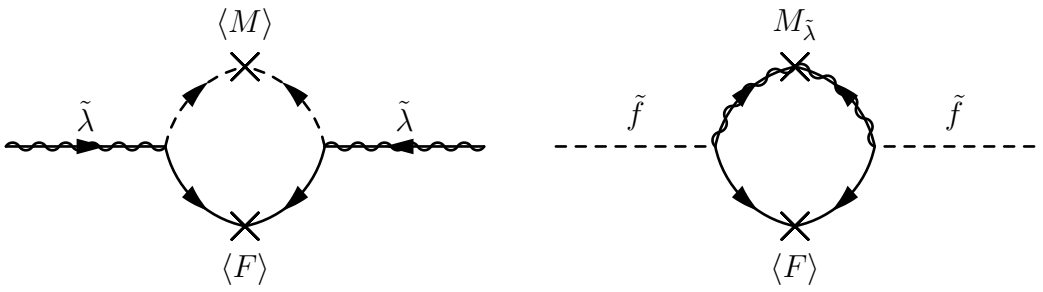

Figure 2.6: Left: a one-loop diagram contributing to $M_{\tilde{\lambda}}$. Right: a diagram contributing to $m^2_{\tilde{f}}$. The insertion of $M_{\tilde{\lambda}}$ (the diagram on the left) makes this diagram two-loop.

are essentially zero at input scale, and only materialize after RG flow. However, as previously discussed, vanishing trilinears are detrimental for a viable Higgs phenomenology, as seen in Eq. 2.20 and its discussion. Furthermore, the μ problem is still looming (and possibly worse than before); mGBSB does not generate μ as the messengers engage with the MSSM exclusively through gauge interactions, and therefore cannot generate the PQ-violating $\mu H_u H_d$ term[6]. Another problematic Higgs-sector quantity, b, does not arise until at least order $(g^2/16\pi^2)^3$, whereas consistency with the other terms in $\mathcal{L}_{\text{soft}}$ would require it to be at order $(g^2/16\pi^2)^2$. This brings us to a major difficulty in implementations of mGMSB: the μ/B_μ problem. To wit: Defining $b \equiv B_\mu \mu$, we should have that $B_\mu \sim \mu \sim g^2/16\pi^2\Lambda$. This is generically not the case, and this poses specific problems in models of gauge mediation[127–129].

2.4 Extended GMSB and Flavored Gauge Mediation

Allowing for direct matter-messenger avoids the disaster with the bounds on $m^2_{h^0}$ [7]. There are numerous ways to do so, but following the taxonomy of [130], we can categorize them. The authors divide such models into two types. Type I are models wherein the superpotential has MSSM-messenger-messenger couplings. Type II contain couplings of the form MSSM-MSSM-messenger. What we shall do is construct a type II theory, where

[6] If supersymmetry and the PQ symmetry are broken at the same scale, this is not a problem, see [103]
[7] The B_μ/μ problem unfortunately still remains.

the MSSM-MSSM-messenger terms are Yukawa-like. There are numerous explorations of such constructions, for instance [124, 125, 131–147].

More concretely, we may notice that the messengers – which operate as $\mathbf{5}$ and $\overline{\mathbf{5}}$ of $SU(5)$ – can be reduced to $\mathbf{3}\oplus\mathbf{2}$ and $\overline{\mathbf{3}}\oplus\mathbf{2}$ of $SU(3)_c\times SU(2)_L$. Furthermore, the $\mathbf{2}$ components of the messengers have the same quantum numbers as the MSSM Higgses, so it is possible to couple them to the MSSM in the same way. If one has a flavor symmetry used to construct the MSSM Yukawas and extends this symmetry to cover the messenger-MSSM couplings, such a paradigm is called *flavored gauge mediation* (FGM)[130, 132, 139–150].

This framework is promising in that it raises the possibility that the mechanism underlying the Standard Model Yukawas might also determine the structure by which the messengers communicate supersymmetry breaking to the MSSM. Conversely, one might try to go the other direction: use the mechanism of supersymmetry breaking to build the Standard Model Yukawas.

The one of the first implementations of FGM was done in [132], and expanded in [139, 142, 144]. In those works, the Froggatt-Nielsen [62] $U(1)$ symmetry that leads to the Standard Model Yukawa structures is also applied to the messenger-matter couplings. One might think that models in which the messengers directly couple to Standard Model fields would have disastrous flavor consequences, but FGM theories in fact lead to heavily suppressed FCNC and CP-violating effects that are phenomenologically acceptable [146].

	Q_1	Q_2	Q_3	u_1	u_2	u_3	d_1	d_2	d_3
$U(1)$	5	4	2	1	-1	-2	1	0	0

Table 2.2: The $U(1)$ charge assignments in the model given in [147]

It is illustrative to consider a benchmark analysis. Consider the model given in Eq. 2.1 of [147]. In this scenario, they impose a $U(1)$ flavor symmetry as described by their Eq. 3.1. The charges of the fields under this symmetry are given in Table 2.2. The Higgses and messengers are neutral under this symmetry. Note that at the level of the superpotential,

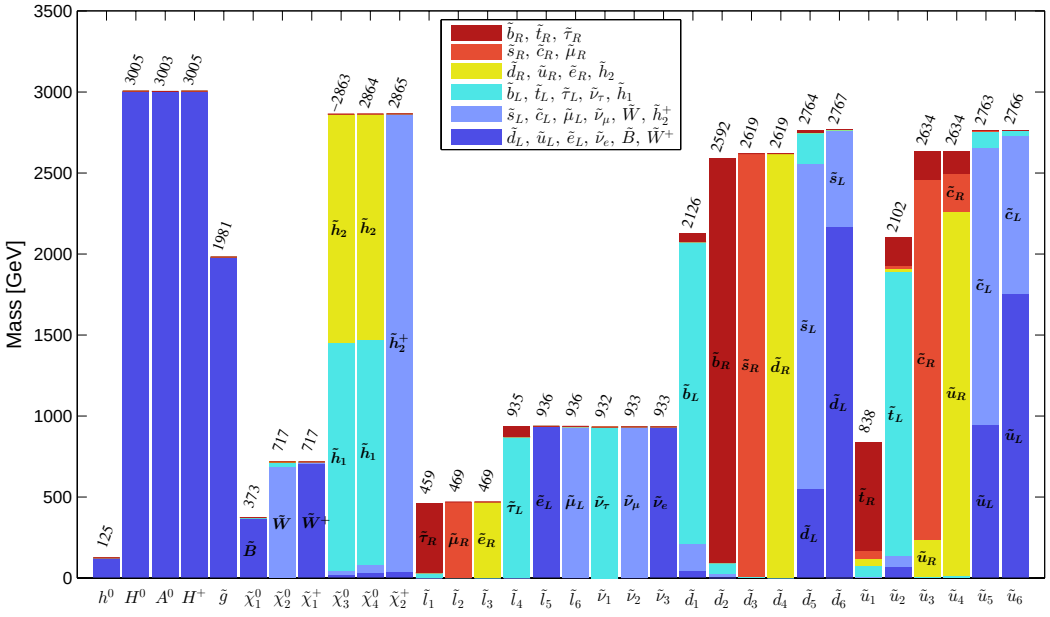

Figure 2.7: A benchmark spectrum of a MFV Abelian FGM model. $(y_u)_{33}(10^{15}\text{GeV}) = 2.9$ at input, and the scales are $M = 9 \times 10^5$ GeV and $F/M = 2.7 \times 10^5$ GeV. In this scenario, it is found that $-(A_u)_{33} = 1920$ GeV, and as a consequence the colored superpartners are very light. Taken from Figure 3 in [147].

this model contains a global symmetry to only allow for H_u to mix with one messenger, and to forbid all other Higgs-messenger couplings. This is a minimally flavor-violating (MFV) model, as the Yukawa matrices for the Higgs and messenger are aligned.

It is notable that this scenario allows for the generation of non-trivial A terms, while keeping the squark masses relatively light. This is demonstrated in the spectrum in Figure 2.7. It is found that a large negative value of $(A_u)_{33} = -1920$ GeV is achieved, which allows for a correct Higgs mass while keeping the colored superpartners light. This is to be contrasted with mGMSB, where the stops must be very heavy to overcome vanishing A terms. The flavor violation of this model is minimal, as even with $\mathcal{O}(1)$ phases in the $(12)_{LL/RR}$ entries of the up squark mixing matrix lead to flavor-violating effects within experimental bounds (c.f Table 1 and Table 5 in [147]).

Nevertheless, the $U(1)$ implementation of FGM has a few shortcomings, namely the existence of an unknown flavon sector driving the $U(1)$ symmetry breaking, where the assignment of $U(1)$ charges to the fields are put in by hand. Moreover, the arbitrariness of such assignments indicates the while the mechanism of supersymmetry breaking requires relatively few parameters, the top down source of flavor is unknown. Of course, the usual folklore is that " never the twain shall supersymmetry and flavor-symmetry breaking meet;" $U(1)$ FGM adheres to this, but we will see that there are folklore-contravening – and viable – FGM models. Specifically, we will investigate scenarios in which the messengers and Higgs mix under a non-Abelian family symmetry.

2.4.1 Non-Abelian Flavored Gauge Mediation Using $\mathcal{S}_3$

The first implementation of this scenario was detailed by Pérez, Ramond and Zhang (PRZ) in [140]. In their two-generation toy model, the messenger and Higgs fields mix under a family symmetry given by the symmetric group on three elements, $\mathcal{S}_3$[8]. We now repeat the details of this model, as it is central in understanding the remainder of Part 2 of this dissertation.

[8]See Appendix A for an overview of the properties and representations of $\mathcal{S}_3$

Pérez, Ramond and Zhang

Consider a scenario of gauge mediation with $N = 1$ messenger pairs, a canonical Kähler potential and a mimimal gauge kinetic function. Denote the $SU(2)$-doublet components of those messengers as $M_{u,d}$[9]. These messengers mix with the MSSM Higgs superfields as a **2** of $\mathcal{S}_3$, *viz.*

$$\mathcal{H}_u = \begin{pmatrix} \mathcal{H}_{u1} \\ \mathcal{H}_{u2} \end{pmatrix} = \mathcal{R}_u \begin{pmatrix} H_u \\ M_u \end{pmatrix}, \qquad \mathcal{H}_d = \begin{pmatrix} \mathcal{H}_{d1} \\ \mathcal{H}_{d2} \end{pmatrix} = \mathcal{R}_d \begin{pmatrix} H_d \\ M_d \end{pmatrix}, \tag{2.26}$$

where $\mathcal{R}_{u,d}$ rotate the mixed Higgs-messenger fields into their mass basis after supersymmetry breaking. In this two-family model, all matter exists in doublet representations of $\mathcal{S}_3$ and couples to the messenger-Higgs fields in an $\mathcal{S}_3$ invariant fashion. These Higgs-messenger fields couple to a supersymmetry breaking field X_H, which is also an $\mathcal{S}_3$ doublet. Their coupling is given by (c.f Eq. 2.22)

$$W_H = (\lambda X_H \mathcal{H}_u \mathcal{H}_d) + m \mathcal{H}_u \mathcal{H}_d, \tag{2.27}$$

where parenthesis indicate contraction under $\mathcal{S}_3$. X_H acquires a VEV, parameterized as

$$\langle X_H \rangle = M \begin{pmatrix} \sin\phi \\ \cos\phi \end{pmatrix} + \theta^2 F \begin{pmatrix} \sin\xi \\ \cos\xi \end{pmatrix}, \tag{2.28}$$

and in doing so breaks supersymmetry. Thereafter, the superpotential in Eq. 2.27 becomes

$$\begin{aligned} W_H &= \mathcal{H}_u^T \begin{pmatrix} M\sin\phi & m \\ m & M\cos\phi \end{pmatrix} \mathcal{H}_d + \theta^2 \mathcal{H}_u^T \begin{pmatrix} F\sin\xi & 0 \\ 0 & F\cos\xi \end{pmatrix} \mathcal{H}_d \\ &\equiv \mathcal{H}_u^T (\mathbb{M} + \theta^2 \mathbb{F}) \mathcal{H}_u. \end{aligned} \tag{2.29}$$

As shown in [140], $\mathbb{M}$ and $\mathbb{F}$ must commute, otherwise $\mathcal{L}_{\text{soft}}$ is pathological; its terms would be dominated by one-loop corrections and sfermion mass-squareds may be negative, initiating tree-level EWSB breaking, which results in mass spectra incompatible with

[9] The $SU(3)$-triplet components are $T_{u,d}$, which are $\mathcal{S}_3$ singlets that communicate supersymmetry breaking caused by X_T, which itself has no other couplings.

the Standard Model. Additionally, the effective theory obtained after integretating out the heavy messengers would not be soft and UV-divergences would remain.

With the assertion that $[\mathbb{M}, \mathbb{F}] = 0$, this model's phenomenology is promising, predicting a see-sawed μ, a hierarchical Yukawa matrix for the Standard Model Higgs interactions, and an inverted, hierarchical Yukawa matrix for the messenger interactions. Nevertheless, this model generically has a significant μ/B_μ problem, as B_μ is much too large; it is the case that the μ/B_μ problem is even more severe than it would be in minimal gauge mediation. Furthermore, it is known that the coupling $\lambda X_H H_u H_d$ – which is required by the $\mathcal{S}_3$ symmetry of the theory – automatically leads to μ/B_μ problem [125]. For this reason, as well for the lack of a third family in the model, that the PRZ paradigm must be expanded.

One such possibility that allows for an alleviation of this significant μ/B_μ problem is to expand the messenger-Higgs sector by including an additional $\mathcal{S}_3$ singlet messenger-Higgs field. This expansion, first done in [149], and continued in the author's papers [151, 152], still contains the compulsory and problematic $\lambda X_H H_u H_d$ term, but allows for enough parametric freedom in the messenger-Higgs sector to mitigate its effects. Furthermore it allows for the natural introduction of a third family of MSSM fields. It must be remarked upon, however, that the introduction of this third messenger-Higgs field increases the number of messenger pairs to $N = 2$, which necessitates a heavier low-energy spectrum than seen in $U(1)$ flavored gauge mediation.

PRZ Extended to Three Families

In [149, 151, 152], the Higgs-messenger sector is expanded by introducing an $\mathcal{S}_3$ singlet Higgs-messenger field to both the down-type and up-type sectors. These singlet fields are denoted by $\mathcal{H}^{(1)}_{u,d}$, and the doublet fields defined in Eq. 2.26 are re-notated as $\mathcal{H}^{(2)}_{u,d}$. Combining all up(down)-type fields in one reducible representation, the Higgs-messenger fields

are $\mathcal{H}_{u,d} = (\mathcal{H}^{(2)}_{u,d}, \mathcal{H}^{(1)}_{u,d}) = (\mathcal{H}_{u,d1}, \mathcal{H}_{u,d2}, \mathcal{H}_{u,d3})$. In terms of the physical Higgs and messenger eigenstates, we have

$$\mathcal{H}_u = \begin{pmatrix} \mathcal{H}_{u1} \\ \mathcal{H}_{u2} \\ \mathcal{H}_{u3} \end{pmatrix} = \mathcal{R}_u \begin{pmatrix} H_u \\ M_{u1} \\ M_{u2} \end{pmatrix}, \qquad \mathcal{H}_d = \begin{pmatrix} \mathcal{H}_{d1} \\ \mathcal{H}_{d2} \\ \mathcal{H}_{d3} \end{pmatrix} = \mathcal{R}_d \begin{pmatrix} H_d \\ M_{d1} \\ M_{d2} \end{pmatrix}. \tag{2.30}$$

In [149], it was shown that this extended Higgs-messenger sector provides sufficient freedom to achieve the required hierarchy between B_μ and μ by tuning the ϕ and ξ parameters in $\langle X_H \rangle$ (c.f. Eq. 2.28). With this extended, the next question that arose is how the MSSM fields may be charged under $\mathcal{S}_3$. One requirement in model-building is that the top Yukawa operator must be renormalizable. If the top quark is neutral under $\mathcal{S}_3$, it must therefore couple to the singlet field $\mathcal{H}^{(1)}_u$. The authors refer to this scenario as case A.

If, instead, the top quark and other generation three fermions are doublets under $\mathcal{S}_3$, the authors arrive at what they call case B. The rest of the MSSM fields are also charged under $\mathcal{S}_3$, detailed in Table 2.3.

	$\mathcal{H}^{(2)}_u$	$\mathcal{H}^{(1)}_u$	$\mathcal{H}^{(2)}_d$	$\mathcal{H}^{(1)}_d$	$Q_{\mathbf{2}}$	$Q_{\mathbf{1}}$	$\bar{u}_{\mathbf{2}}$	$\bar{u}_{\mathbf{1}}$	$\bar{d}_{\mathbf{2}}$	$\bar{d}_{\mathbf{1}}$	$L_{\mathbf{2}}$	$L_{\mathbf{1}}$	$\bar{e}_{\mathbf{2}}$	$\bar{e}_{\mathbf{1}}$	X_H
$\mathcal{S}_3$	**2**	**1**	**2**	**1**	**2**	**1**	**2**	**1**	**2**	**1**	**2**	**1**	**2**	**1**	**2**

Table 2.3: Charges for an $\mathcal{S}_3$ model of the Higgs-messenger fields and the MSSM matter fields as given in scenario B of [149].

In this case, a general superpotential can be constructed, namely

$$W^{(u)} = y_u \left[Q_{\mathbf{2}} \bar{u}_{\mathbf{2}} \mathcal{H}^{(2)}_u + \beta_1 Q_{\mathbf{2}} \bar{u}_{\mathbf{2}} \mathcal{H}^{(1)}_u + \beta_2 Q_{\mathbf{2}} \bar{u}_{\mathbf{1}} \mathcal{H}^{(2)}_u + \beta_3 Q_{\mathbf{1}} \bar{u}_{\mathbf{2}} \mathcal{H}^{(2)}_u + \beta_4 Q_{\mathbf{1}} \bar{u}_{\mathbf{1}} \mathcal{H}^{(1)}_u \right]. \tag{2.31}$$

The values for β_i are not known, and as such are free parameters. Nevertheless, they must be constrained in such a way that the top acquires a large mass as compared to the other generations.

The authors of [149] analyzed a point of enhanced symmetry in the β_i parameter space, namely the democratic limit of every $\beta_i = 1$. With this choice, a nontrivial hierarchy in the

Standard Model Yukawas was attained, at the expense of the inversion of the corresponding messenger Yukawa couplings. The consequence of this is that the trilinear A terms vanish, requiring very large masses for the $SU(3)$-charged superpartners, a consequence noted at the end of Subsection 2.2.1.

There are, of course, many sets of β_i such that a Yukawa hierarchy is achieved. For instance, the point $\beta_1 = -1, \beta_4 = 0$ and $\beta_2 = \beta_3$ achieves a hierarchy. This can be thought of as a doublet-dominated regime, as the operator comprised entirely of $\mathcal{S}_3$ singlets vanishes.

What we will do in this thesis is to consider the opposite, wherein the superpotential is singlet-dominated. Specifically, we will take $\beta_1 = 1$, $\beta_3 = \beta_2$, $\beta_4 = \beta_2\beta_3$, and $\beta_{2,3} \gg 1$. This point of enhanced symmetry may be possible if we consider the $\mathcal{S}_3$ symmetry group as being descended from a larger, broken symmetry. It would therefore be natural to consider the operators independent of this symmetry breaking to dominate.

In the next two Chapters, we will develop this scenario, and find that it achieves sizable stop mixing, and as such we find that the $SU(3)$-charged superpartners are much lighter; this is detailed in Chapter 3). This scenario is then further refined in such a way that a reasonable value for the Cabibbo angle of the quark sector is achieved, as discussed in Chapter 4.

Chapter 3

Obtaining Sizable Stop Mixing in Non-Abelian Flavored Gauge Mediation[1]

3.1 Introduction

The 2012 discovery of the 125 GeV Higgs particle [44, 45] and subsequent detailed measurements of its properties at the Large Hadron Collider (LHC) has provided significant limits on the allowed possibilities for extensions of the Standard Model (SM). In the context of theories with softly broken supersymmetry at the TeV scale (for reviews, see e.g. [115, 153]), the Higgs mass is known to be within the theoretically allowed range for perturbative theories, but its relatively high value either requires large radiative corrections in the minimal supersymmetric standard model (MSSM), or an enlarged Higgs sector to boost the tree-level contributions. As such, it has long been known in the MSSM that large stop mixing or very heavy stops are needed (see e.g. [104]). This can place stringent constraints on specific models of the soft supersymmetry breaking terms, and also has important implications for the potential observability of superpartners at the LHC.

The model-building constraints imposed by the Higgs measurements are particularly striking in the context of gauge mediation. In its minimal implementation, gauge-mediated supersymmetry breaking [110, 116–125] predicts highly suppressed scalar trilinear couplings (A terms) at the messenger scale, leading to small stop mixing. As a result, consistency with the Higgs data [107, 108, 154] generally requires very heavy $SU(3)$-charged

[1] Chapter adapted from [151].

superpartner masses and/or high values of the messenger scale. This conclusion can be circumvented if the messenger fields can couple directly to the MSSM fields, as explored in [124, 125, 130–147] Of particular interest are the "flavored gauge mediation" models [130, 132, 139–150], for which there is nontrivial mixing of the $SU(2)$ messenger doublets and the MSSM Higgs fields. These models allow for the generation of one-loop A terms at the messenger scale, alleviating the Higgs mass problem of minimal gauge mediation in the MSSM.

In building models of flavored gauge mediation, an underlying Higgs-messenger symmetry is typically employed to control the mixing of these fields. A logical and now-standard choice is to use a $U(1)$ symmetry as the Higgs-messenger symmetry, and many interesting examples of this type have been proposed in the literature (see e.g. [147] for a recent analysis and set of LHC benchmark points). In this case, the $U(1)$ charges are chosen judiciously to control the couplings of the Higgs and messenger fields so as to obtain nontrivial third generation A terms and to avoid generating dangerous interactions between the MSSM Higgs fields and the supersymmetry breaking sector.

An alternative is to choose a discrete non-Abelian symmetry as the Higgs-messenger symmetry, as proposed in [140]. This idea was studied using the specific choice of $\mathcal{S}_3$, the permutation group on three objects, for the case of two families in [140], and extended to three families in [149]. In these analyses, it was shown that if the SM quarks and leptons transform nontrivially with respect to the $\mathcal{S}_3$ symmetry (as required for at least a subset of the SM matter particles), obtaining nontrivial SM Yukawa coupling entries in the diagonal fermion mass basis led to vanishing entries in the corresponding messenger Yukawa couplings, as a direct consequence of the non-Abelian symmetry. As a result, generating the needed large top quark Yukawa couplings thus led to vanishing top quark messenger Yukawa couplings, unless the relevant fields are all taken to be $\mathcal{S}_3$ singlets. The phenomenological implications of this correlation are that the resulting stop mixing is generically very small, such the superpartner masses must be quite heavy to be consistent with the Higgs data.

In this work, we analyze a three-family flavored gauge mediation model based on the $\mathcal{S}_3$ Higgs-messenger symmetry in which sizable third generation Yukawa couplings to both the Higgs and the messengers can be simultaneously generated. We show that a fermion mass hierarchy and flavor-diagonal messenger Yukawa coupling structure can emerge in a specific limit of the renormalizable superpotential interactions of these fields that can result from additional symmetries placed on the system. The resulting model of the soft supersymmetry breaking parameters is a minimal scenario with two pairs of vectorlike messenger fields. As this yields larger stop mixing than was possible in previously studied examples of this type with renormalizable couplings of the MSSM fields and the Higgs-messenger fields only [140, 149], the superpartner masses can be significantly lighter, with the heaviest superpartners at or below 5-6 TeV.

The structure of the chapter is as follows. In the next section, we present a brief overview of the general model framework as well as the detailed model inputs of this specific scenario based on the choice of $\mathcal{S}_3$ as the Higgs-messenger symmetry. We then present the resulting soft supersymmetry parameters and carry out a numerical analysis of the superpartner spectra. Finally, we summarize and discuss prospects for future model-building directions along these lines.

3.2 Model

In this section, we provide a self-contained review of the model framework and present the details of the specific scenario that is the focus of this chapter.

As a prelude, we note several salient features of the group theory of $\mathcal{S}_3$, as can be found in many references (see e.g. [140] or Appendix A). The irreducible representations of $\mathcal{S}_3$ are the singlet $\mathbf{1}$, a one-dimensional representation $\mathbf{1}'$, and a doublet, $\mathbf{2}$, with tensor products

$$\mathbf{1} \otimes \mathbf{2} = \mathbf{2}, \qquad \mathbf{1}' \otimes \mathbf{2} = \mathbf{2}, \qquad \mathbf{2} \otimes \mathbf{2} = \mathbf{1} \oplus \mathbf{1}' \oplus \mathbf{2}. \tag{3.1}$$

As in [140] and [149], all fields will be taken to be either singlet or doublet representations. We use the basis in which the singlets obtained from the tensor products of two or three doublets are

$$(\mathbf{2}\otimes\mathbf{2})_{\mathbf{1}} = \left[\begin{pmatrix} a_1 \\ a_2 \end{pmatrix}\otimes\begin{pmatrix} b_1 \\ b_2 \end{pmatrix}\right]_{\mathbf{1}} = a_1 b_2 + a_2 b_1. \tag{3.2}$$

$$(\mathbf{2}\otimes\mathbf{2}\otimes\mathbf{2})_{\mathbf{1}} = \left[\begin{pmatrix} a_1 \\ a_2 \end{pmatrix}\otimes\begin{pmatrix} b_1 \\ b_2 \end{pmatrix}\otimes\begin{pmatrix} c_1 \\ c_2 \end{pmatrix}\right]_{\mathbf{1}} = a_1 b_1 c_1 + a_2 b_2 c_2. \tag{3.3}$$

In this model framework, the minimal viable Higgs-messenger sector consists of one $\mathcal{S}_3$ doublet $\mathcal{H}^{(2)}_{u,d}$ and one $\mathcal{S}_3$ singlet $\mathcal{H}^{(1)}_{u,d}$ for the up-type and down-type Higgs-messenger fields. This is to stave off an otherwise severe μ/B_μ problem (see [127–129] for a discussion of this issue within gauge mediation models), as discussed shortly. Taking $\mathcal{H}_u = (\mathcal{H}^{(2)}_u, \mathcal{H}^{(1)}_u) = (\mathcal{H}_{u1}, \mathcal{H}_{u2}, \mathcal{H}_{u3})$ (and analogously for $u \to d$), we have

$$\mathcal{H}_u = \begin{pmatrix} \mathcal{H}_{u1} \\ \mathcal{H}_{u2} \\ \mathcal{H}_{u3} \end{pmatrix} = \mathcal{R}_u \begin{pmatrix} H_u \\ M_{u1} \\ M_{u2} \end{pmatrix}, \qquad \mathcal{H}_d = \begin{pmatrix} \mathcal{H}_{d1} \\ \mathcal{H}_{d2} \\ \mathcal{H}_{d3} \end{pmatrix} = \mathcal{R}_d \begin{pmatrix} H_d \\ M_{d1} \\ M_{d2} \end{pmatrix}, \tag{3.4}$$

in which the electroweak Higgs fields are denoted as usual by $H_{u,d}$, the $SU(2)$ doublet messengers are $M_{ui,di}$ $(i = 1, 2)$, and $\mathcal{R}_{u/d}$ are unitary matrices that result from the diagonalization of the Higgs-messenger mass matrices (more on this shortly). We also have $SU(3)$ triplet messengers $T_{ui,di}$ $(i = 1, 2)$ that are $\mathcal{S}_3$ singlets. The $T_{ui,di}$ and the messenger doublets $M_{ui,di}$ together form two pairs of $\mathbf{5}$, $\overline{\mathbf{5}}$ representations of $SU(5)$ (i.e., the number of messenger pairs $N_5 = 2$).

The model also includes two supersymmetry breaking fields: the $\mathcal{S}_3$ doublet X_H and a $\mathcal{S}_3$ singlet chiral superfield X_T, where X_H couples only to the Higgs-messenger doublets and X_T couples only to the triplet messengers. We assume that X_T couples only to the triplet messengers and X_H couples only to the messenger doublets or the MSSM fields, as

needed to avoid the possibility of rapid proton decay (this requires additional symmetries, which is not difficult to implement in a concrete scenario) [2]. This field content and the relevant $\mathcal{S}_3$ charges are given in Table 3.1.

	$\mathcal{H}_u^{(2)}$	$\mathcal{H}_u^{(1)}$	$\mathcal{H}_d^{(2)}$	$\mathcal{H}_d^{(1)}$	T_{ui}	T_{di}	X_H	X_T
$\mathcal{S}_3$	**2**	**1**	**2**	**1**	**1**	**1**	**2**	**1**

Table 3.1: The $\mathcal{S}_3$ charges for the extended Higgs-messenger model described in this section.

The superpotential couplings of X_H to the Higgs-messenger sector are given by

$$W_H = \lambda X_H \mathcal{H}_u^{(2)}\mathcal{H}_d^{(2)} + \lambda' X_H \mathcal{H}_u^{(1)}\mathcal{H}_d^{(2)} + \lambda'' X_H \mathcal{H}_u^{(2)}\mathcal{H}_d^{(1)} + \kappa M \mathcal{H}_u^{(2)}\mathcal{H}_d^{(2)} + \kappa' M \mathcal{H}_u^{(1)}\mathcal{H}_d^{(1)}. \quad (3.5)$$

Here we will assume all couplings are real, and take $\lambda' = \lambda'' = \lambda$ for simplicity. The supersymmetry-breaking field X_H is then parametrized as follows:

$$\langle X_H \rangle = M \begin{pmatrix} \sin\phi \\ \cos\phi \end{pmatrix} + \theta^2 F \begin{pmatrix} \sin\xi \\ \cos\xi \end{pmatrix}, \quad (3.6)$$

where ϕ and ξ characterize the vev directions of the scalar and F components, respectively, and we take $F \ll M^2$. After symmetry breaking, the effective superpotential takes the following form:

$$\begin{aligned} W_H &= M\mathcal{H}_u^T \begin{pmatrix} \sin\phi & \kappa & \cos\phi \\ \kappa & \cos\phi & \sin\phi \\ \cos\phi & \sin\phi & \kappa' \end{pmatrix} \mathcal{H}_d + \theta^2 F \mathcal{H}_u^T \begin{pmatrix} \sin\xi & 0 & \cos\xi \\ 0 & \cos\xi & \sin\xi \\ \cos\xi & \sin\xi & 0 \end{pmatrix} \mathcal{H}_d \\ &\equiv \mathcal{H}_u^T \mathbb{M} \mathcal{H}_d + \theta^2 \mathcal{H}_u^T \mathbb{F} \mathcal{H}_d. \end{aligned} \quad (3.7)$$

As outlined in [140], we require $[\mathbb{M}, \mathbb{F}] = 0$, such that $\mathbb{M}$ and $\mathbb{F}$ are diagonalized by the same unitary transformation. It is also necessary to have hierarchy of eigenvalues for both $\mathbb{M}$

[2] We also note for that the different treatment of the doublet and triplet sectors undoubtedly poses challenges for any serious attempt to embed this scenario within grand unification; a thorough treatment of this question is beyond the scope of the present work.

and $\mathbb{F}$, to distinguish the MSSM Higgs fields from the messenger fields. Simultaneously incorporating both constraints is the underlying reason why we need to include the $\mathcal{S}_3$ singlet $\mathcal{H}^{(1)}_{u,d}$ in the Higgs-messenger sector within this framework, as these two conditions are incompatible if only $\mathcal{H}^{(2)}_{u,d}$ is included.

As shown in [149] for the case of Eq. (3.7), upon imposing $[\mathbb{M}, \mathbb{F}] = 0$, which requires $\kappa' = \kappa = \sin(\phi - \xi)/(\cos\xi - \sin\xi)$ (for $\xi \neq \pi/4$), a viable solution with a distinct hierarchy of eigenvalues for both $\mathbb{M}$ and $\mathbb{F}$ can be obtained. This distinct hierarchy is needed for the possibility of separate fine-tunings of the μ and $b = B_\mu \mu$ parameters, otherwise the scenario suffers from a severe μ/B_μ problem. The solution occurs for $\xi \to -\pi/4$ and $\phi \neq \xi$, with a small detuning between ϕ and ξ that controls the size of the μ term. In this limit, the $\mathcal{R}_{u,d}$ are given to leading order by

$$\mathcal{R}_{u,d} = \begin{pmatrix} \frac{1}{\sqrt{3}} & \mp\frac{1}{2}\left(1 + \frac{1}{\sqrt{3}}\right) & \frac{1}{2}\left(1 - \frac{1}{\sqrt{3}}\right) \\ \frac{1}{\sqrt{3}} & \pm\frac{1}{2}\left(1 - \frac{1}{\sqrt{3}}\right) & -\frac{1}{2}\left(1 + \frac{1}{\sqrt{3}}\right) \\ \frac{1}{\sqrt{3}} & \pm\frac{1}{\sqrt{3}} & \frac{1}{\sqrt{3}} \end{pmatrix}. \tag{3.8}$$

Note that the trimaximal column is associated with the light eigenstate, which is precisely the state that corresponds to the electroweak doublets $H_{u,d}$. More precisely, the eigenvalues corresponding to this light eigenstate are $\mu \ll M$ for the case of $\mathbb{M}$, and $b \ll F$ for the case of $\mathbb{F}$. The heavy states in this limit have equal masses M_{mess}, that are of order M. The larger eigenvalues of $\mathbb{F}$ are $F_{2,3} \sim F$ (the detailed relations can be found in [149]).

The next step is to consider the couplings of the Higgs-messenger fields to the MSSM matter fields. Of the variety of possibilities (see [149] for a classification), let us focus here on renormalizable interactions of all three generations. This results from the specific $\mathcal{S}_3$ charge assignments summarized in Table 3.2. The renormalizable superpotential Yukawa couplings, for example in the up quark sector, are given as follows:

$$W^{(u)} = y_u \left[Q_{\mathbf{2}} \bar{u}_{\mathbf{2}} \mathcal{H}^{(2)}_u + \beta_1 Q_{\mathbf{2}} \bar{u}_{\mathbf{2}} \mathcal{H}^{(1)}_u + \beta_2 Q_{\mathbf{2}} \bar{u}_{\mathbf{1}} \mathcal{H}^{(2)}_u + \beta_3 Q_{\mathbf{1}} \bar{u}_{\mathbf{2}} \mathcal{H}^{(2)}_u + \beta_4 Q_{\mathbf{1}} \bar{u}_{\mathbf{1}} \mathcal{H}^{(1)}_u \right], \tag{3.9}$$

in which the β_i are arbitrary coefficients in the absence of further model structure, and the overall scaling y_u is also a free parameter. In the basis given by $Q = (Q_{\mathbf{2}}, Q_{\mathbf{1}})^T$ and

	$\mathcal{H}_u^{(2)}$	$\mathcal{H}_u^{(1)}$	$\mathcal{H}_d^{(2)}$	$\mathcal{H}_d^{(1)}$	$Q_{\mathbf{2}}$	$Q_{\mathbf{1}}$	$\bar{u}_{\mathbf{2}}$	$\bar{u}_{\mathbf{1}}$	$\bar{d}_{\mathbf{2}}$	$\bar{d}_{\mathbf{1}}$	$L_{\mathbf{2}}$	$L_{\mathbf{1}}$	$\bar{e}_{\mathbf{2}}$	$\bar{e}_{\mathbf{1}}$	X_H
$\mathcal{S}_3$	**2**	**1**	**2**	**1**	**2**	**1**	**2**	**1**	**2**	**1**	**2**	**1**	**2**	**1**	**2**

Table 3.2: Charges for an $\mathcal{S}_3$ model of the Higgs-messenger fields and the MSSM matter fields. Here the $SU(3)$ triplet messengers and the associated X_T field are not displayed for simplicity.

$\overline{u} = (\overline{u}_{\mathbf{2}}, \overline{u}_{\mathbf{1}})^T$, these couplings can be expressed in matrix form as

$$W^{(u)} = y_u Q^T \begin{pmatrix} \mathcal{H}_{u1}^{(2)} & \beta_1 \mathcal{H}_u^{(1)} & \beta_2 \mathcal{H}_{u2}^{(2)} \\ \beta_1 \mathcal{H}_u^{(1)} & \mathcal{H}_{u2}^{(2)} & \beta_2 \mathcal{H}_{u1}^{(2)} \\ \beta_3 \mathcal{H}_{u2}^{(2)} & \beta_3 \mathcal{H}_{u1}^{(2)} & \beta_4 \mathcal{H}_u^{(1)} \end{pmatrix} \bar{u}. \tag{3.10}$$

Analogous coupling matrices would hold in the down quark and charged lepton sectors, with the replacements $\beta_i \to \beta_{di}, \beta_{ei}$ [3]. Here we will focus on the up quark sector only, and later assume that the other charged fermions follow similar patterns. (Let us also comment that Eq. (3.9) and its generalizations to other charged SM fermions correct a typo in the corresponding expressions for the superpotential in [149], for which there was an incorrect interchange of β_1 and β_2.)

From Eq. (3.10) and the definition of the Higgs-messenger diagonalization matrices $\mathcal{R}_{u,d}$ as given in Eq. (3.4) and Eq. (3.8), it is straightforward to see that the SM Yukawa matrix takes the form

$$Y_u = \frac{y_u}{\sqrt{3}} \begin{pmatrix} 1 & \beta_1 & \beta_2 \\ \beta_1 & 1 & \beta_2 \\ \beta_3 & \beta_3 & \beta_4 \end{pmatrix}, \tag{3.11}$$

while the messenger Yukawas are given by

$$Y'_{u1} = y_u \begin{pmatrix} -\frac{1}{2} - \frac{1}{2\sqrt{3}} & \frac{\beta_1}{\sqrt{3}} & \frac{\beta_2}{2} - \frac{\beta_2}{2\sqrt{3}} \\ \frac{\beta_1}{\sqrt{3}} & \frac{1}{2} - \frac{1}{2\sqrt{3}} & -\frac{\beta_2}{2} - \frac{\beta_2}{2\sqrt{3}} \\ \frac{\beta_3}{2} - \frac{\beta_3}{2\sqrt{3}} & -\frac{\beta_3}{2} - \frac{\beta_3}{2\sqrt{3}} & \frac{\beta_4}{\sqrt{3}} \end{pmatrix} \tag{3.12}$$

[3] We neglect issues of neutrino mass generation for simplicity.

$$Y'_{u2} = y_u \begin{pmatrix} \frac{1}{2} - \frac{1}{2\sqrt{3}} & \frac{\beta_1}{\sqrt{3}} & -\frac{\beta_2}{2} - \frac{\beta_2}{2\sqrt{3}} \\ \frac{\beta_1}{\sqrt{3}} & -\frac{1}{2} - \frac{1}{2\sqrt{3}} & \frac{\beta_2}{2} - \frac{\beta_2}{2\sqrt{3}} \\ -\frac{\beta_3}{2} - \frac{\beta_3}{2\sqrt{3}} & \frac{\beta_3}{2} - \frac{\beta_3}{2\sqrt{3}} & \frac{\beta_4}{\sqrt{3}} \end{pmatrix}. \tag{3.13}$$

There are a variety of ways in which a hierarchy of fermion masses can be achieved. For example, in [149], the β_i were all taken to be equal and set to unity, which led to two massless quark mass eigenvalues and one heavy (third generation) state. Rather than classifying all possibilities, here we consider a specific example in which the β_i parameters obey the following constraint:

$$\beta_1 = 1, \qquad \beta_4 = \beta_2\beta_3. \tag{3.14}$$

Diagonalizing Eq. (3.11) subject to the constraint of Eq. (3.14) results in two massless eigenvalues, and one nonzero eigenvalue,

$$y_t = y_u \left(\sqrt{2+\beta_2^2}\sqrt{2+\beta_3^2} \right) / \sqrt{3}. \tag{3.15}$$

Furthermore, as y_u and $\beta_{2,3}$ are all arbitrary parameters, we will further consider the limit in which $\beta_{2,3}$ are taken to be very large, while y_u is simultaneously taken to be very small, such that y_t as given above remains fixed. We see from Eq. (3.11) that in this limit, we have

$$Y_u = \frac{y_t}{\sqrt{2+\beta_2^2}\sqrt{2+\beta_3^2}} \begin{pmatrix} 1 & 1 & \beta_2 \\ 1 & 1 & \beta_2 \\ \beta_3 & \beta_3 & \beta_2\beta_3 \end{pmatrix} \overset{\beta_i \gg 1}{\longrightarrow} \text{Diag}(0, 0, y_t). \tag{3.16}$$

Again imposing Eq. (3.14), it is easy to see from Eqs. (3.12) and (3.13) that in the limit of large $\beta_{2,3}$ and fixed y_t, the messenger Yukawa couplings Y'_{u1} and Y'_{u2} also reduce to this form:

$$Y'_{u1} \overset{\beta_i \gg 1}{\longrightarrow} \text{Diag}(0, 0, y_t), \qquad Y'_{u2} \overset{\beta_i \gg 1}{\longrightarrow} \text{Diag}(0, 0, y_t). \tag{3.17}$$

The feature that the messenger Yukawas and the SM Yukawas are flavor-diagonal and have nonzero 33 entries only in this limit is a consequence of the fact that the $\mathcal{S}_3$ singlet contributions have been taken to dominate over the $\mathcal{S}_3$ doublet contributions. Indeed,

an inspection of Eq. (3.9) shows that in the regime in which Eq. (3.14) is satisfied, and $\beta_{2,3} \to \infty$ with $y_u \to 0$ such that y_t is fixed, the only term that remains is $Q_{\mathbf{1}} \bar{u}_{\mathbf{1}} \mathcal{H}_u^{(1)}$. This clearly requires an additional symmetry that allows for the β_4 term to dominate while maintaining consistency with Eq. (3.5) (this is an additional model-building complication, but not an insurmountable one [4]).

To reiterate, we have seen that we can simultaneously obtain sizable third generation SM and messenger Yukawa couplings, and messenger Yukawa couplings that are flavor-diagonal in the limit that the $\mathcal{S}_3$ singlet terms dominate over the interactions involving $\mathcal{S}_3$ doublets. Hence, to leading order in this parameter regime, this case is equivalent to one in which there are only third generation superpotential Yukawa couplings at the renormalizable level, and all other interactions result from higher-dimensional operators [149]. However, despite the equivalency of the two cases at leading order, they can be very different at subleading order. More precisely, the path to this limiting case is highly dependent not only on the $\mathcal{S}_3$ charges of the SM fields, but also the breaking of the additional symmetries that are required to reach this parameter regime. For example, with the $\mathcal{S}_3$ assignment in Table 3.2 and restricting to renormalizable couplings, it is straightforward to see that depending on how the massless eigenvalues are lifted by perturbing about Eq. (3.14), the subleading contributions to the messenger Yukawa interactions in this limit arise in either the 23 or 13 sectors. In contrast, if Eq. (3.14) is maintained, and the first and second generations acquire masses through nonrenormalizable operators, the structure of the subleading corrections to the messenger Yukawa couplings are highly dependent on the model-building details. Both situations have important implications not only for the masses of the superpartners, but also for questions of flavor violation, which is a critically important issue for flavored gauge mediation models. A detailed discussion of

[4] For example, one possibility is to impose a Z_7 symmetry, with charges $Q_{Q_{\mathbf{2}}} = 1$, $Q_{\bar{u}_{\mathbf{2}}} = 1$, $Q_{Q_{\mathbf{1}}} = 2$, $Q_{\bar{u}_{\mathbf{1}}} = 2$, $Q_{\mathcal{H}_u^{(1)}} = 3$, $Q_{\mathcal{H}_u^{(2)}} = 3$, $Q_{X_H} = 1$, and to introduce a flavon field ϕ which has $Q_\phi = 1$. This suppresses the terms in the upper 2×2 block of Y_u such that they require two insertions of the flavon field, while the other off-diagonal terms are generated with one flavon insertion. Please note, however, that the condition that β_1=1 requires additional symmetries to avoid fine-tuning.

these possibilities and their phenomenological implications is the subject of future work – see [152] for the beginnings thereof.

With the simple forms of the SM Yukawa couplings and the messenger Yukawa couplings, as given in Eqs. (3.16) and (3.17), respectively (as well as their analogues in the down quark and charged lepton sectors), the corrections to the soft supersymmetry breaking terms due to the messenger interactions are easily calculated by standard procedures. These procedures have been given in previous literature (see e.g. [130, 139, 148]), and summarized for this set of scenarios in [149].

With the assumption that the doublet and triplet messengers both result in the same quantity $\Lambda = F_{2,3}/M_{\rm mess} \sim F/M$, which we will always assume to be the case in this chapter, the leading order nonvanishing corrections to the soft supersymmetry breaking parameters are given by

$$\left(\delta m^2_{\tilde{u}}\right)_{33} = \frac{\Lambda^2 y_t^2}{(4\pi)^4}\left(-\frac{52}{15}g_1^2 - 12g_2^2 - \frac{64}{3}g_3^2 + 8y_b^2 + 72y_t^2\right), \tag{3.18}$$

$$\left(\delta m^2_{\tilde{d}}\right)_{33} = \frac{\Lambda^2 y_b^2}{(4\pi)^4}\left(-\frac{28}{15}g_1^2 - 12g_2^2 - \frac{64}{3}g_3^2 + 72y_b^2 + 8y_t^2 + 16y_\tau^2\right), \tag{3.19}$$

$$\left(\delta m^2_{\tilde{e}}\right)_{33} = \frac{\Lambda^2 y_\tau^2}{(4\pi)^4}\left(-\frac{36}{5}g_1^2 - 12g_2^2 + 48y_b^2 + 40y_\tau^2\right), \tag{3.20}$$

$$\left(\delta m^2_{\tilde{Q}}\right)_{33} = \frac{1}{2}(\delta m^2_{\tilde{u},33} + \delta m^2_{\tilde{d},33}), \tag{3.21}$$

$$\left(\delta m^2_{\tilde{L}}\right)_{33} = \frac{1}{2}\delta m^2_{\tilde{3},33}, \tag{3.22}$$

$$\delta m^2_{\tilde{H}_u} = -\frac{\Lambda^2}{(4\pi)^4}\left(18y_b^4 + 6y_b^2y_t^2\right), \qquad \delta m^2_{\tilde{H}_d} = -\frac{\Lambda^2}{(4\pi)^4}\left(18y_b^4 + 6y_b^2y_t^2 + 12y_\tau^4\right), \tag{3.23}$$

$$\left(\tilde{A}_u\right)_{33} = -\frac{2y_t\Lambda}{(4\pi)^2}(y_b^2 + 3y_t^2) \equiv \tilde{A}_t, \quad \left(\tilde{A}_d\right)_{33} = -\frac{2y_b\Lambda}{(4\pi)^2}(y_t^2 + 3y_b^2), \quad \left(\tilde{A}_e\right)_{33} = -\frac{6y_\tau^3\Lambda}{(4\pi)^2}. \tag{3.24}$$

All nontrivial corrections in the squark and slepton sectors thus involve only third generation fields [5].

[5] Here we note that the $\tilde{A}$ notation denotes the fact that the trilinear scalar couplings in the Lagrangian are of the form $A_{ijk}\phi_i\phi_j\phi_k$, for scalar fields $\phi_{i,j,k}$ (these are not family indices, but general field labels).

3.3 Results

In this section, we present a detailed numerical exploration of this scenario, as encoded by the soft supersymmetry breaking terms of Eqs. (3.18)–(3.24). The model parameters are $M_{\rm mess}$, Λ, $\tan\beta$, and the sign of μ (sgn(μ)), where we have followed standard procedures and replaced μ and b by $\tan\beta$, sgn(μ), and the Z boson mass. Here we will always set sgn(μ) $= 1$. Note that in comparison to the case of minimal gauge mediation and flavored gauge mediation models based on Abelian symmetries, the number of vectorlike messenger pairs in this scenario is always fixed to be $N_5 = 2$, which is the smallest number that allows for separate fine-tuning of the μ and b parameters. As a result, the model studied here has one fewer discrete parameter than these other scenarios. The renormalization group equations are evaluated using SoftSUSY 4.1.4 [155].

In [149], a preliminary analysis of this scenario was carried out in the context of taking the third generation MSSM matter fields to be inert to the $\mathcal{S}_3$ symmetry, with the primary goal of comparing this case to the case of minimal (flavor-independent) gauge mediation for a fixed value of $\tan\beta$ (of $\tan\beta = 10$). Our main purpose here is to provide a systematic analysis of the superpartner mass spectra, highlighting the dependence on $\tan\beta$ subject to the Higgs mass constraint.

For concreteness, and to connect with the results of our previous work, we begin with the example shown in the top panel of Figure 3.1, for which the messenger scale is $M_{\rm mess} = 10^{12}$ GeV and $\tan\beta = 10$; once these two parameters are fixed, the value of Λ is thus set by the requirement that $m_h \simeq 125$ GeV. This example shows a characteristic pattern also seen in the intermediate scale examples of [149], for which the heavy Higgs particles are between $5-6$ TeV, the gluino is approximately 5 TeV, and the squarks fall into two groupings, a lighter set that is close in mass to the gluino, and a heavier set that is similar in mass to the heavy charginos and neutralinos. The sleptons are close in mass to the lightest chargino and the second-lightest neutralino, which are nearly mass degenerate, and the next-to-lightest superpartner (NLSP) is the lightest neutralino. The needed values of μ

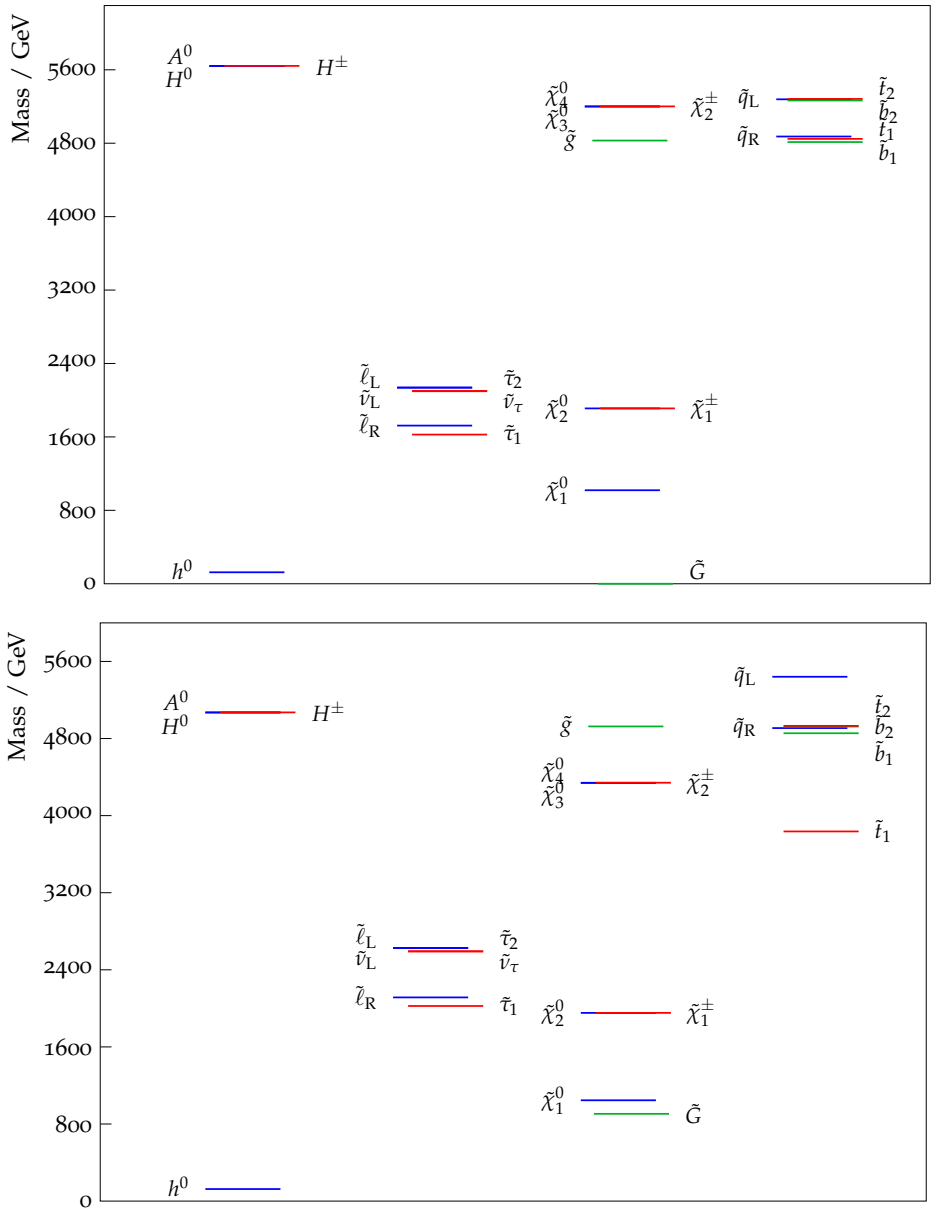

Figure 3.1: The mass spectrum for $M_{\text{Mess}} = 1 \times 10^{12}$ GeV (top panel) and $M_{\text{Mess}} = 1 \times 10^{16}$ GeV (bottom panel), both with $\tan\beta = 10$. In each case, Λ is fixed by the Higgs mass constraint.

and b/μ are in the $5-6$ TeV range. With an intermediate messenger scale, the gluino is lighter than the masses of the sparticles controlled by μ. In the bottom panel of Figure 3.1, we show an example with $M_{\rm mess} = 10^{16}$ GeV and $\tan\beta = 10$. Due to increased renormalization group running effects, the μ and b/μ terms are lighter than in the previous case, which leads to lighter masses for the heavy Higgs states. The gluino is now heavier than the heavy charginos and neutralinos, which have masses controlled by μ. There are also larger stop mixing effects, with the lighter stop mass just below 4 TeV, and a heavier gravitino due to the high messenger scale.

For smaller values of the messenger scale, the spectra are generally heavier for a fixed $\tan\beta$, as the stop mixing is smaller, requiring an increase in the value of Λ to obtain the same value of the light Higgs mass. This is seen in Figure 3.2, which shows points with $M_{\rm mess} = 10^6$ GeV (top panel) and $M_{\rm mess} = 10^{10}$ GeV (bottom panel), both with $\tan\beta = 10$. We note the lighter sleptons, lighter gluino mass, and greater squark mass splitting for low messenger scales.

Let us now consider smaller values of $\tan\beta$. In Figure 3.3, we show a low messenger scale example with $M_{\rm mess} = 10^6$ GeV (top panel) and a high messenger scale example with $M_{\rm mess} = 10^{12}$ GeV (bottom panel), both now with $\tan\beta = 5$. The sparticle masses are expected to be heavier for smaller $\tan\beta$, since the tree-level contribution to the light Higgs mass has decreased, requiring even larger radiative corrections to boost the light Higgs mass to its experimentally measured value. As a result, the mass spectra in these cases are highly split, and even the lighter sparticles have masses at and above 2 TeV. For higher values of the messenger scale, this splitting is amplified, as a larger value of Λ is needed to compensate for smaller A terms at low energies. These features are clearly exhibited in Figure 3.3, where we note that in each case, the heavy Higgs bosons and many of the squark masses are in the 10 TeV range, and thus out of the range shown in the figure.

We now consider the limit of large $\tan\beta$, for which the effects of the bottom and tau Yukawa couplings are more significant than in the lower $\tan\beta$ regime. In Figure 3.4, we show spectra with $M_{\rm mess} = 10^{12}$ GeV (top panel) and $M_{\rm mess} = 10^{16}$ GeV (bottom panel),

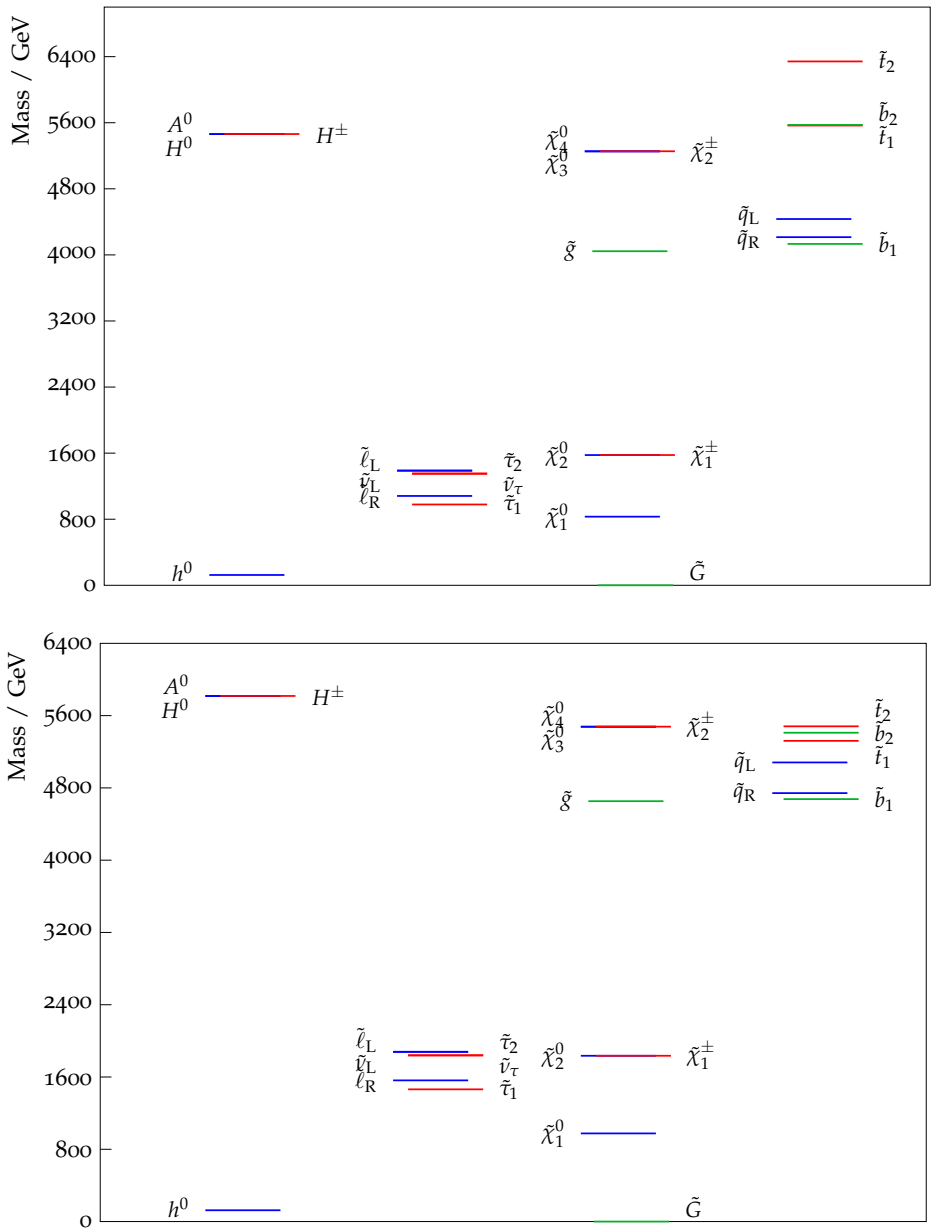

Figure 3.2: The mass spectrum for $M_{\text{Mess}} = 1 \times 10^6$ GeV (top panel) and $M_{\text{Mess}} = 1 \times 10^{10}$ GeV (bottom panel), both with $\tan\beta = 10$. In each case, Λ is fixed by the Higgs mass constraint.

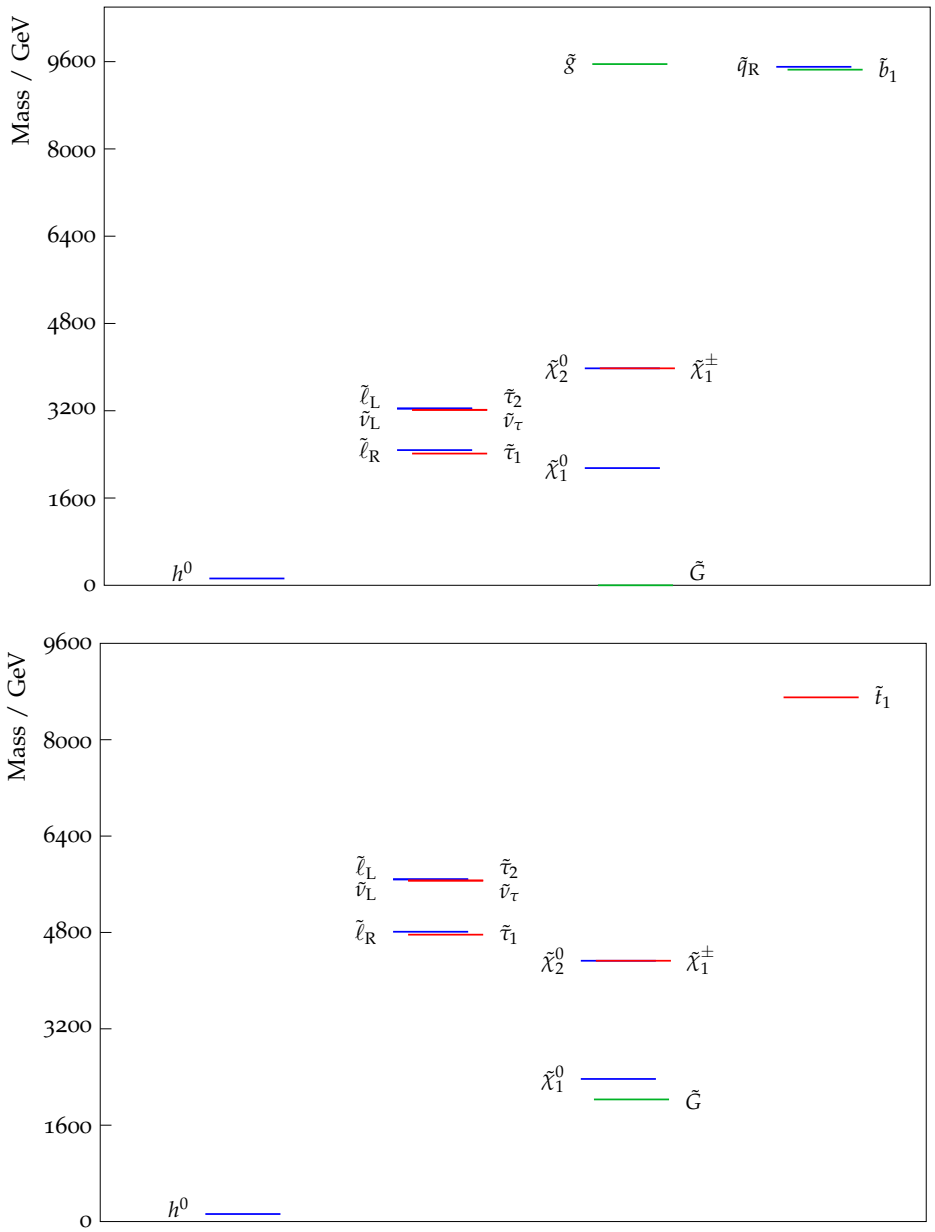

Figure 3.3: The mass spectrum for $M_{\text{Mess}} = 1 \times 10^6$ GeV (top panel) and $M_{\text{Mess}} = 1 \times 10^{12}$ GeV (bottom panel), both with $\tan\beta = 5$. In each case, Λ is fixed by the Higgs mass constraint.

both with $\tan\beta = 40$. In comparison to the analogous $\tan\beta = 10$ cases as shown in Figure 3.1, the higher $\tan\beta$ spectra are compressed, with the heaviest superpartner masses in the 5 TeV range. The two cases again differ in their values of μ and b/μ, with the high messenger scale example again displaying smaller values for these quantities, such that the gluino is heavier than the heavy charginos and neutralinos, and the heavy Higgs particles are lighter than their counterparts in the intermediate scale case. We also see a greater splitting of the squark masses in the high messenger scale case. These similarities continue in Figure 3.5, which is the analogous set of mass spectra to Figure 3.2, with $M_{\rm mess} = 10^6$ GeV (top panel) and $M_{\rm mess} = 10^{10}$ GeV, but now with $\tan\beta = 40$. As expected, the superpartner mass spectrum is again compressed compared to lighter values of $\tan\beta$, though slightly less so than what occurs for higher messenger scale values. For the low messenger scale example, there is a relatively light gluino and light bottom squark, with masses in the 3 TeV range. The NLSP remains the lightest neutralino, though the lighter stau mass continues to approach the NLSP mass as the messenger scale increases, due to the larger value of the tau Yukawa coupling in the large $\tan\beta$ regime.

These representative examples of the superpartner mass spectra demonstrate that as $\tan\beta$ is varied, there is a range of cases in the low $\tan\beta$ regime that have very heavy sparticle masses, but otherwise we have a range of superpartner masses that tend to be at most in the $5-6$ TeV range. This behavior in fact is quite robust. In Figure 3.6, the range of gluino masses in the $\log(M_{\rm mess}) - \tan\beta$ plane is shown, with the NLSP (lightest neutralino) mass given by the dotted contours. There is a tiny sliver of parameter space, corresponding to the lowest allowed values of $\tan\beta$, for which the gluino mass (and Λ) increases substantially, and increases as the messenger scale increases. Otherwise, the parameter regime is dominated by gluino masses within the $4-5$ TeV range, as seen repeatedly in the example spectra shown here.

It is also illuminating to explore the Higgs mass prediction and its correlation with the gluino mass within the parameter space of this model. In Figure 3.7, we show the $\log_{10}(\Lambda) - \tan\beta$ plane for two fixed values of the messenger scale: $M_{\rm mess} = 10^6$ GeV (top

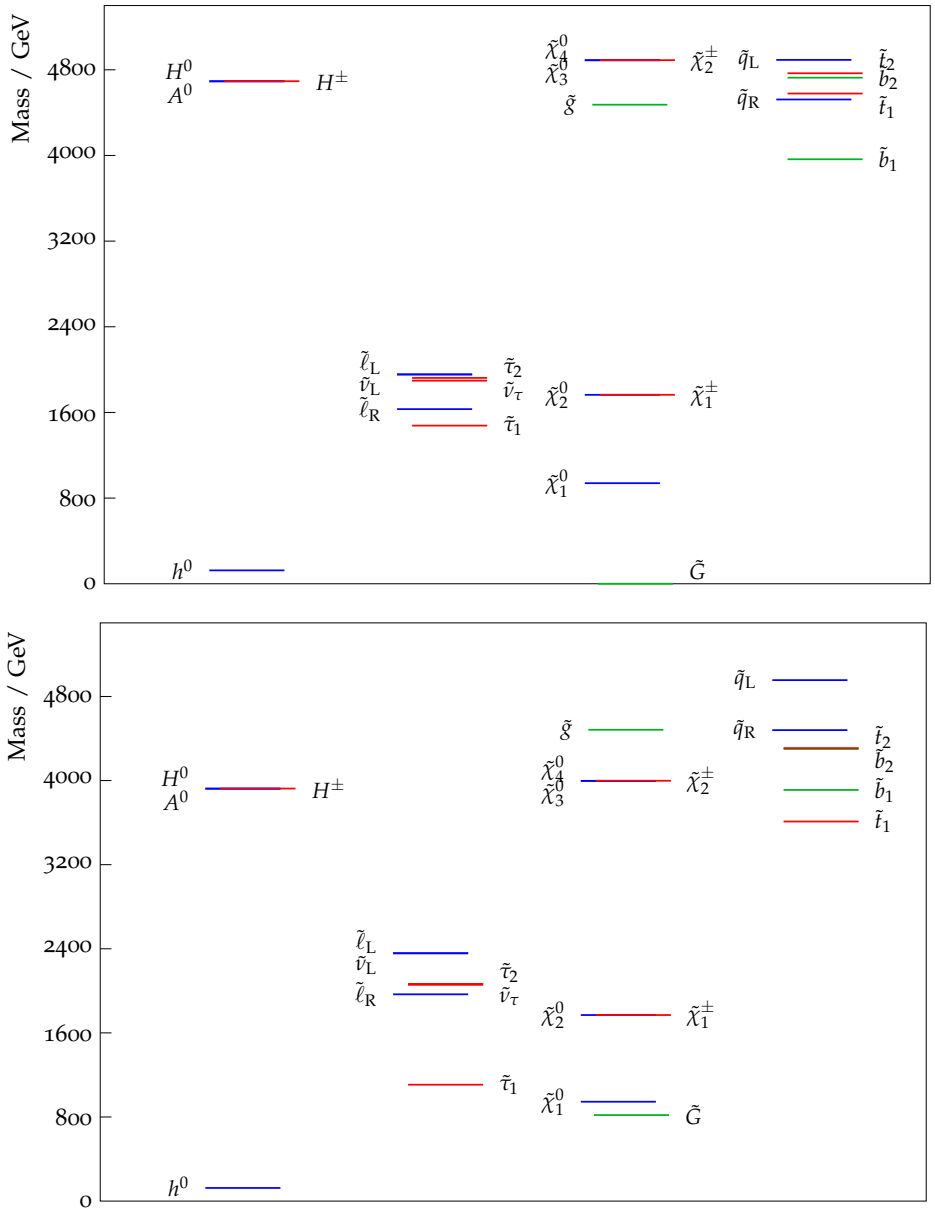

Figure 3.4: The mass spectrum for $M_{\text{Mess}} = 1 \times 10^{12}$ GeV (top panel) and $M_{\text{Mess}} = 1 \times 10^{16}$ GeV (bottom panel), both with $\tan\beta = 40$. In each case, Λ is fixed by the Higgs mass constraint.

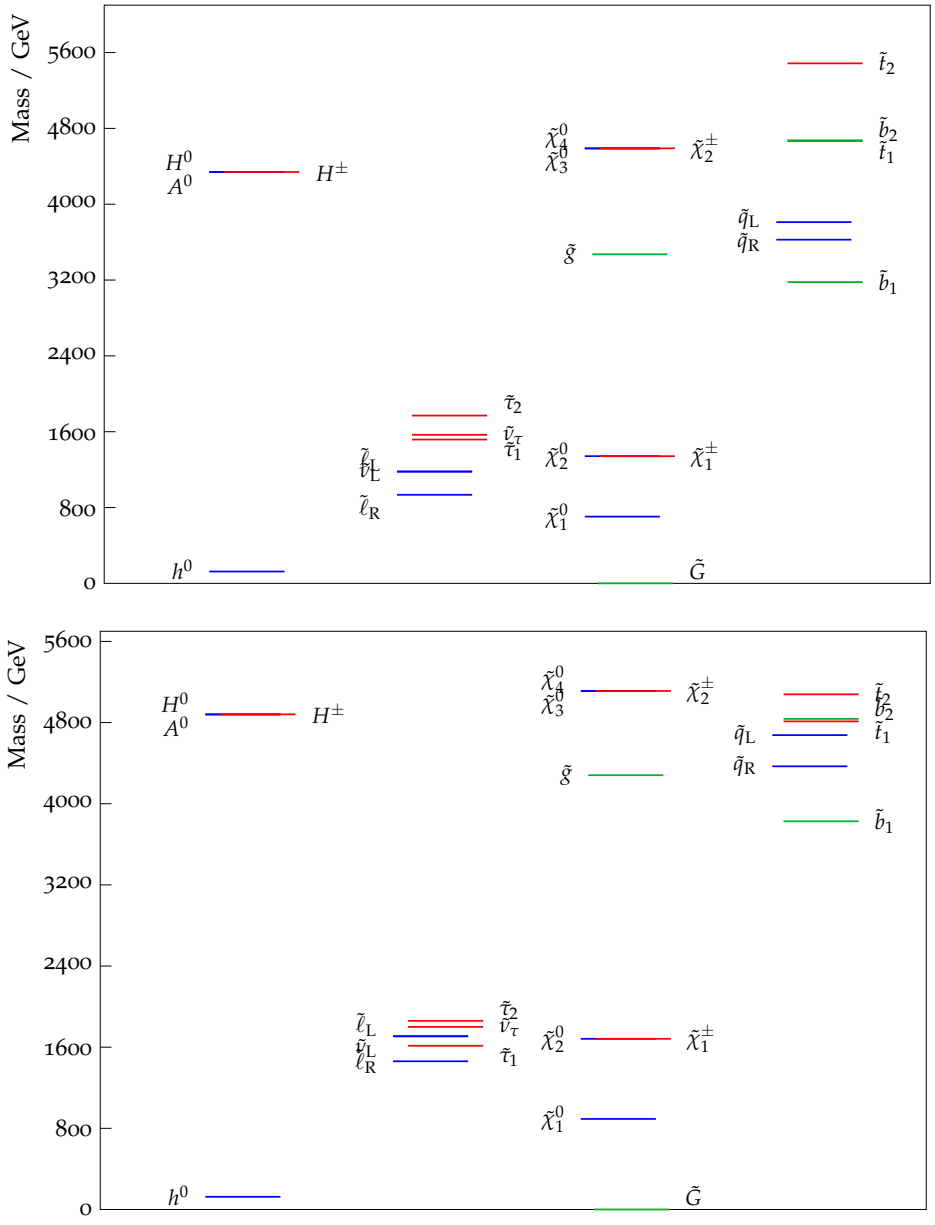

Figure 3.5: The mass spectrum for $M_{\text{Mess}} = 1 \times 10^6$ GeV (top panel) and $M_{\text{Mess}} = 1 \times 10^{10}$ GeV (bottom panel), both with $\tan\beta = 40$. In each case, Λ is fixed by the Higgs mass constraint.

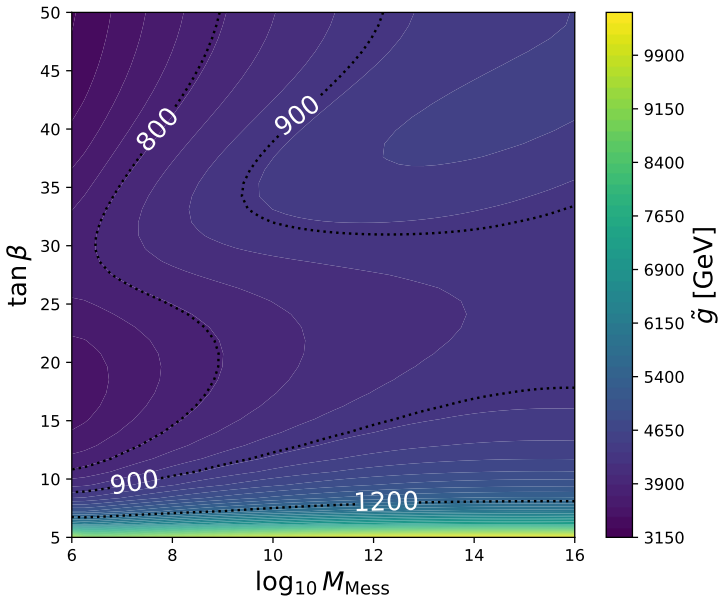

Figure 3.6: The range of gluino masses in this scenario, as displayed in the $\log M_{\text{mess}} - \tan\beta$ plane. The dotted contours denote the lightest neutralino mass.

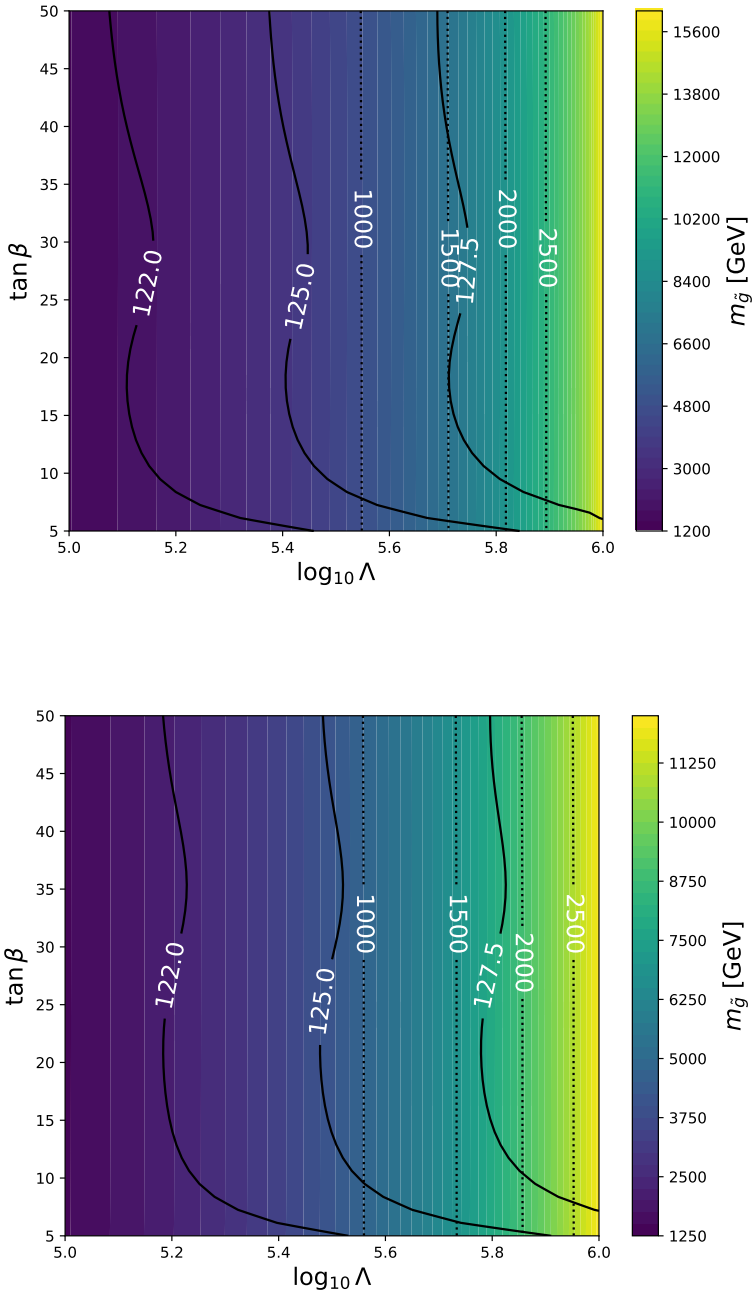

Figure 3.7: The Higgs mass (solid contours) and gluino masses (color shading) in this scenario, as displayed in the $\log_{10}\Lambda - \tan\beta$ plane for $M_{\rm mess} = 10^6$ GeV (top panel) and $M_{\rm mess} = 10^{10}$ GeV (bottom panel). The dotted contours show the lightest neutralino mass.

panel) and $M_{\rm mess} = 10^{10}$ GeV (bottom panel). The Higgs mass contours are given by solid lines, the gluino mass is labeled by color shading, and the dotted contours represent the lightest neutralino (NLSP) mass. Here we see the correlation in this model between the needed values of the gluino mass and the Higgs mass constraint, with gluino masses in the range of 4 TeV or greater for the experimentally preferred range of the lightest Higgs mass. The NLSP mass in the allowed parameter region is correspondingly lighter for lower messenger scale values than for higher values. The general features of the $M_{\rm mess} = 10^{10}$ GeV case persist for higher values of the messenger scale (not displayed here for simplicity).

In Figure 3.8, the Higgs and gluino mass predictions are displayed in the $\log_{10} M_{\rm mess} - \log_{10} \Lambda$ plane for $\tan\beta = 5$ (top panel) and $\tan\beta = 20$ (bottom panel). The contour labeling is identical to Figure 3.7, with the Higgs mass given by solid contours, the NLSP mass by dotted contours, and the gluino mass as color shading; note the different scale of the color shading compared to the previous figure. Here we see the differences in the gluino mass predictions between the low $\tan\beta$ regime and the intermediate to high $\tan\beta$ regimes, with significantly heavier gluino masses needed for very low $\tan\beta$, and the < 5 TeV range for intermediate to high $\tan\beta$. Note that as seen in Figure 3.6, the crossover between the low $\tan\beta$ range and this intermediate to high $\tan\beta$ range occurs at quite modest values of $\tan\beta$ (~ 10 and above); hence, the results shown here for $\tan\beta = 20$ are quite similar to those at higher values of $\tan\beta$ (hence these higher values are not displayed separately). In addition, the NLSP mass scales trivially with Λ, and thus as we've seen, the preferred Higgs mass region is associated with heavier neutralinos (and other superpartner masses) for low $\tan\beta$.

It is illustrative to examine the stop mixing parameter $X_t = \tilde{A}_t - \mu \cot\beta$. In Figure 3.9, we plot $|X_t/m_S|$ as a function of the messenger scale and $\tan\beta$, where the mass scale m_S is given by the geometric mean of the stop masses ($m_S = \sqrt{m_{\tilde{t}_1} m_{\tilde{t}_2}}$). We see that we obtain sizable stop mixing throughout the parameter space in this scenario, with higher values in the case of high messenger scales, and lower values for low messenger scales, consistent with the mass spectra shown earlier.

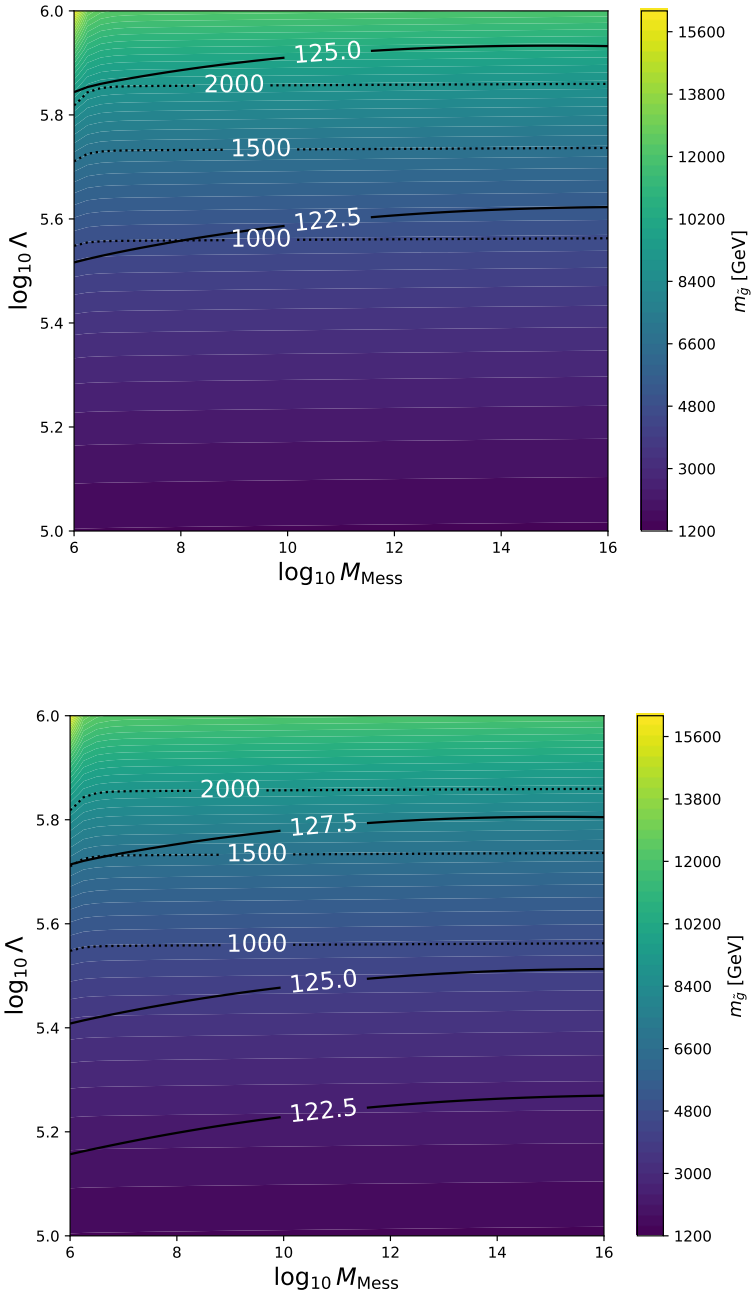

Figure 3.8: The Higgs mass (solid contours) and gluino masses (color shading) in this scenario, as displayed in the $\log_{10}\Lambda - \log_{10} M_{\rm mess}$ plane for $\tan\beta = 5$ (top panel) and $\tan\beta = 20$ (bottom panel). The dotted contours show the lightest neutralino mass.

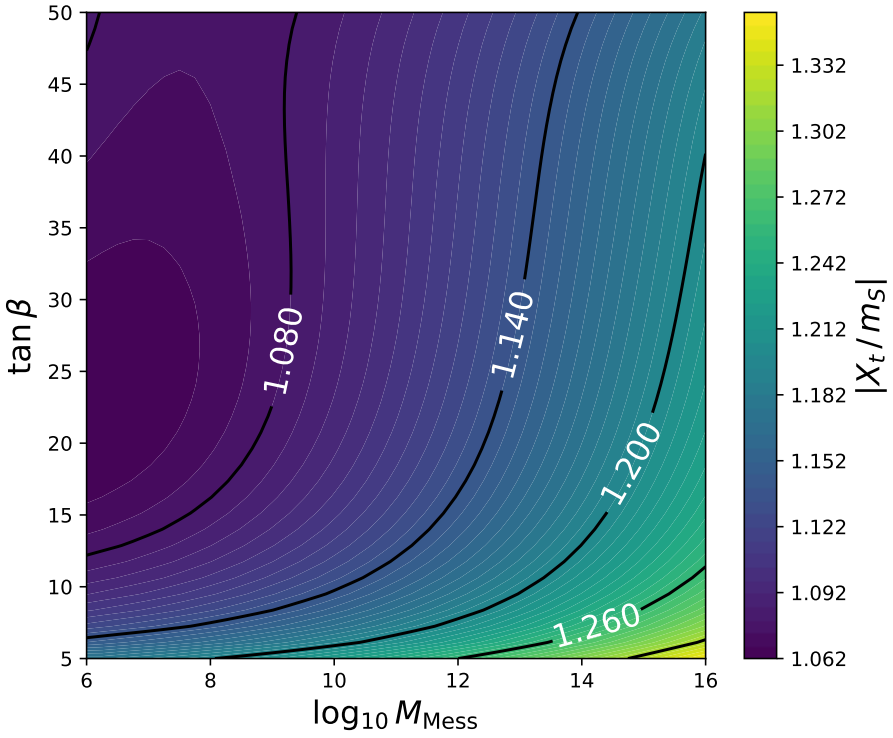

Figure 3.9: The values of $|X_t/m_S|$ in this scenario, where X_t is the stop mixing parameter, and $m_S = \sqrt{m_{\tilde{t}_1} m_{\tilde{t}_2}}$, as displayed in the $\log M_{\rm mess} - \tan\beta$ plane.

We close this section by commenting that the superpartner mass range in this scenario is generally heavier than what is possible in flavored gauge mediation models based on $U(1)$ symmetries. This can be seen for example for some of the benchmark points of [147], for which all superpartner masses can be at the 2 TeV range or less. In such models, the $U(1)$ charges can be chosen such that problematic couplings between the electroweak Higgs fields and the supersymmetry breaking field can be forbidden, whereas for non-Abelian Higgs-messenger symmetries, these couplings cannot be avoided. Therefore, in the non-Abelian case, we need to augment the field degrees of freedom to ameliorate the effects of these couplings and arrive at a phenomenologically acceptable model. As stated previously, this is the reason why we have $N_5 \geq 2$ in the non-Abelian case. For Abelian models, N_5 is a parameter that can be chosen, and thus one can obtain light spectra with $N_5 = 1$.

3.4 Conclusions

In this chapter, we have explored a specific flavored gauge mediation model of the MSSM soft supersymmetry breaking parameters that can result from postulating that the electroweak Higgs fields and the $SU(2)$ messenger doublets are related by a discrete non-Abelian gauge symmetry. This Higgs-messenger symmetry is taken to be $\mathcal{S}_3$, as first studied in this context for two families in [140], and later extended to three families in [149]. The model predicts two pairs of messenger fields, which transform as $\mathbf{5}$, $\bar{\mathbf{5}}$ representations of $SU(5)$; as discussed in [149], this arises from the need to have an enlarged Higgs-messenger field content that includes $\mathcal{S}_3$ doublet and singlet representation to mitigate an otherwise severe μ/B_μ problem. The extended Higgs-messenger sector allows for a rich variety of possible renormalizeble superpotential couplings of the Higgs-messenger fields to the SM matter fields, depending on the assumed $\mathcal{S}_3$ charges of the quark and lepton superfields. In a specific limit in which these couplings are dominated by the interactions among the $\mathcal{S}_3$ singlet representations, the resulting SM and messenger Yukawas both involve only third generation fields.

As a result, a minimal flavored gauge mediation model is obtained in which the sfermion masses are flavor diagonal, and there is sizable stop mixing due to the one-loop third generation A terms that arise from the messenger-matter interactions. The model has three continuous parameters: the messenger scale $M_{\rm mess}$, the scale Λ, which sets the scale of the soft supersymmetry breaking terms (together with loop factors), and $\tan\beta$, and one discrete parameter (the sign of the μ parameter), which yields a highly predictive scenario. We showed in this chapter that in much of the parameter space, the superpartner masses are at most $5-6$ TeV, with the gluino typically in the $4-5$ TeV range. The exceptions to this general pattern occur at small values of $\tan\beta$, for which the need for large radiative corrections to bolster the light Higgs mass requires much heavier squark masses. This highly predictive model of the MSSM soft parameters is thus one to keep in mind as the LHC continues to probe the paradigm of TeV-scale supersymmetry.

While the $\mathcal{S}_3$ singlet-dominated regime can arise trivially by requiring that the MSSM matter fields are inert to the Higgs-messenger symmetry, we have shown in this chapter that it can also result in a specific limit in the case that the quark and lepton superfields have nontrivial $\mathcal{S}_3$ charges. Hence, it is possible in this limit to sidestep the previously established correlation between the SM and messenger Yukawa couplings in this class of models [140, 149], which had disallowed sizable third generation couplings for both the SM and messenger couplings, and consequently required heavier superpartner masses to obtain the experimentally determined value of the light Higgs mass.

It is important to note that in the intriguing case that the quark and lepton superfields transform nontrivially with respect to the Higgs-messenger symmetry, reaching this limit requires additional symmetries that are also directly connected to the origin of the SM fermion masses and mixing parameters. Indeed, given that in the scenario studied here, the first and second matter fermion generations are massless, extending this simple model to a fully realistic theory requires a detailed examination of subleading corrections as this limit is relaxed. These corrections will yield flavor-changing interactions that are a hallmark of this class of flavored gauge mediation models. Though it is known that these effects can often be more strongly suppressed in flavored gauge mediation models than what naive estimates might suggest [146, 147], the question remains open as to whether a viable, fully-fledged three-family model can be constructed in which the Higgs-messenger symmetry is also a nontrivial part of the full family symmetry. In the next chapter, we detail the first step in such explorations along these lines.

Chapter 4

Cabbibo Mixing in Non-Abelian Flavored Gauge Mediation[1]

4.1 Introduction

In this chapter, as a next step in our exploration of this class of flavored gauge mediation models, we build upon the model in the previous chapter to investigate the generation of the quark and charged lepton masses and the quark mixing angles. Our focus in this work is to elucidate the conditions for achieving a mass hierarchy for the lighter generations of SM charged mattter fields and obtaining a reasonable value for the Cabibbo mixing angle of the quark sector (here we will ignore the issue of neutrino mass generation, and return to this question in future work). While $\mathcal{S}_3$ has been considered as a family symmetry in prior work (see e.g. [156–158], among others, for works in which S_3 symmetry is used to predict the Cabibbo angle), our approach differs from previous literature that it is an investigation of this question within the context of the MSSM with flavored gauge mediated supersymmetry breaking. More precisely, in this scenario, the electroweak Higgs doublets $H_{u,d}$ emerge after $\mathcal{S}_3$ breaking as specific linear combinations of Higgs-messenger fields in singlet and doublet representations of $\mathcal{S}_3$, while the orthogonal combinations of the Higgs-messenger fields are two sets of heavy messenger states that are decoupled at the messenger scale of gauge mediation. As a result, within this setting there are specific

[1] Chapter adapted from [152]

relations among the SM and messenger Yukawa couplings, and constraints on each sector that must be jointly satisfied. We find that while specific perturbations of the Yukawa couplings associated with the renormalizable superpotential interactions do not in general lead to the appropriate mixing of the first and second generations, the Cabibbo angle can be generated via higher-dimensional superpotential operators, with corresponding implications for the mass spectrum of the theory.

The structure of this chapter is as follows. We begin with an restatement of the discrete non-Abelian Higgs-messenger symmetry and the resulting model structure, which again assumes case of the discrete group $\mathcal{S}_3$, as in [140, 149, 151]. We present the model and discuss the generation of masses and mixing angles among the first and second quark families. The phenomenological implications are then discussed. Finally, we present our summary and conclusions.

4.2 Fermion Masses: Renormalizable Couplings[2]

As studied in [151], a key assumption of this scenario is that the three generations of SM quarks and leptons are embedded into doublet and singlet represenations of $\mathcal{S}_3$. The charge assignments for the fields in the theory is summarized in Table 4.1.

	$\mathcal{H}_u^{(2)}$	$\mathcal{H}_u^{(1)}$	$\mathcal{H}_d^{(2)}$	$\mathcal{H}_d^{(1)}$	$Q_{\mathbf{2}}$	$Q_{\mathbf{1}}$	$\bar{u}_{\mathbf{2}}$	$\bar{u}_{\mathbf{1}}$	$\bar{d}_{\mathbf{2}}$	$\bar{d}_{\mathbf{1}}$	$L_{\mathbf{2}}$	$L_{\mathbf{1}}$	$\bar{e}_{\mathbf{2}}$	$\bar{e}_{\mathbf{1}}$	X_H
$\mathcal{S}_3$	**2**	**1**	**2**	**1**	**2**	**1**	**2**	**1**	**2**	**1**	**2**	**1**	**2**	**1**	**2**

Table 4.1: Charges for an $\mathcal{S}_3$ model of the Higgs-messenger fields and the MSSM matter fields. Here the $SU(3)$ triplet messengers and the associated X_T field are not displayed for simplicity.

The renormalizable superpotential Yukawa couplings of the MSSM matter fields and the Higgs-messenger fields, for example for the up quarks, are given by

$$W^{(u)} = y_u\left[Q_{\mathbf{2}}\bar{u}_{\mathbf{2}}\mathcal{H}_u^{(2)} + \beta_1 Q_{\mathbf{2}}\bar{u}_{\mathbf{2}}\mathcal{H}_u^{(1)} + \beta_2 Q_{\mathbf{2}}\bar{u}_{\mathbf{1}}\mathcal{H}_u^{(2)} + \beta_3 Q_{\mathbf{1}}\bar{u}_{\mathbf{2}}\mathcal{H}_u^{(2)} + \beta_4 Q_{\mathbf{1}}\bar{u}_{\mathbf{1}}\mathcal{H}_u^{(1)}\right], \quad (4.1)$$

[2]Note that this subsection up until Eq. 4.9 is a restatement of Section 3.2, and is retained for narrative continuity.

in which the β_i are arbitrary coefficients in the absence of further model structure. We note that here we will take them to be real, for simplicity [3]. In the basis given by $Q = (Q_{\mathbf{2}}, Q_{\mathbf{1}})^T$ and $\overline{u} = (\overline{u}_{\mathbf{2}}, \overline{u}_{\mathbf{1}})^T$, these couplings can be expressed in matrix form as [4]:

$$W^{(u)} = y_u Q^T \begin{pmatrix} \mathcal{H}^{(2)}_{u1} & \beta_1 \mathcal{H}^{(1)}_u & \beta_2 \mathcal{H}^{(2)}_{u2} \\ \beta_1 \mathcal{H}^{(1)}_u & \mathcal{H}^{(2)}_{u2} & \beta_2 \mathcal{H}^{(2)}_{u1} \\ \beta_3 \mathcal{H}^{(2)}_{u2} & \beta_3 \mathcal{H}^{(2)}_{u1} & \beta_4 \mathcal{H}^{(1)}_u \end{pmatrix} \bar{u}. \tag{4.2}$$

Analogous coupling matrices would hold in the down quark and charged lepton sectors, with the replacements $\beta_i \to \beta_{di}, \beta_{ei}$.

A key feature of this scenario compared to previous work using $\mathcal{S}_3$ as a family symmetry (see e.g.[156–158]) is that there is a specific decomposition of the Higgs-messenger fields into the electroweak Higgs pair, $H_{u,d}$, and two heavy pairs of doublet messengers that acquire masses of the order of $M_{\rm mess}$ and thus decouple at scales much higher than the TeV scale, as summarized in the previous section. This decomposition of the Higgs-messenger fields, which is obtained using using Eqs. (3.4) and (3.8), are given for the up-type Higgs and messenger fields as follows:

$$\begin{aligned} \mathcal{H}^{(1)}_u &= \frac{1}{\sqrt{3}}(H_u + M_{u1} + M_{u2}) \\ (\mathcal{H}^{(2)}_u)_1 &= \frac{1}{\sqrt{3}} H_u - \frac{1}{2}\left(1 + \frac{1}{\sqrt{3}}\right) M_{u1} + \frac{1}{2}\left(1 - \frac{1}{\sqrt{3}}\right) M_{u1} \\ (\mathcal{H}^{(2)}_u)_2 &= \frac{1}{\sqrt{3}} H_u + \frac{1}{2}\left(1 - \frac{1}{\sqrt{3}}\right) M_{u1} - \frac{1}{2}\left(1 - \frac{1}{\sqrt{3}}\right) M_{u1}. \end{aligned} \tag{4.3}$$

(Analogous results hold for the down-type Higgs and messenger fields, from Eqs. (3.4) and (3.8).)

[3] The assumption of real β_i clearly has an effect on options for generating the CKM quark mixing phase angle $\delta_{\rm CKM}$. We defer the detailed discussion of generating a viable $\delta_{\rm CKM}$ for a future study.

[4] Eq. (4.2) and its generalizations to other charged SM fermions correct a typo in the corresponding expressions for the renormalizable superpotential in [149], for which there was an incorrect interchange of β_1 and β_2; these expressions are correct in [151].

Using the results of Eq. (4.3) in Eq. (4.2), it is straightforward to see that the SM up quark sector Yukawa couplings are given by

$$Y_u = \frac{y_u}{\sqrt{3}} \begin{pmatrix} 1 & \beta_1 & \beta_2 \\ \beta_1 & 1 & \beta_2 \\ \beta_3 & \beta_3 & \beta_4 \end{pmatrix}, \tag{4.4}$$

and the messenger Yukawa couplings Y'_{u1} and Y'_{u2} take the form

$$Y'_{u1} = y_u \begin{pmatrix} -\frac{1}{2} - \frac{1}{2\sqrt{3}} & \frac{\beta_1}{\sqrt{3}} & \frac{\beta_2}{2} - \frac{\beta_2}{2\sqrt{3}} \\ \frac{\beta_1}{\sqrt{3}} & \frac{1}{2} - \frac{1}{2\sqrt{3}} & -\frac{\beta_2}{2} - \frac{\beta_2}{2\sqrt{3}} \\ \frac{\beta_3}{2} - \frac{\beta_3}{2\sqrt{3}} & -\frac{\beta_3}{2} - \frac{\beta_3}{2\sqrt{3}} & \frac{\beta_4}{\sqrt{3}} \end{pmatrix} \tag{4.5}$$

$$Y'_2 = y_{u2} \begin{pmatrix} \frac{1}{2} - \frac{1}{2\sqrt{3}} & \frac{\beta_1}{\sqrt{3}} & -\frac{\beta_2}{2} - \frac{\beta_2}{2\sqrt{3}} \\ \frac{\beta_1}{\sqrt{3}} & -\frac{1}{2} - \frac{1}{2\sqrt{3}} & \frac{\beta_2}{2} - \frac{\beta_2}{2\sqrt{3}} \\ -\frac{\beta_3}{2} - \frac{\beta_3}{2\sqrt{3}} & \frac{\beta_3}{2} - \frac{\beta_3}{2\sqrt{3}} & \frac{\beta_4}{\sqrt{3}} \end{pmatrix}. \tag{4.6}$$

In this section, we will focus on the diagonalization of the SM Yukawa couplings as given in Eq. (4.4), and save the discussion of the messenger Yukawa couplings for later in this chapter.

It is straightforward to diagonalize Eq. (4.4) for arbitrary (real) β_i via a standard biunitary transformation, in which

$$U_{uL}^\dagger Y_u U_{uR} = Y_u^{\text{diag}}, \tag{4.7}$$

with

$$U_{uL}^\dagger Y_u Y_u^\dagger U_{uL}, \qquad U_{uR}^\dagger Y_u^\dagger Y_u U_{uR}. \tag{4.8}$$

It is clear from the structure of Eq. (4.4) that the eigenvalues are not hierarchical for arbitary values of the β_i. Hence, specific relations among the β_i are required for this scenario to be phenomenologically viable of this scenario. Any such relations correspond to additional symmetry structures, together with the $\mathcal{S}_3$ Higgs-messenger symmetry. As

discussed in [151], one possible solution that guarantees two zero mass eigenvalues and one nonzero mass eigenvalue is to require that

$$\beta_1 = 1, \qquad \beta_2\beta_3 = \beta_4. \tag{4.9}$$

The nonzero eigenvalue is then to be identified with the top quark Yukawa coupling, y_t. As discussed in [151], this requires the specific identification that $y_u = y_t/(\sqrt{2+\beta_2^2}\sqrt{2+\beta_3^2})$.

Furthermore, from Eq. (4.4) and Eq. (4.9), we see that one of the zero mass eigenvalues arises from the upper 2×2 block of Y_u and is controlled by $\beta_1 \to 1$, while the other arises from the symmetry of the third column and row of Y_u and is controlled by $\beta_2\beta_3 \to \beta_4$. Note that Eq. (4.9) includes the possibility that all $\beta_i = 1$, for which there is the enhanced symmetry $\mathcal{S}_{3L} \times \mathcal{S}_{3R}$. This is the flavor "democratic" limit, which was studied in this context in [149], and which has a long and extensive literature (see e.g. [159–175]). However, Eq. (4.9) also encompasses other possibilities. This includes the option that $\beta_4 \gg \beta_{2,3} \gg \beta_1$, in which the term involving $\mathcal{S}_3$ singlet representations only in Eq. (4.1) is dominant, which was explored in [151].

Given that there is a degenerate subspace corresponding to the two zero mass eigenvalues, the diagonalization matrices U_{uL} and U_{uR} should generally involve linear combinations of the associated eigenvectors, with the linear combinations parametrized by a continuous parameter. More precisely, the (unnormalized) eigenvector corresponding to the zero eigenvalue controlled by $\beta_1 \to 1$ is given by $(1, -1, 0)$, while the (unnormalized) eigenvector corresponding to the other zero eigenvalue is given by $(-\beta_{3,2}, -\beta_{3,2}, 1)$, with $\beta_{3,2}$ corresponding to the eigenvectors for $Y_u Y_u^\dagger$ and $Y_u^\dagger Y_u$, respectively. With this in mind, the diagonalization matrices U_{uL} and U_{uR} are given by

$$U_{uL} = \begin{pmatrix} \frac{\cos\tilde{\theta}}{\sqrt{2}} - \frac{\beta_3 \sin\tilde{\theta}}{\sqrt{2}\sqrt{2+\beta_3^2}} & -\frac{\beta_3 \cos\tilde{\theta}}{\sqrt{2}\sqrt{2+\beta_3^2}} - \frac{\sin\tilde{\theta}}{\sqrt{2}} & \frac{1}{\sqrt{2+\beta_3^2}} \\ -\frac{\cos\tilde{\theta}}{\sqrt{2}} - \frac{\beta_3 \sin\tilde{\theta}}{\sqrt{2}\sqrt{2+\beta_3^2}} & -\frac{\beta_3 \cos\tilde{\theta}}{\sqrt{2}\sqrt{2+\beta_3^2}} + \frac{\sin\tilde{\theta}}{\sqrt{2}} & \frac{1}{\sqrt{2+\beta_3^2}} \\ \frac{\sqrt{2}\sin\tilde{\theta}}{\sqrt{2+\beta_3^2}} & \frac{\sqrt{2}\cos\tilde{\theta}}{\sqrt{2+\beta_3^2}} & \frac{\beta_3}{\sqrt{2+\beta_3^2}} \end{pmatrix} \tag{4.10}$$

$$U_{uR} = \begin{pmatrix} \frac{\cos\tilde{\theta}}{\sqrt{2}} - \frac{\beta_2 \sin\tilde{\theta}}{\sqrt{2}\sqrt{2+\beta_2^2}} & -\frac{\beta_2 \cos\tilde{\theta}}{\sqrt{2}\sqrt{2+\beta_2^2}} - \frac{\sin\tilde{\theta}}{\sqrt{2}} & \frac{1}{\sqrt{2+\beta_2^2}} \\ -\frac{\cos\tilde{\theta}}{\sqrt{2}} - \frac{\beta_2 \sin\tilde{\theta}}{\sqrt{2}\sqrt{2+\beta_2^2}} & -\frac{\beta_2 \cos\tilde{\theta}}{\sqrt{2}\sqrt{2+\beta_2^2}} + \frac{\sin\tilde{\theta}}{\sqrt{2}} & \frac{1}{\sqrt{2+\beta_2^2}} \\ \frac{\sqrt{2}\sin\tilde{\theta}}{\sqrt{2+\beta_2^2}} & \frac{\sqrt{2}\cos\tilde{\theta}}{\sqrt{2+\beta_2^2}} & \frac{\beta_2}{\sqrt{2+\beta_2^2}} \end{pmatrix}, \tag{4.11}$$

in which we have written the linear combinations of degenerate eigenvectors in terms of the parameter $\tilde{\theta}$, with $0 \leq \tilde{\theta} \leq \pi/2$. In the case that $\tilde{\theta} = 0$, the mass ordering is such that the eigenvalue controlled by β_1 would correspond to the first generation, and U_{uL}, U_{uR} then reduce to the forms given in [151]. In contrast, for $\tilde{\theta} = \pi/2$, it is the other eigenvalue that is to be identified with the first generation, and the corresponding U_{uL}, U_{uR} have their first two columns interchanged compared to the forms given in [151]. Here it is important to recall that $\tilde{\theta}$ is an unphysical parameter in the degenerate (massless) limit, as studied in [151], and hence it has no observable consequences in this limit. However, when perturbations to this leading order structure are incorporated such that there are three distinct hierarchical mass eigenvalues, a specific value of $\tilde{\theta}$ is determined. Once this is done for both the up and down quark sector, the CKM matrix can be explicitly predicted. Indeed, a primary goal of this work is to explore such perturbations to see if viable quark masses and mixing can be obtained in this scenario.

To this end, we note that if identical structures are assumed within the down quark sector, such that the U_{dL}, U_{dR} that satisfy $U_{dL}^\dagger Y_d U_{dR} = Y_d^{\text{diag}}$ are given by Eqs. (4.10)–(4.11) with $\beta_{3,2} \to \beta_{3d,2d}$ and $\tilde{\theta} \to \tilde{\theta}_d$, the Cabibbo-Kobayashi-Maskawa matrix $U_{\text{CKM}} = U_{uL}^\dagger U_{dL}$ takes the general form

$$U_{\text{CKM}} = \begin{pmatrix} \cos\tilde{\theta}\cos\tilde{\theta}_d + \frac{(2+\beta_3\beta_{3d})\sin\tilde{\theta}\sin\tilde{\theta}_d}{\sqrt{2+\beta_3^2}\sqrt{2+\beta_{3d}^2}} & \frac{(2+\beta_3\beta_{3d})\cos\tilde{\theta}_d\sin\tilde{\theta}}{\sqrt{2+\beta_3^2}\sqrt{2+\beta_{3d}^2}} - \cos\tilde{\theta}\sin\tilde{\theta}_d & -\frac{\sqrt{2}(\beta_3-\beta_{3d})\sin\tilde{\theta}}{\sqrt{2+\beta_3^2}\sqrt{2+\beta_{3d}^2}} \\ -\cos\tilde{\theta}_d\sin\tilde{\theta} + \frac{(2+\beta_3\beta_{3d})\cos\tilde{\theta}\sin\tilde{\theta}_d}{\sqrt{2+\beta_3^2}\sqrt{2+\beta_{3d}^2}} & \frac{(2+\beta_3\beta_{3d})\cos\tilde{\theta}\cos\tilde{\theta}_d}{\sqrt{2+\beta_3^2}\sqrt{2+\beta_{3d}^2}} + \sin\tilde{\theta}\sin\tilde{\theta}_d & -\frac{\sqrt{2}(\beta_3-\beta_{3d})\cos\tilde{\theta}}{\sqrt{2+\beta_3^2}\sqrt{2+\beta_{3d}^2}} \\ \frac{\sqrt{2}(\beta_3-\beta_{3d})\sin\tilde{\theta}_d}{\sqrt{2+\beta_3^2}\sqrt{2+\beta_{3d}^2}} & \frac{\sqrt{2}(\beta_3-\beta_{3d})\cos\tilde{\theta}_d}{\sqrt{2+\beta_3^2}\sqrt{2+\beta_{3d}^2}} & \frac{2+\beta_3\beta_{3d}}{\sqrt{2+\beta_3^2}\sqrt{2+\beta_{3d}^2}} \end{pmatrix}. \tag{4.12}$$

There are several illuminating features of Eq. (4.12). First, Eq.(4.12) shows that the $2-3$ and $1-3$ mixing angles of U_{CKM} both depend linearly on the quantity $\beta_3 - \beta_{3d}$. In contrast, the Cabibbo $(1-2)$ mixing angle λ is largely independent of this factor, and

instead depends primarily on the difference between $\tilde{\theta}$ and $\tilde{\theta}_d$. In the case that $\tilde{\theta}$ takes intermediate values such that $\sin\tilde{\theta} \sim \cos\tilde{\theta}$, it is necessary to take $\beta_{3d} \to \beta_3 + O(\lambda^3)$. This a very delicate balance that is needed between the up and down quark sectors, and ensuring that this condition is satisfied certainly requires additional model-building input. In this case, further corrections are required to fill in the needed value of the $2-3$ CKM mixing angle. Second, it is possible to envision a scenario in which $\tilde{\theta} \to O(\lambda)$, such that we can take the still-stringent but slightly milder condition that $\beta_{3d} \to \beta_3 + O(\lambda^2)$. Indeed, in the limit that $\beta_{3d} \to \beta_3$, Eq. (4.12) simplifies to the following form:

$$U_{\text{CKM}} = \begin{pmatrix} \cos(\tilde{\theta}-\tilde{\theta}_d) & \sin(\tilde{\theta}-\tilde{\theta}_d) & 0 \\ -\sin(\tilde{\theta}-\tilde{\theta}_d) & \cos(\tilde{\theta}-\tilde{\theta}_d) & 0 \\ 0 & 0 & 1 \end{pmatrix}. \tag{4.13}$$

In this case, we must further require that $\tilde{\theta}_d \to O(\lambda)$ and $\tilde{\theta} - \tilde{\theta}_d \sim O(\lambda)$, which is also a delicate balance between the up and down quark sectors. Further model-building structure must be incorporated to generate such relations dynamically rather than forcing them to occur via fine-tuning.

While it might at first seem plausible that perturbations to Eq. (4.9) could yield a phenomenologically acceptable CKM matrix, we can see right away that this is impossible with only the renormalizable (tree-level) superpotential couplings of Eq. (4.1). The reason is that Eq. (4.4) is exactly diagonalizable for arbitrary β_i, and the eigenvectors of the Hermitian combinations $Y_u Y_u^\dagger$ and $Y_u^\dagger Y_u$ in the general case include the (unnormalized) eigenvector $(1,-1,0)$, with the associated eigenvalue controlled by the parameter β_1. Hence, once the β_i no longer satisfy Eq. (4.9), the hierarchy of the eigenvalues is immediately fixed (up to the possible but uninteresting case of masses that are nonzero, but still degenerate) such that either $\tilde{\theta} = 0$ or $\tilde{\theta} = \pi/2$. (Analogous results hold for $\tilde{\theta}_d$.) As a result, the Cabibbo angle is predicted to be either vanishingly small if $\tilde{\theta} = \tilde{\theta}_d$, or $O(1)$ if $\tilde{\theta} - \tilde{\theta}_d \sim \pi/2$, neither of which are phenomenologically viable.

4.3 Fermion Masses: Nonrenormalizable Operators

As discussed in the previous section, the Yukawa couplings at the renormalizable level do not give rise to a phenomenologically acceptable CKM matrix. Hence, we now explore the possibility that the renormalizable couplings listed in Eq. (4.2) are supplemented by couplings of the Higgs-messenger fields to the matter fields that arise from higher-dimensional (nonrenormalizable) operators in the superpotential. Such operators arise from new physics associated with the cutoff scale of the operator. In the canonical Froggatt-Nielsen approach [62] based on family symmetries, such operators originate from renormalizable Yukawa couplings of the SM fields to new heavy fields (known as Froggatt-Nielsen fields) and flavon fields that receive vacuum expectation values and thus participate in the breaking of the family symmetry. Upon family symmetry breaking, therefore, these operators contribute to fermion masses; in supersymmetric models they result in effective operator contributions to the superpotential.

Here we are interested in effective operators that preserve the $\mathcal{S}_3$ symmetry at high scales (at or close to the messenger scale). Given the quantum numbers of the matter and Higgs fields as given in Table 4.1, this clearly requires augmenting the theory to include a flavon sector that consists of chiral superfields that have vacuum expectation values in their scalar components (but no associated F terms). Furthermore, the flavon sector must include fields with nontrivial $\mathcal{S}_3$ quantum numbers, which then can easily resemble the corresponding $\mathcal{H}^{(2)}_{u,d}$ fields. Quite generally, with the introduction of such flavon fields, additional model-building constraints are required to ensure, for example, that such flavons do not couple directly to the $X_{H,T}$ fields of the theory, for example. Our purpose here is to not to provide a comprehensive analysis of all operators and the associated detailed dynamics of the flavon sector, but rather to provide an explicit working example of a higher-dimensional operator that can satisfy the requirements of the previous section for generating a viable Cabibbo mixing angle.

The working example we construct is as follows. Let us consider the following contribution to the superpotential:

$$W_{NR}^{(u)} = \frac{\epsilon}{\Lambda'}\Big(Q_{\mathbf{2}}\phi_{\mathbf{2}}\Big)\Big(\mathcal{H}_u^{(2)}\bar{u}_{\mathbf{2}}\Big), \tag{4.14}$$

in which $\phi_{\mathbf{2}}$ is a flavon in the $\mathbf{2}$ representation of $\mathcal{S}_3$. Here ϵ is a dimensionless parameter, and Λ' is the scale of the new physics that is responsible for generating this operator. Through some dynamics (that as stated we will leave unspecified in this work), $\phi_{\mathbf{2}}$ acquires a vacuum expectation value in its scalar component, but as previously just discussed, not its F-component, so it does not participate in the mediation of supersymmetry breaking. We parametrize this field's vacuum expectation value as

$$\langle\phi_{\mathbf{2}}\rangle = v\begin{pmatrix}\cos\theta\\ \sin\theta\end{pmatrix}, \tag{4.15}$$

in which v is a dimensionful parameter, and the dimensionless parameter θ has been introduced (and we will shortly see its identification with the parameter θ as given in the previous section). After this flavon acquires a vev, the strength of the operator of Eq. (4.14) is given by $\beta_\epsilon \equiv v\epsilon/\Lambda'$. We then obtain an additional contribution to the SM up quark Yukawa matrix:

$$Y_u^{NR} = \frac{\beta_\epsilon}{\sqrt{3}}\begin{pmatrix}\sin\theta & \sin\theta & 0\\ \cos\theta & \cos\theta & 0\\ 0 & 0 & 0\end{pmatrix}, \tag{4.16}$$

as well as contributions to the messenger Yukawa couplings, as follows:

$$\begin{aligned} Y_{u1}^{\prime NR} &= \frac{\beta_\epsilon}{2}\begin{pmatrix}\left(1-\frac{1}{\sqrt{3}}\right)\sin\theta & -\left(1+\frac{1}{\sqrt{3}}\right)\sin\theta & 0\\ \left(1-\frac{1}{\sqrt{3}}\right)\cos\theta & -\left(1+\frac{1}{\sqrt{3}}\right)\cos\theta & 0\\ 0 & 0 & 0\end{pmatrix}\\ Y_{u2}^{\prime NR} &= \frac{\beta_\epsilon}{2}\begin{pmatrix}-\left(1+\frac{1}{\sqrt{3}}\right)\sin\theta & \left(1-\frac{1}{\sqrt{3}}\right)\sin\theta & 0\\ -\left(1+\frac{1}{\sqrt{3}}\right)\cos\theta & \left(1-\frac{1}{\sqrt{3}}\right)\cos\theta & 0\\ 0 & 0 & 0\end{pmatrix}, \end{aligned} \tag{4.17}$$

and we assume there are analogous relations for the down quark and charged lepton sectors. The task at hand is once again to diagonalize the SM Yukawa couplings, which now take the form $Y_u \to Y_u + Y_u^{NR}$. Again, in this section we will focus on the SM fermion masses, and defer the discussion of the associated messenger Yukawa couplings to the next section.

Here we will focus our attention on the case in which we retain the relations of Eq. (4.9) for the renormalizable couplings, such that $\beta_1 = 1$ and $\beta_2\beta_3 = \beta_4$. The SM up quark Yukawa matrix then takes the form

$$Y_u \to \frac{1}{\sqrt{3}} \begin{pmatrix} y_u + \beta_\epsilon \sin\theta & y_u + \beta_\epsilon \sin\theta & y_u\beta_2 \\ y_u + \beta_\epsilon \cos\theta & y_u + \beta_\epsilon \cos\theta & y_u\beta_2 \\ y_u\beta_3 & y_u\beta_3 & y_u\beta_2\beta_3 \end{pmatrix}. \tag{4.18}$$

Diagonalizing this matrix in the usual manner, the eigenvalues are easily shown to be nondegenerate. As we will see, one eigenvalue remains massless, the second has mass of order $\beta_\epsilon \ll 1$, and the third is to be identified with the top quark Yukawa coupling y_t.

While it is straightforward to obtain the diagonalization matrices for arbitrary values of the parameters $\beta_{2,3}$ and β_ϵ, here we focus on leading order effects in β_ϵ. We also focus on the limit studied in [151], wherein $\beta_{2,3}$ are taken to be very large while y_u is set such that y_t remains constant. This is done not only for simplicity, but also because deviations from that limit generically result in flavor off-diagonal couplings in the messenger sector, which require more detailed analysis [5]. In this paradigm, the SM up quark Yukawa becomes

$$Y_u = \begin{pmatrix} \frac{\beta_\epsilon \sin\theta}{\sqrt{3}} & \frac{\beta_\epsilon \sin\theta}{\sqrt{3}} & 0 \\ \frac{\beta_\epsilon \cos\theta}{\sqrt{3}} & \frac{\beta_\epsilon \cos\theta}{\sqrt{3}} & 0 \\ 0 & 0 & y_t \end{pmatrix}, \tag{4.19}$$

[5] A notable exception is the "democratic" limit in which the β_i couplings of the renormalizable sector are all equal to 1; we defer a detailed discussion of this case to a future study.

while the messenger Yukawas take the form

$$Y'_{u1} = \begin{pmatrix} \beta_\epsilon \left(\frac{1}{2} - \frac{1}{2\sqrt{3}}\right) \sin\theta & -\beta_\epsilon \left(\frac{1}{2} + \frac{1}{2\sqrt{3}}\right) \sin\theta & 0 \\ \beta_\epsilon \left(\frac{1}{2} - \frac{1}{2\sqrt{3}}\right) \cos\theta & -\beta_\epsilon \left(\frac{1}{2} + \frac{1}{2\sqrt{3}}\right) \cos\theta & 0 \\ 0 & 0 & y_t \end{pmatrix}$$

$$Y'_{u2} = \begin{pmatrix} -\beta_\epsilon \left(\frac{1}{2} + \frac{1}{2\sqrt{3}}\right) \sin\theta & \beta_\epsilon \left(\frac{1}{2} - \frac{1}{2\sqrt{3}}\right) \sin\theta & 0 \\ -\beta_\epsilon \left(\frac{1}{2} + \frac{1}{2\sqrt{3}}\right) \cos\theta & \beta_\epsilon \left(\frac{1}{2} - \frac{1}{2\sqrt{3}}\right) \cos\theta & 0 \\ 0 & 0 & y_t \end{pmatrix}. \tag{4.20}$$

Upon first inspection, it appears that the Yukawa matrices are dependent on the direction of the flavon vacuum expectation value, and as such one might expect the eigenvalues of Y_u to also carry this dependence. However, this is not the case, as we will soon see.

Following the standard procedure of rotating the SM up quark Yukawa in Eq. (4.19) into the diagonal quark mass basis using a biunitary transformation, the diagonalization matrices U_{uL} and U_{uR} are found to take the simple forms

$$U_{uL} = \begin{pmatrix} -\cos\theta & \sin\theta & 0 \\ \sin\theta & \cos\theta & 0 \\ 0 & 0 & 1 \end{pmatrix} \qquad U_{uR} = \begin{pmatrix} -\frac{1}{\sqrt{2}} & \frac{1}{\sqrt{2}} & 0 \\ \frac{1}{\sqrt{2}} & \frac{1}{\sqrt{2}} & 0 \\ 0 & 0 & 1 \end{pmatrix}. \tag{4.21}$$

In this basis, the SM up quark Yukawa matrix is

$$Y_u = \text{Diag}\left(0, \sqrt{\frac{2}{3}}\beta_\epsilon, y_t\right). \tag{4.22}$$

We now see that the dependence on the direction of the vacuum expectation value of the flavon field drops out in the Yukawa matrices, but is now carried by the unitary matrices $U_{u:}$ and U_{uR}. It is immediately clear, however, that θ enters into the flavor structure of this model. Explicitly, assuming a corresponding structure in the down quarks, ($\theta \to \theta_d$,

$y_u \to y_d$, and $\beta_i \to \beta_{di}$), we obtain a CKM matrix of the form

$$U_{\rm CKM} = U_{uL}^\dagger U_{dL} = \begin{pmatrix} \cos(\theta - \theta_d) & \sin(\theta - \theta_d) & 0 \\ -\sin(\theta - \theta_d) & \cos(\theta - \theta_d) & 0 \\ 0 & 0 & 1 \end{pmatrix}. \tag{4.23}$$

We note that the structure of the CKM as given in Eq. (4.23) is unambiguous, as the quark masses are non-degenerate (as seen in Eq. (4.22)), and it describes mixing between the first and second generations. This form explicitly allows for the generation of appropriately Cabibbo-sized mixing between the first and second families if $\sin(\theta - \theta_d) \simeq \lambda$, as anticipated from the general discussion of the last section. Indeed, upon a comparison of Eq. (4.23) with the renormalizable level structure of Eq. (4.12), we see that we have obtained a viable CKM matrix to leading order in the Cabibbo angle λ, and that the parameters $\tilde{\theta}$ and $\tilde{\theta}_d$ of the previous section can be identified with the quantities θ and θ_d of this section, which parametrize the vacuum expectation values of the flavon fields in the up and down quark sectors (compare Eq. (4.13) and Eq. (4.23)). Furthermore, we note that as we have explicitly taken the limit that $\beta_{2,3} \gg 1$ and $\beta_{2d,3d} \gg 1$, at this order no $1-3$ or $2-3$ CKM mixing is generated. To summarize, this operator has indeed led to a working example of lifting the mass degeneracy of the couplings of the renormalizable sector in the case that $\beta_1 = 1$, $\beta_4 = \beta_2\beta_3$ (and analogously for the down quark sector), in such a way that a Cabibbo mixing angle of the appropriate size can be generated within this framework.

4.4 Messenger Yukawa Couplings and Superpartner Mass Spectra

In this section, we turn our attention to the messenger Yukawa couplings and resulting mass spectra of the MSSM superpartners. Here we will confine our attention to the large $\beta_{2,3}$ regime, for which the structure of the resulting soft terms is particularly simple, and is flavor diagonal. We defer a more comprehensive analysis of general $\beta_{2,3}$ that satisfy

Eq. (4.9) for a future study.

Messenger Yukawa couplings and soft supersymmetry breaking terms. We begin by writing the messenger Yukawa couplings in the diagonal SM fermion mass basis. For the up quark sector, it is straightforward to determine that starting from Eq. (4.17), the messenger Yukawas in the diagonal quark mass basis, in the limit that $\beta_{2,3} \gg 1$, are given by

$$Y'_{u1} = \begin{pmatrix} 0 & 0 & 0 \\ -\frac{\beta_\epsilon}{\sqrt{2}} & -\frac{\beta_\epsilon}{\sqrt{6}} & 0 \\ 0 & 0 & y_t \end{pmatrix} \qquad Y'_{u2} = \begin{pmatrix} 0 & 0 & 0 \\ \frac{\beta_\epsilon}{\sqrt{2}} & -\frac{\beta_\epsilon}{\sqrt{6}} & 0 \\ 0 & 0 & y_t \end{pmatrix}. \tag{4.24}$$

With these simple forms of the up quark and messenger Yukawa matrices as given in Eqs. (4.22) and (4.24), the corrections to the soft supersymmetry breaking terms are easily calculated. The methods for doing so are standard in the literature, (see e.g. [139], [130], [148]), and are summarized for these classes of models in [149].

As before, we assume that the doublet and triplet messengers are determined by the same value of $\Lambda = F_{2,3}/M_{Mess} \approx F/M$, and that the down quark and charged lepton sectors are analogous to the up quark sector. As a first step in exploring the phenomenology of this scenario, and to examine in detail the effects of Eq. (4.14), for simplicity we assume a single β_ϵ parameter for each of the sectors, and allow it to vary (while keeping $\beta_\epsilon \ll 1$). The soft terms include the usual gauge-mediated contributions (not shown for simplicity), as well as corrections due to the messenger Yukawa couplings.

The nonvanishing corrections to the soft terms from the messenger Yukawas are presented below (here the relevant factors of $\Lambda/(4\pi)^2$ are suppressed for notational convenience):

$$\left(\delta m^2_{\tilde{Q}}\right)_{22} = \left(-2y_b^2 - 2y_t^2 - \frac{2y_\tau^2}{3} - \frac{16g_1^2}{9} - 8g_2^2 - \frac{128g_3^2}{9}\right)\beta_\epsilon^2$$

$$\left(\delta m^2_{\tilde{Q}}\right)_{33} = 36y_b^4 + 8y_t^2y_b^2 + 8y_\tau^2y_b^2 - \frac{14g_1^2y_b^2}{15} - 6g_2^2y_b^2 - \frac{32g_3^2y_b^2}{3} + 36y_t^4 - \frac{26g_1^2y_t^2}{15} - 6g_2^2y_t^2 - \frac{32g_3^2y_t^2}{3} + \left(-\frac{8y_b^2}{3} - 2y_t^2\right)\beta_\epsilon^2$$

$$\left(\delta m^2_{\tilde{u}}\right)_{11} = \left(-\frac{26g_1^2}{15} - 6g_2^2 - \frac{32g_3^2}{3}\right)\beta_\epsilon^2, \qquad \left(\delta m^2_{\tilde{u}}\right)_{22} = \left(-4y_t^2 - \frac{26g_1^2}{45} - 2g_2^2 - \frac{32g_3^2}{9}\right)\beta_\epsilon^2$$

$$\left(\delta m^2_{\tilde{u}}\right)_{33} = 72y_t^4 + 8y_b^2y_t^2 - \frac{52g_1^2y_t^2}{15} - 12g_2^2y_t^2 - \frac{64g_3^2y_t^2}{3} - 4\beta_\epsilon^2y_t^2$$

$$\left(\delta m^2_{\tilde{d}}\right)_{11} = \left(4y_\tau^2 - \frac{14g_1^2}{15} - 6g_2^2 - \frac{32g_3^2}{3}\right)\beta_\epsilon^2, \quad \left(\delta m^2_{\tilde{d}}\right)_{22} = \left(-4y_b^2 - \frac{14g_1^2}{45} - 2g_2^2 - \frac{32g_3^2}{9}\right)\beta_\epsilon^2$$

$$\left(\delta m^2_{\tilde{d}}\right)_{33} = 72y_b^4 + 8y_t^2y_b^2 + 24y_\tau^2y_b^2 - \frac{28g_1^2y_b^2}{15} - 12g_2^2y_b^2 - \frac{64g_3^2y_b^2}{3}$$

$$\left(\delta m^2_{\tilde{L}}\right)_{22} = \left(-2y_b^2 - \frac{2y_\tau^2}{3} - \frac{12g_1^2}{5} - 4g_2^2\right)\beta_\epsilon^2$$

$$\left(\delta m^2_{\tilde{L}}\right)_{33} = 20y_\tau^4 + 24y_b^2y_\tau^2 - \frac{18g_1^2y_\tau^2}{5} - 6g_2^2y_\tau^2 - \frac{8\beta_\epsilon^2y_\tau^2}{3}$$

$$\left(\delta m^2_{\tilde{e}}\right)_{11} = \left(-\frac{18g_1^2}{5} - 6g_2^2\right)\beta_\epsilon^2 \qquad \left(\delta m^2_{\tilde{e}}\right)_{22} = \left(-4y_b^2 - \frac{4y_\tau^2}{3} - \frac{6g_1^2}{5} - 2g_2^2\right)\beta_\epsilon^2$$

$$\left(\delta m^2_{\tilde{e}}\right)_{33} = 40y_\tau^4 + 48y_b^2y_\tau^2 - \frac{36g_1^2y_\tau^2}{5} - 12g_2^2y_\tau^2 - \frac{16\beta_\epsilon^2y_\tau^2}{3}$$

$$\delta m^2_{\tilde{H}_u} = -6y_t^2(y_b^2 + 3y_t^2), \qquad \delta m^2_{\tilde{H}_d} = -6(3y_b^4 + y_b^2y_t^2 + 3y_\tau^4)$$

$$\left(\tilde{A}_u\right)_{33} = -2y_t\left(y_b^2 + 3y_t^2\right), \qquad \left(\tilde{A}_d\right)_{33} = -2y_b\left(3y_b^2 + y_t^2\right), \qquad \left(\tilde{A}_e\right)_{33} = -6y_\tau^3. \quad (4.25)$$

We see that there is no introduction of off-diagonal flavor-violating couplings at leading order in this limiting case in which for the up, down, and charged lepton sectors, Eq. (4.9) is satisfied and the relevant $\beta_{2,3}$ are taken to be very large while keeping the third generation SM fermion masses fixed. Furthermore, the corrections to the first two generations

arise at order β_ϵ^2.

Superpartner mass spectra. We now explore the phenomenology of the soft terms as given in Eqs. (4.25). As is *de rigueur*, our model parameters are $M_{\rm Mess}$, Λ, $\tan\beta$, and the sign of μ, where we have replaced μ and b by $\tan\beta$, $\mathrm{sgn}(\mu)$ and the Z boson mass. We set $\mathrm{sgn}(\mu) = 1$. The renormalization group equations are run using SoftSUSY 4.1.4 [155].

In previous work [151], we explored the behavior of the superpartner mass spectra for the renormalizable sector Yukawa couplings in the large β_i limit, focusing on the dependence of the spectra on $\tan\beta$ and the messenger scale. For continuity, as well as a check on the phenomenological consistency of the higher-dimensional operator correction introduced in Eq. (4.14), we begin with the example spectra as shown in Figure 4.1. The top of Figure 4.1 shows results for the model studied in [151]. The messenger scale is $M_{\rm Mess} = 1 \times 10^{12}$ GeV and $\tan\beta = 10$. The value of Λ is set such that $m_h \simeq 125$ GeV. The bottom of Figure 4.1 displays the Higgs and superpartner mass spectra that arise from the soft supersymmetry breaking terms as given in Eq. (4.25), but with $\beta_\epsilon = 0$. The spectra are in agreement, as expected.

In the $\beta_\epsilon \to 0$ limit, the heavy Higgs particles are between $5 - 6$ TeV, along with the gluino at around 5 TeV. The squark masses fall into two general categories, one significantly heavier than the other. The heavier squarks are the left-handed sdown, sup and scharm squarks, as well as the both scharms and the heavier of the two stops. Their masses are close to the heavier charginos and neutralinos. The lower group is comprised of the right-handed sdown, sup and scharm squarks, as well as both sbottoms, and the lighter stop, whose masses are closer to the gluino. The next-to-lightest supersymmetric particle (NSLP) in this scenario is a bino-like neutralino.

Let us now include the effects of Eq. (4.14), such that β_ϵ is now nonzero. Here we note that as β_ϵ is connected with the masses of the charged SM fermions of the second generation, this quantity is expected to take small values. As explicit examples, the resulting spectra for small values of the coupling strengths β_ϵ are given in Figure 4.2. The top

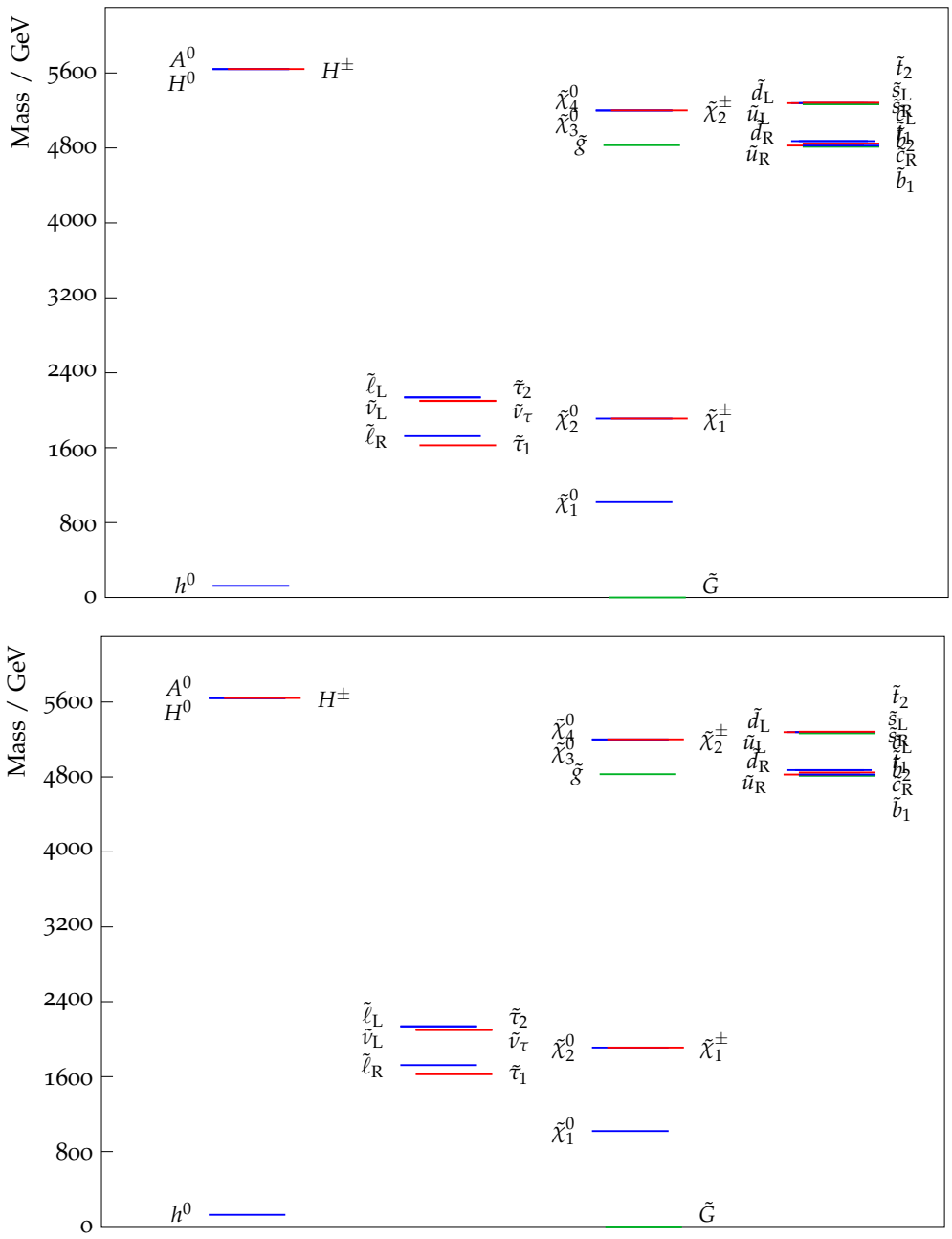

Figure 4.1: The mass spectra for $M_{\text{Mess}} = 1 \times 10^{12}$ GeV and $\tan\beta = 10$ for the scenario explored in [151] (top) and for the case explored here with $\beta_\epsilon = 0$ (bottom). In each case, Λ is fixed by the Higgs mass constraint. As expected, the two cases are in agreement.

of Figure 4.2 has taken $\beta_\epsilon = 0.01$, and the bottom has $\beta_\epsilon = 0.05$. The spectra follow the same general pattern as seen in Figure 4.1, but with minor changes to the splitting of the superpartner masses. We see that the masses of the right-handed down and up squarks are pushed down, as well as the lightest left-handed charged slepton and sneutrino. The masses of the heavy Higgses are almost entirely unaffected, as are the masses of the gauginos.

It is illustrative to consider what occurs for larger values of β_ϵ, for comparative purposes (note that significant values of β_ϵ are inconsistent with SM charged fermion mass predictions). We find that the pattern described above continues for such larger values of β_ϵ, as shown in Figure 4.3. On the top, for $\beta_\epsilon = 0.1$, we see that the first two families of charged sleptons and sneutrinos are now lighter than one of the staus, with the other stau being the lightest slepton. Additionally, we see that the tight groupings of the squarks into two bands, as seen in Figure 4.1 are splitting with the right-handed sup becoming the lightest colored superpartner. On the bottom, which has $\beta_\epsilon = 0.2,$ the lightest right-handed charged slepton is now lighter than all third generation sleptons. Furthermore, the squarks continue to display larger mass splittings, with the mass splittings within the original two groupings that appeared for smaller β_ϵ clearly demonstrated.

In Figures 4.4 and 4.5, we consider a smaller messenger mass of $M_{\rm Mess} = 1 \times 10^6$ GeV. Displayed on the top of Figure 4.4 is the superpartner mass spectrum for this messenger mass, with $\beta_\epsilon = 0.01$. As seen previously in [151], a lower messenger scale leads to a large mass spectrum for fixed value of $\tan\beta$, due to the smaller size of the stop mixing. Since we choose Λ such that $m_h \simeq 125$ GeV, a low messenger mass necessitates a larger value of Λ, and therefore leads to a heavier spectrum. The squark masses are no longer demarcated into two distinct groupings, but rather split between 4 and 6.4 TeV. The lightest squark is a sbottom, while the heaviest is a stop. There are four major squark groups. In decreasing mass order they are: the heaviest stop, the lighter stop and heavier sbottom, the left-handed squarks in generations one and two, and lastly the right-handed first and

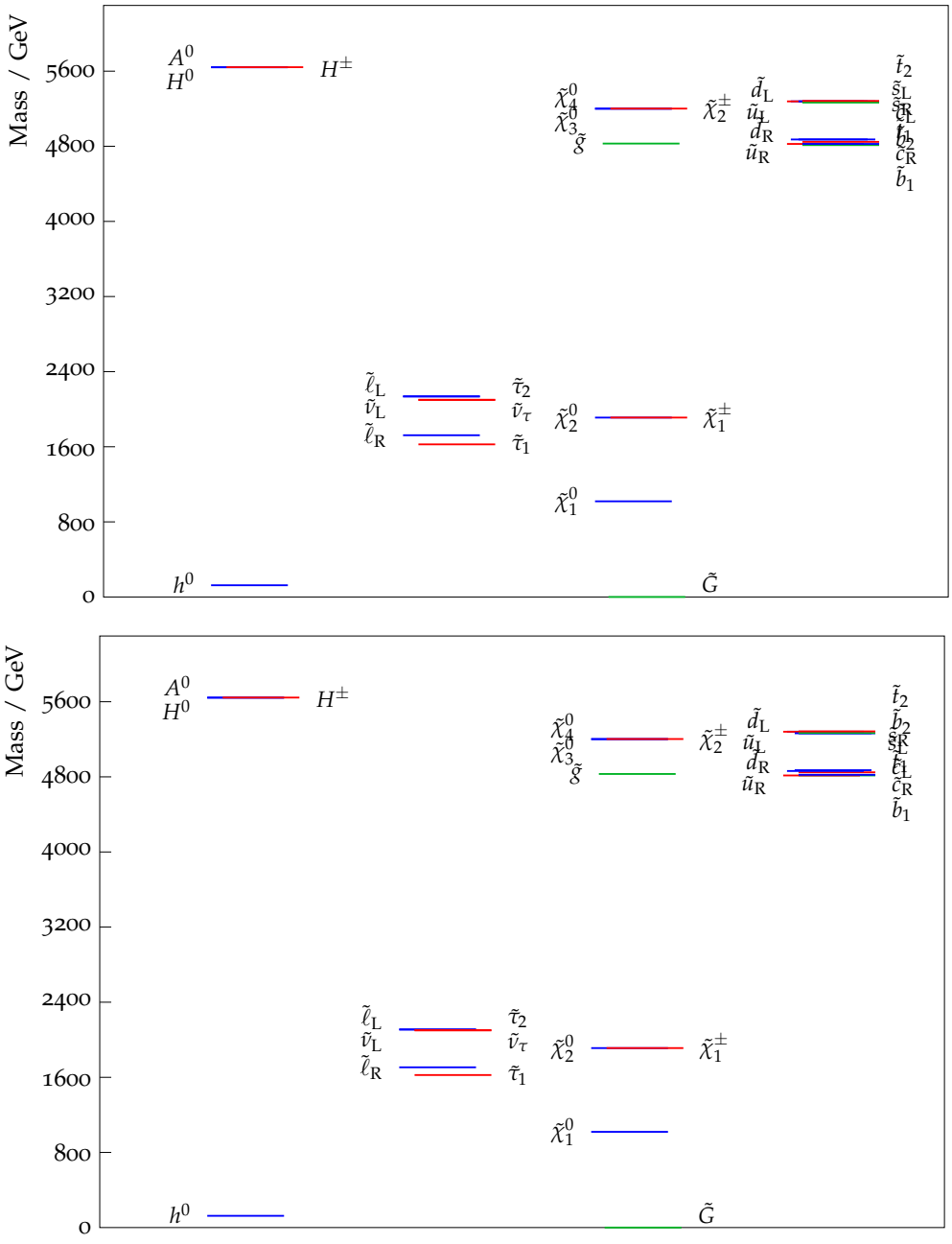

Figure 4.2: Mass spectra for $M_{\text{Mess}} = 1 \times 10^{12}$ GeV (both), $\tan\beta = 10$ and $\beta_\epsilon = 0.01$ (top) and $\beta_\epsilon = 0.05$ (bottom). In each case, Λ is fixed by the Higgs mass constraint.

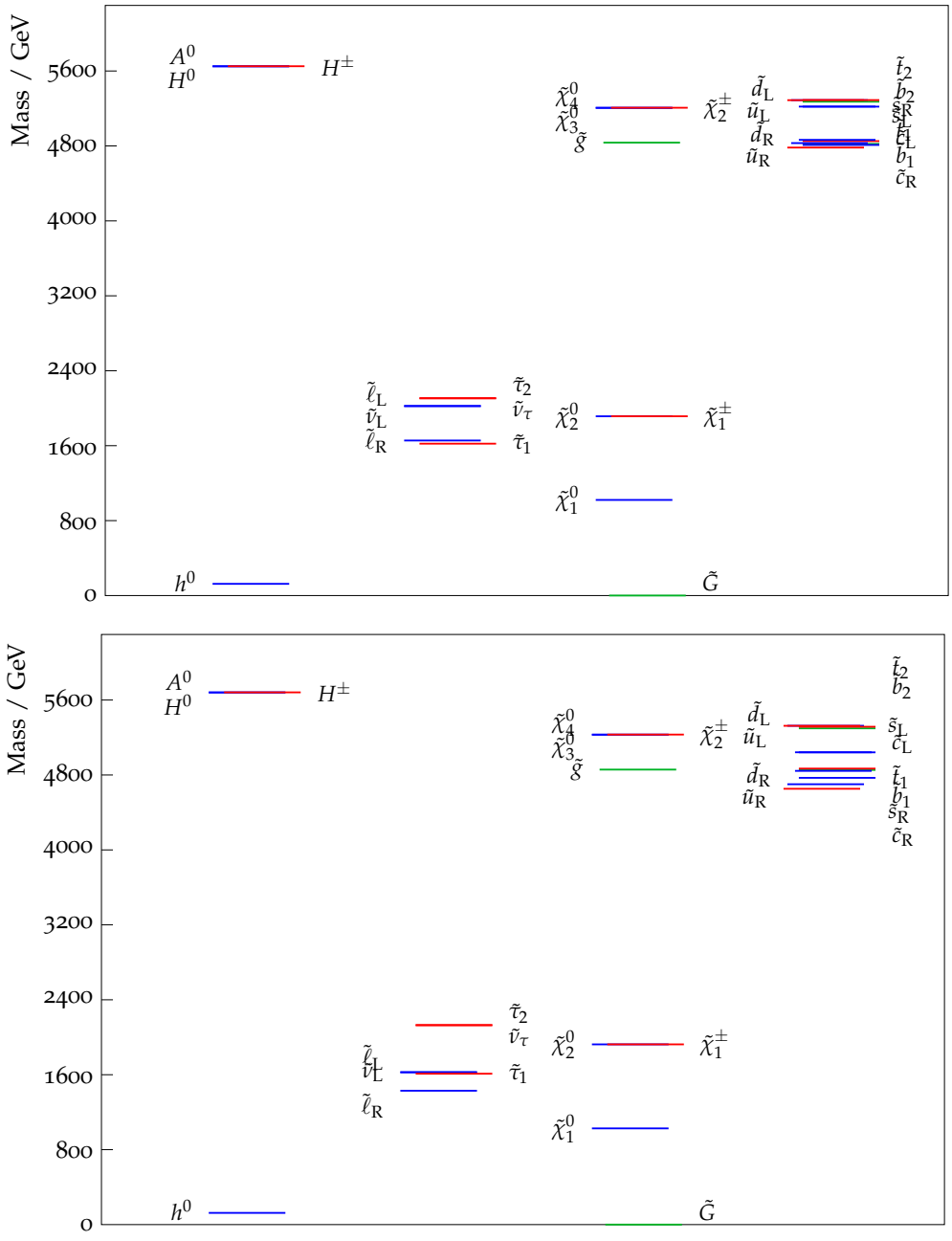

Figure 4.3: Mass spectra for $M_{\text{Mess}} = 1 \times 10^{12}$ GeV (both), $\tan\beta = 10$ and $\beta_\epsilon = 0.1$ (top) and $\beta_\epsilon = 0.2$ (top). In each case, Λ is fixed by the Higgs mass constraint.

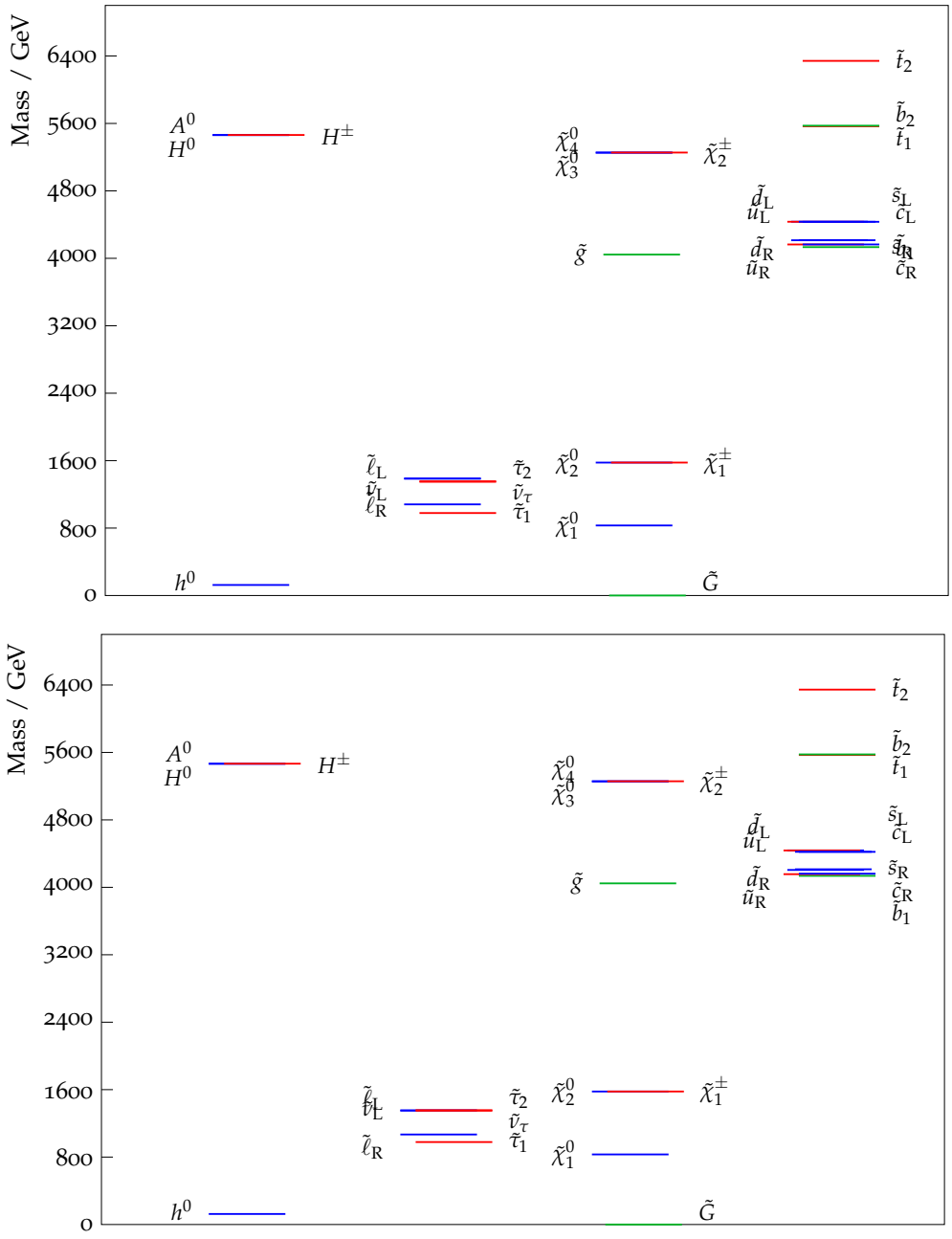

Figure 4.4: Mass spectra for $M_{\text{Mess}} = 1 \times 10^6$ GeV (both), $\tan\beta = 10$ and $\beta_\epsilon = 0.01$ (top) and $\beta_\epsilon = 0.05$ (bottom). In each case, Λ is fixed by the Higgs mass constraint.

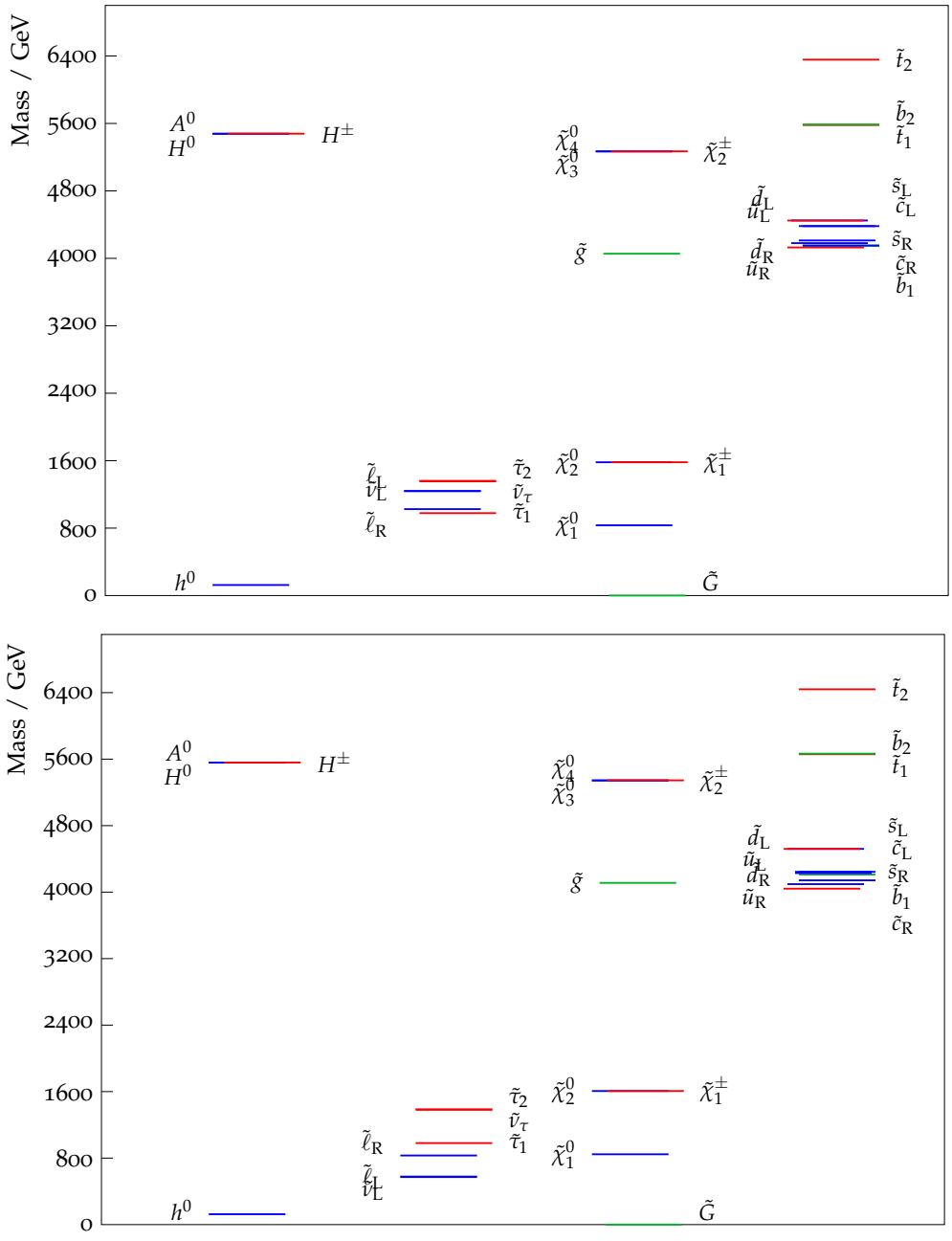

Figure 4.5: Mass spectra for $M_{\text{Mess}} = 1 \times 10^6$ GeV (both), $\tan\beta = 10$ and $\beta_\epsilon = 0.1$ (top) and $\beta_\epsilon = 0.2$ (bottom). In each case, Λ is fixed by the Higgs mass constraint.

second generation squarks along with the other sbottom. The NSLP in this scenario is a bino-like neutralino.

The bottom of Figure 4.4 shows the spectrum for $\beta_\epsilon = 0.05$. Much like Figure 4.2, the increase in β_ϵ pushes the masses of the right-handed sdown and sup down, as well as the lightest left-handed charged slepton and sneutrino. The lightest squark continues to be a sbottom, but one can see the splitting amongst the masses of the lighter squarks begin to take shape. If now turn to the top of Figure 4.5, where $\beta_\epsilon = 0.1$, we see that the the general behavior as seen in the previous three spectra for $M_{\text{Mess}} = 1 \times 10^6$ GeV continues. What is new, however, is that the lightest squark is now a right-handed sup, much like was the case for the messenger scale $M_{\text{Mess}} = 1 \times 10^{12}$ GeV. We see that the lighter squark masses continue to split. Lastly, the bottom of Figure 4.5 exhibits new behavior as compared to the spectra for a higher messenger mass. For example, the NSLP is left-handed slepton, as opposed to a neutralino.

It is instructive to investigate the behavior of this model over a wider range of Λ and messenger mass. In Figures 4.6 and 4.7, we plot the predicted Higgs mass (solid contours), lightest slepton mass (dotted contours) and right-handed sup mass as Λ and M_{Mess} are varied. We do this for four different values of β_ϵ. We see that for a phenemonologically viable point of parameter space (i.e $m_H = 125$ GeV), the mass of the lightest slepton decreases. Eventually, there are points in $(\Lambda, M_{\text{Mess}})$ parameter space that both provide a viable Higgs mass, and predict a slepton NLSP of less than 1 TeV.

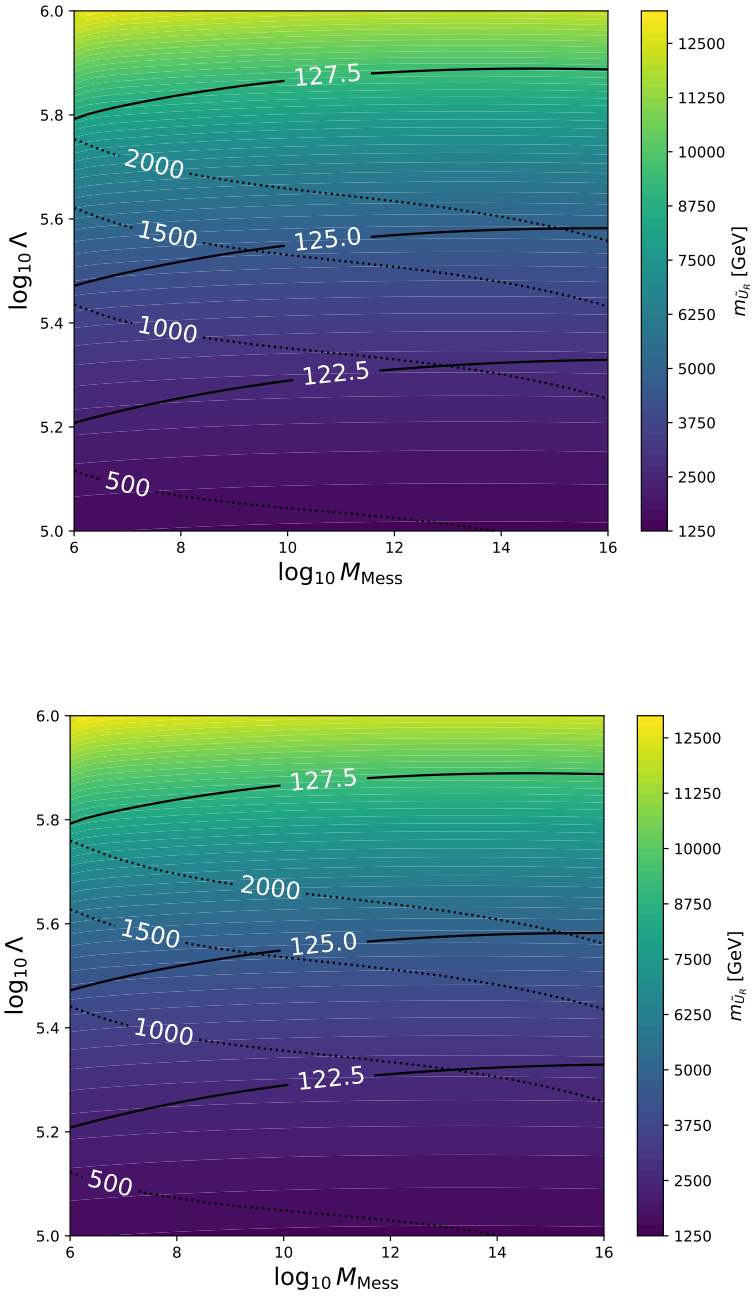

Figure 4.6: The Higgs mass (solid contours), right-handed sup mass (color shading) and right-handed selectron masses (dotted contours) in this scenario with $\beta_\epsilon = 0$ (top) and $\beta_\epsilon = 0.05$ (bottom).

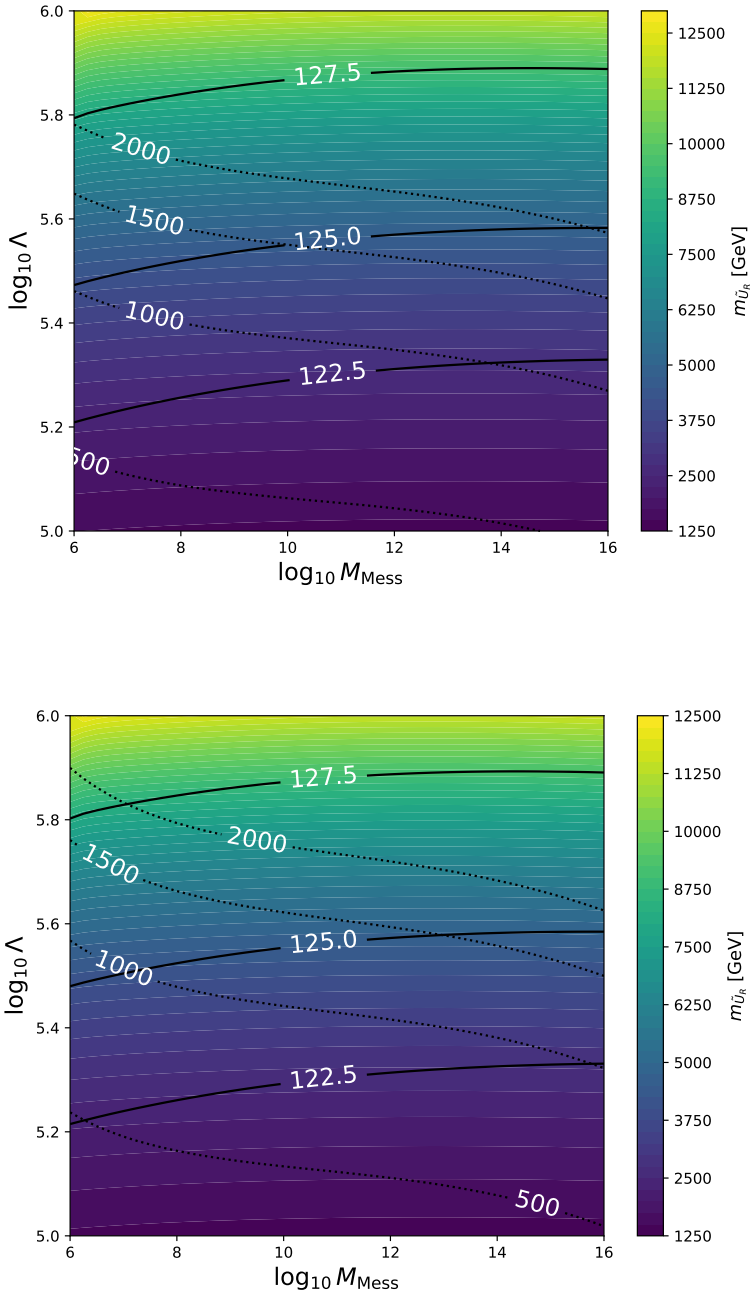

Figure 4.7: The Higgs mass (solid contours), right-handed sup mass (color shading) and right-handed selectron masses (dotted contours) in this scenario with $\beta_\epsilon = 0.1$ (top) and $\beta_\epsilon = 0.2$ (bottom).

4.5 Conclusions

In this chapter, as the next step in a broader program of exploring the phenomenological implications of a specific flavored gauge mediation framework in which discrete non-Abelian symmetries govern the Higgs-messenger mixing, we have investigated the generation of fermion masses and quark mixing angles within a three-family scenario. The discrete non-Abelian symmetry group is chosen to be $\mathcal{S}_3$, and one hypothesis of this line of exploration is that this symmetry group also provides a framework for a partial family symmetry. This scenario requires the introduction of two messenger doublets that mix with the electroweak Higgs doublets via the $\mathcal{S}_3$ symmetry, rendering it an effective $N = 2$ gauge mediation model with messenger Yukawa corrections. The phenemenology of this scenario in the case that only MSSM Yukawa couplings at the renormalizable level were included, and only the third generation SM fermions had nonzero masses, was investigated in [149] and [151].

We build on those previous analyses with the introduction of a higher-dimensional operator perturbation of the superpotential couplings, which generates a hierarchically smaller mass for the second generation SM fermions, and leaves the first generation massless. In this chapter, we showed that with a judicious choice of this operator, mixing among the first and second generation can result, and a Cabibbo angle of an appropriate size was able to be generated. While the scenario generically results in the possibility of flavor-violating couplings, we show that in a specific limiting case of the model parameters, the resulting messenger Yukawas in the diagonal quark mass basis yield flavor-diagonal corrections to the soft supersymmetry parameters, resulting in a scenario with few input parameters. We see in this context that the superparticle spectra are at most $4 - 6$ TeV, with the distribution of sparticle masses within this range being affected by the strength of the higher-dimensional operator.

Part 2 Conclusion

In Part 2, we introduced one of the most robust and well-explored BSM theories: supersymmetry. We focused on constructing a specific implementation of flavored gauge mediated supersymmetry breaking wherein the Higgs-messenger mixing is governed by the discrete non-Abelian group $\mathcal{S}_3$. In this model, we also embeded the Standard Model matter fields in representations of the same non-Abelian discrete group as a first step in combining supersymmetry and flavor symmetry breaking.

We first explored the phenemenology of this scenario in the case that only MSSM Yukawa couplings at the renormalizable level were included, and that only the third generation SM fermions had nonzero masses. This occurred at the enhanced symmetry point where the singlet β_4 term dominated. As one may think of our $\mathcal{S}_3$ symmetry group as being the remnant of a larger symmetry, it is reasonable to posit that terms related to this symmetry breaking are suppressed. However, the subleading $\mathcal{S}_3$ structure is important, as we saw with the introduction of a non-renormalizable operator.

We found that sizable stop mixing is achieved due to the one-loop trilinear terms arising from the messenger-matter interactions. This arose without introducing significant off-diagonal flavor mixing. In much of the parameter space, we found that the superpartner masses are at most $5 - 6$ TeV, with gluinos around $4 - 5$ TeV.

We then extended this theory with the introduction of a non-renormalizable perturbation of the superpotential which allowed us to generate smaller second generation fermion masses. We were also able to show that the introduction of this operator allowed for the generation of appropriately sized Cabbibo mixing.

As before, we obtained superparticle spectra that are at most $4 - 6$ TeV, with the distribution of sparticle masses within this range being determined by the strength of the higher-dimensional operator. Importantly, this model was generically open to further flavor structure.

Part 3: Neutrinos, Discrete Symmetries and Sum Rules

Chapter 5

Neutrino Masses and Mixings

5.1 Evidence of Neutrino Masses and Mixings

In the original formulation of the Standard Model, neutrinos are massless. This is because the Standard Model only contains left-handed neutrinos, and without a right-handed partner neutrinos cannot acquire mass via renormalizable operators. For years, experimental observations – while still in tension with Standard Model predictions – had not definitively shown that neutrinos were massive. Nevertheless, even before the Standard Model was formulated, there was experimental evidence that neutrinos behaved in ways that may be inconsistent with the behavior of massless particles.

Beginning with the Homestake experiment of Davis and Bahcall [54], the past 60 years have brought an accumulation of more and more precise experimental evidence that neutrinos oscillate and have mass[55–60]. These experimental observations corroborated earlier theorists who predicted and parameterized neutrino oscillations [176, 177].

Within the Standard Model, neutrinos are defined as the $SU(2)_L$ partners of left-handed charged leptons and are therefore weak interaction eigenstates. For general fermions, this weak eigenbasis is not the same basis as the fermions' free Hamiltonian. In the cases of neutrinos, the Standard Model predicts them to be massless and therefore degenerate. This degeneracy allows the freedom to define the free Hamiltonian eigenstates (i.e. the mass basis) to be the same as the weak interaction basis, and so massless neutrinos would

not oscillate. As neutrino oscillations have been experimentally confirmed, it must be that the neutrino mass eigenstates are non-degenerate.

The neutrinos in the weak basis are related the mass states via a the Maki–Nakagawa–Sakata-Pontecorvo mixing matrix, U_{MNSP}, such that

$$\begin{pmatrix} \nu_e \\ \nu_\mu \\ \nu_\tau \end{pmatrix} = \underbrace{\begin{pmatrix} U_{e1} & U_{e2} & U_{e3} \\ U_{\mu 1} & U_{\mu 2} & U_{\mu 3} \\ U_{\tau 1} & U_{\tau 2} & U_{\tau 3} \end{pmatrix}}_{U_{\text{MNSP}}} \begin{pmatrix} \nu_1 \\ \nu_2 \\ \nu_3 \end{pmatrix}, \tag{5.1}$$

where the left-hand side is the weak interaction basis, and the right is the mass basis. It is usually given the parameterization

$$U_{\text{MNSP}} = \begin{pmatrix} 1 & 0 & 0 \\ 0 & c_{23} & s_{23} \\ 0 & -s_{23} & c_{23} \end{pmatrix} \begin{pmatrix} c_{13} & 0 & s_{13}e^{-i\delta} \\ 0 & 1 & 0 \\ -s_{13}e^{i\delta} & 0 & c_{13} \end{pmatrix} \begin{pmatrix} c_{12} & s_{12} & 0 \\ -s_{12} & c_{12} & 0 \\ 0 & 0 & 0 \end{pmatrix} \begin{pmatrix} 1 & 0 & 0 \\ 0 & e^{i\eta_1/2} & 0 \\ 0 & 0 & 0e^{i\eta_2/2} \end{pmatrix}, \tag{5.2}$$

where $s_{ij} = \sin(\theta_{ij})$, $c_{ij} = \cos(\theta_{ij})$, and the phase matrix at the right is only present if neutrinos are Majorana particles.

The current status of the parameters of U_{MNSP} are given in Table 5.1. Note that the absolute masses of the neutrinos are not yet certain, but mass-squared differences $\Delta m_{ij}^2 = m_i^2 - m_j^2$ have been measured. The exact ordering of the neutrino masses is not known between two possibilities. The first is what is called "normal ordering," in which $m_3^2 \gg m_s^2 \gtrsim m_1^2$, and the other is referred to as "inverted ordering," where $m_2^2 \gtrsim m_1^2 \gg m_3^2$. At this point, it appears normal ordering is slightly preferred by the data at 2.7σ [179].

It is crucial to note that the behavior of U_{MNSP} and V_{CKM} differ greatly. As we have seen, V_{CKM} is close to diagonal, with cross-generation transitions suppressed. This is not the case for U_{MNSP}, as two mixing angles θ_{12} and θ_{23} are close to maximal and θ_{13} is small but definitively nonzero. We therefore must approach neutrino mass models in a completely different way than for quarks.

Neutrino Mixing Parameter	Normal Ordering	Inverted Ordering
s^2_{12}	$0.304^{+0.013}_{-0.012}$	$0.304^{+0.013}_{-0.012}$
s^2_{23}	$0.570^{+0.018}_{-0.024}$	$0.575^{+0.017}_{-0.021}$
s^2_{13}	$0.02221^{+0.00068}_{-0.00062}$	$0.02240^{+0.00062}_{-0.00062}$
$\delta(^\circ)$	195^{+51}_{-25}	286^{+27}_{-32}
Δm^2_{21}	$7.42^{+0.21}_{-0.20} \times 10^{-5}$ eV^2	$7.42^{+0.21}_{-0.20} \times 10^{-5}$ eV^2
Δm^2_{31}	$2.517^{+0.026}_{-0.028} \times 10^{-3}$ eV^2	–
Δm^2_{32}	–	$-2.498^{+0.028}_{-0.028} \times 10^{-3}$ eV^2

Table 5.1: The current global fits for oscillation parameters from experimental data as reported in the July 2020 global fit of the NuFit collaboration [178, 179]. Note that these fits are more recent than those used in Chapter 6, which were current at the time of publication.

5.2 Mass Generation Mechanisms

Firstly, the exact mechanism by which neutrinos acquire mass is unknown. There is nothing precluding the introduction of right-handed neutrinos to form Yukawa terms to generate masses, i.e

$$\mathcal{L}^{\nu}_{\text{Yukuwa}} = -Y^{\nu}_{ij}\overline{L}_i \nu_{Rj}\tilde{H}. \tag{5.3}$$

However, as the mass of a Dirac fermion is proportional to the Higgs VEV, $v = 246$ GeV, the Yukawa coupling Y^{ν}_{ij} in Eq. 5.3 would have to be highly suppressed to accommodate the observed sub-eV masses of neutrinos. This parametric suppression is obtainable, but it may be desirable to have that neutrinos acquire masses in a more natural way.

One may instead assume that a neutrino is a Majorana fermion. It is known that a neutral spin-1/2 fermion may be described as a completely real field, indicating that it can be its own anti-particle [180]. Note that a general spin-1/2 field ψ may be represented as $\psi = \psi_L + \psi_R$, where ψ_L is the left-handed component and ψ_R is the right-handed.

This can be seen from the fact that a spin 1/2 Dirac field exists as a $(1/2,0)_L \oplus (0,1/2)_R$ representation of the Lorentz group.

If the neutrino were a Majorana particle, its wave function would be expressable as $\nu = \nu_L + \nu_L^c$, where ν_L^c is the charge conjugation of $\nu_L : \nu_L^c = \mathcal{C}\bar{\nu_L}^T$ explicitly. It can be shown that ν_L^c exists in the $(0,1/2)_R$ of the Lorentz group, and as such $\nu = \nu_L + \nu_L^c$ transforms as a spin 1/2 Dirac field. This field is its own charge-conjugate, $\nu^c = \nu$ and has half the degrees of freedom as a Dirac field. This loss of two degrees of freedom has a significant consequence on U_{MNSP}. Much like V_{CKM}, U_{MNSP} is a three-by-three unitary matrix, and therefore can be parameterized by three mixing angles and six phases. While the quark fields admitted arbitrary rephasings whereby five of the phases in V_{CKM} could be absorbed, only three phases can be can absorbed in U_{MNSP} in the case of Majorana neutrinos, hence the last matrix to the right in Eq. 5.2

Looking at one generation for now, one may then build a Majorana mass term,

$$-\mathcal{L}_{m_{\text{Majorana}}} = \frac{m}{2}\left(\bar{\nu}_L \mathcal{C}\bar{\nu}_L^T - \nu_L^T \mathcal{C}^\dagger \nu_L\right), \tag{5.4}$$

but it should be noted that this term cannot be produced via a standard Yukawa coupling, or any renormalizable operator containing existing Standard Model fields, and is in itself not valid before electroweak symmetry breaking.

Therefore, the minimal operator consistent with the Standard Model leading to Eq. 5.4 is the five dimensional Weinberg operator [181]. Schematically, this operator is

$$-\mathcal{L}_{\text{Weinberg}} = \frac{y}{\Lambda}\left(\overline{L}\tilde{H}\right)\left(L^c\tilde{H}\right), \tag{5.5}$$

After electroweak symmetry, the operator in Eq. 5.5 becomes the operator in Eq. 5.4, with

$$-\mathcal{L}_{m_{\text{Majorana}}} = \frac{yv^2}{2\Lambda}\left(\bar{\nu}_L \mathcal{C}\bar{\nu}_L^T - \nu_L^T \mathcal{C}^\dagger \nu_L\right), \tag{5.6}$$

giving ν_L a mass of yv^2/Λ. Note that this construction leads a naturally small neutrino masses. Of course this is an effective operator, and as such it must descend from a higher-energy process.

If we introduce three additional Majorana neutrinos, but instead make them right-handed, the operator

$$-\mathcal{L}_{M_{\text{Majorana}}} = \frac{M_{ij}}{2}\left(\bar{\nu}_{Ri}\mathcal{C}\bar{\nu}^T_{Rj} - \nu^T_{Ri}\mathcal{C}^\dagger\nu_{Rj}\right), \tag{5.7}$$

is no longer forbidden. We let us now reconsider the Yukawa term

$$\mathcal{L}^\nu_{\text{Yukuwa}} = -Y^\nu_{ij}\overline{L}_i\nu_{Rj}\tilde{H} + \text{h.c}, \tag{5.8}$$

where we allow Y^ν to be the same relative order as the other fermions. Both of these mass terms are allowable in the Standard Model, even above the weak scale. These interactions allow for the tree-level diagram in Figure 5.1. If one takes the right-handed fields very

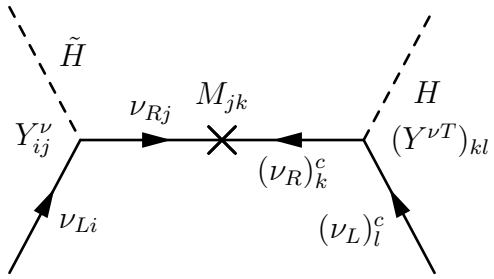

Figure 5.1: A tree-level implementation of a type-I seesaw mechanism.

heavy, they may be integrated out of the diagram to give an effective operator

$$\mathcal{L}_{\text{Effective}} = -Y^{\nu T}M^{-1}Y^\nu(\bar{L}\tilde{H})(L^c\tilde{H}). \tag{5.9}$$

After electroweak symmetry breaking, this generates Eq. 5.4 for ν_L, with mass matrix $(-Y^{\nu T}M^{-1}Y^\nu)_{ij}v^2$. The eigenvalues of this matrix will be very small, as M is large. This mechanism by which heavy neutrinos leads to light Standard Model neutrinos is called the "seesaw mechanism" [182, 183]. The process in Figure 5.1 is known as a type-I seesaw, but other seesaw expansions of the Weinberg operator are known [184]. Of course, the seesaw mechanism isn't the only method of mass generation, and models using supersymmetry, extra dimensions, string theory or modular forms are also actively considered [185, 186].

5.3 Flavor Symmetries

Nevertheless, even with a mechanism of mass generation, the introduction of neutrino masses adds an additional six unconstrained parameters onto the existing 19 of the Standard Model. As the form of U_{MNSP} is qualitatively different than that of V_{CKM}, a different paradigm of flavor symmetry is needed.

Since U_{MNSP} has two large mixing angles and a single small one, the sorts of symmetries behooving neutrino flavors models may be discrete[1]. U_{MNSP} being so far from a diagonal form indicates that neutrino flavor symmetries must be "sharp,"" i.e not a smooth deformation away from diagonal.

The paradigm we shall use is to assume that the neutrino and charged lepton mass matrices have discrete non-Abelian flavor symmetries that are broken differently, leading to a nontrivial U_{MNSP}. There are numerous models, such as: tribimaximal (TBM) mixing[187–191], where $s^2_{12} = 1/3$, $s^2_{23} = 1/2$ $s_{13} = 0$, predicted by embedding fields into representations of the tetrahedral group; bimaximal (BM) mixing[192–196], where $\sin^2(2\theta_{12})\sin^2(2\theta_{23}) = 1$; the two golden ratio mixing schemes, GR1 [197–200] and GR2 [201, 202], where the mixing angles relate to the golden ratio $\phi = 1/2(1+\sqrt{5})$ and are governed by an icosahedral symmetry; or hexagonal (HEX) [203] mixing, governed by $D_{12,}$ the symmetry group of the hexagon. For a review on the use of discrete non-Abelian symmetries in model-building theories of neutrino masses and mixings, see [204].

5.3.1 A_4 Tribimaximal Mixing

As a concrete example, let us briefly describe one possible construction of a tribimaximal mixing scenario with tetrahedral symmetry following the work in [205]. It is important to note that tribimaximal mixing is an *ansatz*, and therefore the construction that follows is only one specific implementation of arriving at tribimaximal mixing.

[1] Despite Part 2 detailing a model of quark flavor built on a discrete symmetry, the usual paradigm for the quarks is to perturbatively introduce off-diagonal elements using a continuous symmetry.

Consider the discrete group A_4, the alternating group on four elements, or equivalently the group of isometries of the tetrahedron. It admits four irreducible representations, $\mathbf{1}$, $\mathbf{1}'$, $\mathbf{1}''$, and $\mathbf{3}$. Much like we did for the MSSM fields in Part 2, we will charge the lepton sector under the assignments listed in Table 5.2.

	L_i	e^c_{L1}	e^c_{L2}	e^c_{L3}	Φ_i	ξ_1	ξ_2	ξ_3	$\xi_{i=4,5,6}$
A_4	$\mathbf{3}$	$\mathbf{1}$	$\mathbf{1}'$	$\mathbf{1}''$	$\mathbf{3}$	$\mathbf{1}$	$\mathbf{1}'$	$\mathbf{1}''$	$\mathbf{3}$

Table 5.2: The A_4 charges for the leptonic and extended Higgs sector.

L_i are the three usual lepton doublets, e^c_{Li} are the left-handed conjugates of the charged lepton singlets, Φ_i are three Higgs doublets and χ_i are six Higgs triplets. We will not write down the resulting Lagrangian or scalar potential and dynamics, which are detailed in [206, 207]. After electroweak symmetry breaking, the resulting charged lepton mass matrix is

$$M_l = v \begin{pmatrix} h_1 & h_2 & h_3 \\ h_1 & h_2\omega & h_3\omega^2 \\ h_1 & h_2\omega^2 & h_3\omega \end{pmatrix}, \tag{5.10}$$

where $\omega = e^{2\pi i/3}$ and $v = \langle \Phi^0_1 \rangle = \langle \Phi^0_2 \rangle = \langle \Phi^0_3 \rangle$.

The neutrino mass matrix is generated by the small VEVs of the heavy Higgs triplets, producing the mass matrix

$$M_\nu = \begin{pmatrix} a+b+c & 0 & 0 \\ 0 & a+\omega b+\omega^2 c & d \\ 0 & d & a+\omega^2 b+\omega c \end{pmatrix}, \tag{5.11}$$

where a, b, c, and d are the VEVs of the neutral components of $\xi_{i=1,2,3,4}$ respectively, and $\langle \xi^0_5 \rangle = \langle \xi^0_6 \rangle$. The lepton mass matrix M_l may be diagonalized by

$$U_L = \frac{1}{\sqrt{3}} \begin{pmatrix} 1 & 1 & 1 \\ 1 & \omega & \omega^2 \\ 1 & \omega^2 & \omega \end{pmatrix}, \tag{5.12}$$

and therefore, in the charged lepton basis, the mass matrix for the neutrinos becomes

$$M_\nu^L = U_L^T M_\nu U_L^* = \begin{pmatrix} a+\frac{2d}{3} & b-\frac{d}{3} & c-\frac{d}{3} \\ b-\frac{d}{3} & c+\frac{2d}{3} & a-\frac{d}{3} \\ c-\frac{d}{3} & a-\frac{d}{3} & b+\frac{2d}{3} \end{pmatrix}. \tag{5.13}$$

It is this matrix M_ν^L that is diagonalized by U_{MNSP}. If one considers a scenario in which $b = c$, such as a model with a Z_2 $\nu_\mu - \nu_\tau$ symmetry, one finds that the resulting U_{MNSP} is the tribimaximal mixing matrix,

$$U_{\text{MNSP}}^{(\text{TBM})} = \begin{pmatrix} \sqrt{\frac{2}{3}} & \frac{1}{\sqrt{3}} & 0 \\ -\frac{1}{\sqrt{6}} & \frac{1}{\sqrt{3}} & -\frac{1}{\sqrt{2}} \\ -\frac{1}{\sqrt{6}} & \frac{1}{\sqrt{3}} & \frac{1}{\sqrt{2}} \end{pmatrix} \tag{5.14}$$

i.e. where $s_{12}^2 = 1/3$, $s_{23}^2 = 1/2$ and $s_{13} = 0$.

5.3.2 Sum Rules

Of course, the tribimaximal and other mixing scenarios mentioned are ruled out by current experimental data, and as such the paradigm is to allow for charged lepton corrections to U_{MNSP}. The procedure is to then enforce relations between these charged lepton corrections, the experimentally fit mixing angles and phase, and the predictions for the neutrino mass matrix given a particular symmetry. These relations are called sum rules, and they can be split into two types, atmospheric sum rules[204, 208–216] and solar sum rules [217–220]. The sum rules paradigm has a long history, beginning with [221–225] and continuing until today [226–249].

Sum rules enforce relations between the observed global fits and the internal model parameters describing the neutrino family symmetry and charged lepton corrections. In the next chapter, we will take the observed global fits as inputs and use sum rules to predict the most likely value for the CP-violating Dirac phase in U_{MNSP}.

Chapter 6

Predictions for the Leptonic Dirac CP-Violating Phase[1]

6.1 Introduction

The confirmation of a non-zero and sizable reactor mixing angle[58–60] has opened the window to detecting CP violation in the lepton sector through the direct measurement of the Dirac CP-violating phase δ of the Maki-Nakagawa-Sakata-Pontecorvo (MNSP) lepton mixing matrix, U_{MNSP}[176, 177]; see also the PDG review [53]. There are already experimental hints that its value may exist around $\delta \sim \pm\pi/2$ from the T2K [251] and NOνA [252] collaborations. Additionally, input from recent global fits favor $\delta \sim -\pi/2$ at 3σ[253–256]. In either case, the impending confirmation of the value of this CP-violating phase forces physicists to revisit theories of its possible origin which can explain its measured value, as well as all of the other measured values of the lepton mixing angles contained in U_{MNSP}. The arguably most popular approach to address the origin the lepton mixing parameters of U_{MNSP} is with the implementation of a discrete flavor symmetry. In this framework, a given mixing pattern is related to residual symmetries of the leptonic mass matrices which may arise from the spontaneous breaking of the flavor symmetry group. Such models that utilize a spontaneously broken discrete flavor symmetry usually predict a zero leading order reactor mixing angle and a maximal atmospheric mixing angle due to

[1] Chapter adapted from [250]

their popularity before the aforementioned measurement of a nonzero reactor mixing angle. Furthermore, they are usually constructed in a basis where the charged lepton mass matrix is diagonal. Due to these assumptions, these flavor models generally produce a leading order neutrino mixing matrix U_ν described by tribimaximal (TBM) mixing[187–191], bimaximal (BM) mixing[192–196], the two golden ratio mixing schemes (GR1 [197–200] and GR2 [201, 202]), or hexagonal (HEX) [203] mixing. Perhaps the simplest way to accommodate a nonzero reactor mixing angle while still using these popular starting points is to introduce a nontrivial lepton mixing matrix which can rotate $U_{\mathsf{MNSP}} = U_e^\dagger U_\nu$ away from its "problematic" leading order predictions.

The emergence of a third nonzero mixing angle in U_{MNSP} gives rise to the appearance of the Dirac CP-violating phase originating in the charged lepton mixing matrix U_e (when assuming a particular form for U_ν as described above). Together with the initial fixed starting point dictated by U_ν, e.g., tribimaximal or GR1 mixing, and an assumed form of U_e, it is possible to explore the predictions for the Dirac CP-violating phase δ which have mixing angles consistent with the measured experimental data. The simplest of such assumed forms for U_e is just a single rotation in the $1-2$ or $1-3$ planes.[2] The corrections to the reactor mixing angle as well as the other parameters lead to relations (called sum rules) between model parameters contained in U_e, the leading order angle predictions in U_ν, and the experimentally measured angles in U_{MNSP}. One way to characterize the mixing angle predictions resulting from these sum rules has been to classify them into two types: atmospheric sum rules[204, 208–216] and solar sum rules [217–220]. While atmospheric sum rules arise from a variety of scenarios, e.g., semi-direct models, solar sum rules are characteristic of models in which the leading order U_ν matrix is corrected by charged lepton contributions. The idea of correcting the leading order neutrino sector mixing angles by such charged lepton effects has been developed in [221–225]. Recent literature on such sum rules also includes [226–238], as well as the related work of [239–249].

[2] A single rotation in the $2-3$ plane will not generate a correction to the (zero) reactor mixing angle.

For example, for a set of such models that involve a $1-2$ charged lepton rotation, there is a well-known sum rule for $\cos\delta$ [226] (see also [222–225, 229, 230, 244]):

$$\cos\delta = \frac{t_{23}s_{12}^2 + s_{13}^2 c_{12}^2/t_{23} - (s_{12}^{\nu})^2(t_{23} + s_{13}^2/t_{23})}{s'_{12}s_{13}}, \tag{6.1}$$

in which $c_{ij} = \cos\theta_{ij}$, $s_{ij} = \sin\theta_{ij}$, $t_{ij} = \tan\theta_{ij}$, and we have used primed letters to represent the corresponding trigonometric functions of twice the argument, e.g., $s'_{ij} = \sin(2\theta_{ij})$.

As has been discussed extensively in the literature, the form of this sum rule (and the analogous sum rule for models with a $1-3$ charged lepton rotation) is quite striking in that it depends on just one model parameter, $(s_{12}^{\nu})^2$, and functions of the three observable mixing angles. This in turn has led to numerous studies of the posterior probability density function of $\cos\delta$ for a given $(s_{12}^{\nu})^2$, using the results of global fit data for the distributions of the lepton mixing angles as inputs. These results can provide guidance as to the precision needed in the determination of δ at current and forthcoming neutrino experiments to provide some degree of discriminating power in the theory space of possible models of lepton mixing.

In this chapter, we examine the predicted probability distribution for $\cos\delta$ in models that satisfy Eq. (6.1), using a different (complementary) approach. Here we focus for simplicity on models that involve a single $1-2$ charged lepton rotation; the models under consideration have three continuously varying, bounded input parameters, including a single source of CP violation. We assume no non-standard interactions, such that the effects of additional field content such as flavons and other exotics are encoded by the given model parameters. This allows for a phenomenological analysis of a specific class of models that satisfy the sum rule for $\cos\delta$ given in Eq. (6.1). The predicted ranges of the observable mixing angles within this class of models are restricted since there is a small number of model parameters, and the model parameters are theoretically bounded. Hence, not all observable mixing angles in these theories are independent. The theoretical model class-induced relationship among these parameters encode the needed constraints

from the unitarity of the lepton mixing matrix to ensure that $\cos\delta$ is appropriately bounded (*i.e.*, that δ is indeed a physical CP-violating parameter), in all cases.[3]

Our goal is to explore the implications of these theoretical constraints among the observables within this class of models, and their implications for the distribution of theoretically allowed values of $\cos\delta$, depending on assumptions regarding the distributions of the input parameters. With the important assumption that these models can provide a correct description of the observable lepton mixing parameters, we investigate the implications of two specific assumptions regarding the probability distributions of the model parameters, and their resulting implications for the distributions of the physical observables. After first exploring the situation in which all model parameters are assumed to have independent distributions, we then consider conditional probability distributions involving the input parameters that best reproduce the results for s^2_{13}, s^2_{23}, and s^2_{12} from global fit data in this class of models. In both situations, we examine the resulting prediction for the probability distribution of $\cos\delta$ that can be obtained within this class of models.

In our analysis, we use the results from neutrino oscillation experiments as reported in the July 2019 global fit of the NuFit collaboration [253, 254] and summarized in Table 6.1[4]. Indeed, we will see that the great precision that has been achieved in the measurement of s^2_{13} greatly simplifies the analysis and provides nontrivial constraints on the feasibility of this set of models in predicting distributions for the remaining mixing parameters that are in reasonably good agreement with the data.

This chapter is structured as follows. In Section 6.2, we provide an overview of the class of models under consideration. In Section 6.3.1, we consider the implications of the assumption that the model parameters have independent distributions, and describe the resulting predictions for the probability distributions of the observable mixing parameters. Next, we instead assume that the probability distributions of the model parameters

[3]This includes for example the case of bimaximal mixing scenarios, which are known to be particularly constrained in terms of their ability to reproduce the preferred values of the lepton mixing angles as deduced from global fit data.

[4]These fits were updated again in July 2020 after this work was completed.

	3σ range **NO**	3σ range **IO**
s^2_{12}	$0.275 - 0.350$	$0.275 - 0.350$
s^2_{23}	$0.427 - 0.609$	$0.430 - 0.612$
s^2_{13}	$0.02046 - 0.02440$	$0.02066 - 0.02461$

Table 6.1: The lepton mixing angles for the case of normal ordering (NO) and inverted ordering (IO) used in this chapter, as taken from the July 2019 global fit of [253, 254].

are conditional probability distributions, in Section 6.3.2, as this allows for a greater optimization of the match of the model predictions to the experimental observables.

6.2 Background

We consider a class of theoretical models in which the starting point is the assumption that the matrix that diagonalizes the neutrino mass matrix is of the form $U_\nu = R_{23}(\theta^\nu_{23})R_{12}(\theta^\nu_{12})$, where the R_{ij} matrices are given by

$$R^\nu_{23} = \begin{pmatrix} 1 & 0 & 0 \\ 0 & c^\nu_{23} & s^\nu_{23} \\ 0 & -s^\nu_{23} & c^\nu_{23} \end{pmatrix}, \quad R^\nu_{12} = \begin{pmatrix} c^\nu_{12} & s^\nu_{12} & 0 \\ -s^\nu_{12} & c^\nu_{12} & 0 \\ 0 & 0 & 1 \end{pmatrix}, \tag{6.2}$$

and it is assumed that to leading order, the charged lepton mass matrix is diagonal in family space. As a result, at leading order s^2_{23} and s^2_{12} are nonzero, while s^2_{13} is zero. The required shift to the reactor angle arises from corrections to the charged lepton sector, which here are encoded by a diagonalization matrix of the left-handed charged leptons in the $1 - 2$ plane.

More precisely, the charged lepton diagonalization matrix is assumed to be of the form $U_e = U^e_{12}$, in which the U^e_{ij} are defined as

$$U^e_{23} = \begin{pmatrix} 1 & 0 & 0 \\ 0 & c^e_{23} & s^e_{23}e^{-i\delta^e_{23}} \\ 0 & -s^e_{23}e^{i\delta^e_{23}} & c^e_{23} \end{pmatrix}, \quad U^e_{12} = \begin{pmatrix} c^e_{12} & s^e_{12}e^{-i\delta^e_{12}} & 0 \\ -s^e_{12}e^{i\delta^e_{12}} & c^e_{12} & 0 \\ 0 & 0 & 1 \end{pmatrix}, \quad U^e_{13} = \begin{pmatrix} c^e_{13} & 0 & s^e_{13}e^{-i\delta^e_{13}} \\ 0 & 1 & 0 \\ -s^e_{13}e^{i\delta^e_{13}} & 0 & c^e_{13} \end{pmatrix}, \tag{6.3}$$

in which $s^e_{ij} = \sin\theta^e_{ij}$ and $c^e_{ij} = \cos\theta^e_{ij}$.[5] Therefore, in models considered here, we have

$$U_{\text{MNSP}} \equiv U = U_e^\dagger U_\nu = U^{e\dagger}_{12} R^\nu_{23} R^\nu_{12}. \tag{6.4}$$

From this form of the lepton mixing matrix, the observable mixing angles take the form

$$\begin{aligned} s^2_{13} &= (s^e_{12})^2 (s^\nu_{23})^2, \qquad s^2_{23} = \frac{(s^\nu_{23})^2 - (s^e_{12})^2 (s^\nu_{23})^2}{1 - (s^e_{12})^2 (s^\nu_{23})^2}, \\ s^2_{12} &= \frac{(c^\nu_{12})^2 (c^\nu_{23})^2 (s^e_{12})^2 + (c^e_{12})^2 (s^\nu_{12})^2 - 2 c^e_{12} c^\nu_{12} c^\nu_{23} s^e_{12} s^\nu_{12} \cos\delta^e_{12}}{1 - (s^e_{12})^2 (s^\nu_{23})^2}, \end{aligned} \tag{6.5}$$

and the value of $\cos\delta$ is given by Eq. (6.1), subject to the constraints of Eqs. (6.5).

Let us now briefly comment on the model parameters, which we can take to be the following set: $(s^e_{12})^2$, $(s^\nu_{23})^2$, $(s^\nu_{12})^2$, and $\cos\delta^e_{12}$. Within such models, the "bare" atmospheric neutrino mixing angle θ^ν_{23} is often taken (or predicted) to be maximal, *i.e.*, that $(s^\nu_{23})^2 = 1/2$. In this work, we will not fix this parameter to its maximal value, but rather let it float. This class of models can then be taken to be equivalent to the class of models with two rotations in the charged lepton sector, of the form $U_e = U^e_{23}(\theta^e_{23}, \delta^e_{23}) U^e_{12}(\theta^e_{12}, \delta^e_{12})$, with the phase $\delta^e_{23} = 0$.

One of the defining features of the class of models considered here is that there is a single CP-violating phase, δ^e_{12}, that sources the Dirac phase δ. As we will see, this feature

[5] Note that there is an an intrinsic degeneracy in these definitions as $\delta'^e_{ij} \to \delta^e_{ij} - \pi$ and $\theta'^e_{ij} \to \theta^e_{ij} - \pi/2$ yield the same rotation matrix. This will be taken into account in our analysis.

yields a tight connection between the allowed values of s^2_{12} and $\cos\delta$, which would clearly relax in situations with multiple CP-violating phases. We defer the analysis of scenarios with multiple phases to future work.

While the parameters $(s^e_{12})^2$, $(s^\nu_{23})^2$, and $\cos\delta^e_{12}$ are continuous parameters, here we will follow the usual protocol in the literature and consider only particular discrete values of $(s^\nu_{12})^2$. The values taken all correspond to values that can be achieved in specific models based on non-Abelian discrete family symmetries. As previously mentioned, these values correspond to the cases of bimaximal mixing (BM), tribimaximal mixing (TBM), hexagonal mixing (HEX), and two scenarios based on golden ratio mixing (GR1), (GR2). The models considered here thus have three continuous model parameters, and are broadly categorized by their specific value of $(s^\nu_{12})^2$, as given in Table 6.2.

	BM	TBM	HEX	GR1	GR2
$(s^\nu_{12})^2$	$1/2$	$1/3$	$1/4$	$(5-\sqrt{5})/10$	$(5-\sqrt{5})/8$

Table 6.2: The values of $(s^\nu_{12})^2$ for the theoretical scenarios under consideration.

It is useful to simplify the notation. We begin with a relabeling of the model parameters, for the sake of brevity:

$$a \equiv \left(s^e_{12}\right)^2, \qquad b \equiv \left(s^\nu_{23}\right)^2, \qquad c \equiv \cos\delta^e_{12}. \tag{6.6}$$

We also relabel the observable mixing angles s^2_{13}, s^2_{23}, and s^2_{12} as x, y, and z, respectively. Finally, we define $z_0 \equiv (s^\nu_{12})^2$, as this quantity is the "bare" value of $s^2_{12} \equiv z$. In terms of the model parameters, we can rewrite the observable mixing angles as

$$\begin{aligned} x &\equiv s^2_{13} = ab \\ y &\equiv s^2_{23} = \frac{(1-a)b}{1-ab} \\ z &\equiv s^2_{12} = z_0 - \frac{2c\sqrt{a(1-a)(1-b)z_0(1-z_0)}}{1-ab} + \frac{a(1-b)(1-2z_0)}{1-ab}. \end{aligned} \tag{6.7}$$

We save the discussion of the sum rules for $\cos\delta$ in terms of these parameters for later, as it is a straightforward but rather cumbersome expression that follows from Eq. (6.1) and Eq. (6.7).

From this starting point, we now consider the possibilities for the probability distributions for the model parameters a, b, and c, with the goal of predicting distributions for the observables x, y, and z in alignment with the global fit data of [253, 254], and determining the resulting probability distribution for $\cos\delta$. An immediate simplification results from the fact that the reactor angle has been measured with great precision. As such, we can assume to leading order that the distribution for $x \equiv s^2_{13}$ can be effectively modeled as a delta function, fixed about its central value of $(s^2_{13})_0 \equiv x_0 = 0.02241$ [253, 254][6], as follows:

$$P_x(x) = \delta(x - x_0). \tag{6.8}$$

As we will see, this assumption significantly simplifies the analysis of the next sections.

6.3 Predicting $P(\cos\delta)$

6.3.1 Independent Probability Distribution

Within a top-down model, it is plausible to imagine that the continuous model parameters a, b, and c are independent. That is to say that the probability distribution for each continuous model parameter should depend exclusively on that parameter; for example, $P_a = P_a(a)$. With this simple assumption, we can then determine the theoretical probability distributions for each model parameter, as guided by attempting to optimize the agreement with the theoretically predicted distributions of the observable mixing parameters with their experimental distributions, and with the assumption that such a theory can reproduce experimentally allowed results. Once the distributions for the model parameters have been determined based on the experimental inputs for the leptonic mixing angles, it is then possible to characterize the predicted distribution for the cosine of the Dirac CP-violating phase, $\cos\delta$.

[6] Here we take the central value of s^2_{13} for the case of normal ordering, for concreteness.

This assumption, as opposed to the assumption of conditional probabilities among the parameters (which will be discussed in the next section), will quite generally lead to stringent restrictions on the theory, and furthermore can result in the possibility that it is impossible to reproduce the experimental distribution for one or more of the observed mixing parameters. Indeed, we will see in this section that in the set of scenarios considered here, and with this assumption, it is generally not possible to obtain the characteristic Gaussian distribution for $y \equiv s^2_{23}$ with the full experimentally allowed range. Instead, we will see that what results is a much sharper distribution (that becomes a delta function distribution in the limit that the distribution for $x \equiv s^2_{13}$ is taken to be a delta function). This reflects the fact that in this scenario, the same two model parameters predict two observables, one of which (s^2_{13}) is very precisely determined by experimental data, and hence, either the choice of these parameters will lead to physically reasonable results or the model will explicitly fail.

To see this more precisely, we begin with the quantity x, which depends on the continuous model parameters a and b. We assume that each of these model parameters is distributed with an unknown univariate probability density function. It then follows that the probability of measuring a specific value of x should be determined by the total probability of attaining values of a and b such that $x = ab$. Concretely, for $P_x(x)$, one has

$$P_x(x) = \int da\, db\, \delta(ab - x) P_a(a) P_b(b). \tag{6.9}$$

Analogously, we can write

$$P_y(y) = \int da\, db\, \delta(h(a,b) - y) P_a(a) P_b(b), \tag{6.10}$$

with $h(a,b) = (1-a)b/(1-ab)$. $P_z(z)$ takes the form

$$P_z(z) = \int da\, db\, dc\, \delta(f(x(a,b),b,c) - z) P_a(a) P_b(b) P_c(c), \tag{6.11}$$

in which (see the third sum rule in Eq. (6.7)):

$$f(a,b,c) = z_0 - \frac{2c\sqrt{a(1-a)(1-b)z_0(1-z_0)}}{1-ab} + \frac{a(1-b)(1-2z_0)}{1-ab}. \tag{6.12}$$

P_x, P_y, and P_z are each normalized to unity, as P_a, P_b and P_c are each normalized to unity.

To parameterize $P_a(a)$, $P_b(b)$, and $P_c(c)$, we take the simplifying assumption that $P_x(x)$ is well approximated by a delta function. Therefore, to first approximation, $P_a(a)$ and $P_b(b)$ should be delta functions as well, otherwise a smooth distribution for $P_x(x)$ is obtained. Explicitly, we parameterize the two independent distributions $P_a(a)$ and $P_b(b)$ as follows:

$$P_a(a) = A(a)\delta(a - a_1), \qquad P_b(b) = B(b)\delta(b - b_1), \tag{6.13}$$

where $A(a)$ and $B(b)$ are smooth functions that satisfy $A(a_1) = B(b_1) = 1$. Carrying out Eq. (6.9) explicitly, it is straightforward to obtain the expected identification that $x_0 = a_1 b_1$. Similarly, evaluating Eq. (6.10) leads to the identification that

$$P_y(y) = \delta(y - y_0), \tag{6.14}$$

in which

$$y_0 = \frac{b_1(1 - a_1)}{1 - a_1 b_1} = \frac{b_1 - x_0}{1 - x_0}. \tag{6.15}$$

As discussed, with independent distributions for the model parameters a and b, the requirement that the distribution for $x = s^2_{13}$ is a delta function to a good approximation results in a similarly sharp predicted distribution for $y = s^2_{23}$, in contrast to what is currently allowed from the global fits. This is not surprising given that for fixed $x \equiv s^2_{13}$, $y \equiv s^2_{23}$ is also fixed. Once the parameters a and b are allowed to have conditional probability distributions, the distribution for s^2_{23} can better match the currently allowed distribution from global fit data, as we will see explicitly in the next section.

Let us turn now to the expression for $P_z(z)$, as in Eq. (6.11). After doing the integrations in a and b,

$$P_z(z) = \left(\frac{1 - a_1 b_1}{2\sqrt{a_1(1 - a_1)(1 - b_1)z_0(1 - z_0)}}\right) P_c\left(\frac{-(z - z_0)(1 - a_1 b_1) + a_1(1 - b_1)(1 - 2z_0)}{2\sqrt{a_1(1 - a_1)(1 - b_1)(1 - z_0)z_0}}\right). \tag{6.16}$$

where z_0 is defined in Eq. (6.12).

Let us now return to the sum rules for $\cos\delta$, recalling that we can rewrite Eq. (6.1) as

$$\cos\delta = \frac{\sqrt{a(1-a)(1-b)}(1-2z_0) - c(1-2a+ab)\sqrt{z_0(1-z_0)}}{\sqrt{a(1-a)(1-b) + (1-2a+ab)^2 z_0(1-z_0) - 2c\gamma_{ab}(1-2a+ab)(1-2z_0) - 4c^2\gamma_{ab}^2}}, \tag{6.17}$$

where $\gamma_{ab} = \sqrt{a(1-a)(1-b)z_0(1-z_0)}$. Thus, $P_{\cos\delta}$ can be written as

$$P_{\cos\delta} = \int da\, db\, dc\, \delta(g(a,b,c) - \cos\delta) P_a(a) P_b(b) P_c(c). \tag{6.18}$$

Simplifying this expression requires a proper treatment of the roots of the delta function. Upon doing so, it is straightforward to see that $P_{\cos\delta}(\cos\delta)$ takes the form

$$P_{\cos\delta}(\cos\delta) = \left(\left|\frac{dg}{dc}\right|_{c_+}\right)^{-1} P_c(c_+)\Theta(\cos\delta) + \left(\left|\frac{dg}{dc}\right|_{c_-}\right)^{-1} P_c(c_-)\Theta(-\cos\delta), \tag{6.19}$$

in which

$$\begin{aligned} c_\pm = \frac{1}{D}\Big[&(x_0y_0 - x_0 + y_0)\left(1-c_\delta^2\right)(n-2)\sqrt{x_0\left(y_0 - y_0^2\right)} \\ &\pm |c_\delta|\,(x_0y_0 - x_0 - y_0)\sqrt{(n-1)\left(x_0 + y_0 - x_0y_0\right)^2 + \left(c_\delta^2 - 1\right)(1-y_0)\, n^2 x_0 y_0}\Big], \end{aligned} \tag{6.20}$$

with

$$D = \sqrt{n-1}\left[x_0^2\left(y_0-1\right)^2 - 2x_0y_0\left(1-2c_\delta^2\right)(1-y_0) + y_0^2,\right] \tag{6.21}$$

and $n \equiv 1/z_0$ and $c_\delta \equiv \cos\delta$ have been defined for convenience.

To obtain an *ansatz* for $P_c(c)$, we express Eq. (6.7) in terms of x_0, y_0 and $n = 1/z_0$:

$$\begin{aligned} z &= z_0 - 2c\frac{\sqrt{x_0y_0z_0(1-y_0)(1-z_0)}}{y_0(1-x_0)+x_0} + \frac{x_0(1-y_0)(1-2z_0)}{y_0(1-x_0)+x_0} \\ &= \frac{1}{n} - 2c\frac{\sqrt{n-1}}{n}\left(\frac{\sqrt{x_0y_0(1-y_0)}}{y_0(1-x_0)+x_0}\right) + \frac{n-2}{n}\left(\frac{x_0(1-y_0)}{y_0(1-x_0)+x_0}\right). \end{aligned} \tag{6.22}$$

Due to the trivial requirement that $|c| \leq 1$, the allowed bounds for z do not lie at 0 and 1, but within a subset of that interval, which is determined by the specific values of x_0, y_0, and n. The bounds for z with x_0 and y_0 at their central values are given in Table 6.3. From

	BM	TBM	HEX	GR1	GR2
$z \in$	$[0.375, 0.625]$	$[0.221, 0.457]$	$[0.231, 0.469]$	$[0.149, 0.367]$	$[0.173, 0.397]$

Table 6.3: Theoretically allowed ranges for z for various mixing scenarios, with x_0 and y_0 and their central best-fit values.

Table 6.1, the 3σ **NO** range for z is $[0.275, 0.350]$. The allowed ranges for z in tribimaximal, hexagonal, GR1 and GR2 mixing cover this 3σ bound completely, but the allowed range for bimaximal mixing lies outside of this range, as is well known in the literature. Hence, as seen in Eq. (6.22), the value of c needed to to push z as close as possible to the best-fit range is $c = 1$.

These bounds inform our choice for $P_z(z)$, inasmuch as $P_z(z)$ should vanish for values of z outside of the above theoretical bounds. Thus, we assume the following form of $P_z(z)$ for each mixing pattern:

$$P_{z:pat} = \mathcal{K} P_z^{(exp)}(z) | z \in [z_{min}, z_{max}], \tag{6.23}$$

where $P_z^{(exp)}(z)$ is a Gaussian centered around the best-fit value of z, and where $\mathcal{K}$ is an appropriate normalization factor.[7] We note that $P_c(c)$ can be neatly expressed as

$$P_c(c) = \frac{1}{\mathcal{A}} P_z(z(c)), \tag{6.24}$$

where

$$\mathcal{A} = \frac{n}{2\sqrt{n-1}} \sqrt{\frac{y_0}{x_0(1-y_0)}} \left(1 + \frac{x_0(1-y_0)}{y_0}\right).$$

A plot of $P_c(c)$ for each mixing pattern is given in Figure 6.1. We also plot Eq. (6.19), as shown in Figure 6.2. As expected, all mixing patterns other than bimaximal peak well away from unphysical values of $\cos\delta$. The bimaximal mixing pattern has $\cos\delta$ peaked at $\cos\delta = -1$, which is expected, as one expects $c = 1$ to be the most likely value in this mixing pattern. This reflects the well-known result the bimaximal mixing pattern in this

[7] We can make alternative choices for this distribution, as discussed in the Appendix. Here we will restrict ourselves to the standard normal distribution for simplicity, whereas in the next section where the goal is to optimize the overlap with the experimental results, we will consider more refined alternatives.

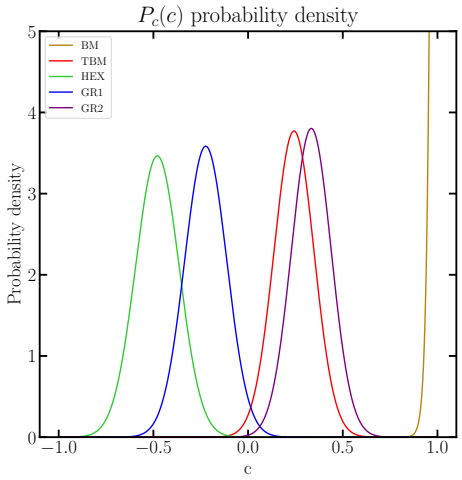

Figure 6.1: A comparison of $P_c(c)$ for various mixing patterns, in the situation that $P_z(z)$ can be represented by a simple Gaussian with parameters given by the empirical best-fit values. As expected, the peak of $P_c(c)$ for bimaximal mixing occurs at $c = 1$, as the value of z must be pushed down significantly to fit into the 3σ best fit bounds.

set of models quite generally is highly constrained. Note that by construction, the full range of possible physical values for $\cos\delta$ is covered, with no possibility that the posterior probability distribution $P_{\cos\delta}(\cos\delta)$ has nontrivial values for values of $\cos\delta$ outside of the physical range.

6.3.2 Conditional Probability Distributions

We now assume that the probability distributions for the model parameters are conditional probability distributions. Indeed, there may be top-down theories in which this is the case (for example, if the parameter values must dynamically satisfy a given constraint, or if there are fixed points). As stated, we remain agnostic in this work as to the details of the theoretical model that gives rise to the lepton mixing matrix of the form of Eq. (6.4).

As before we assume here that the distribution of x is of the form given in Eq. (6.8), such that

$$x = ab = x_0 \quad \Rightarrow \quad a = \frac{x_0}{b} \quad \text{or} \quad b = \frac{x_0}{a}. \tag{6.25}$$

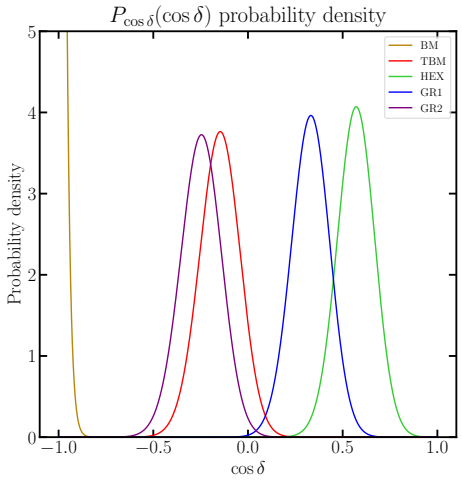

Figure 6.2: $P_{\cos\delta}$ as a function of $\cos\delta$ for various mixing patterns. Here we have assumed that $P_z(z)$ is a Gaussian centered at the experimental best-fit value of z, with width of 1σ.

Clearly, a and b are correlated through x_0. Define

$$P_{a|b}(a) = \delta\left(a - \frac{x_0}{b}\right) \quad \text{and} \quad P_{b|a}(b) = \delta\left(b - \frac{x_0}{a}\right), \tag{6.26}$$

where $P_{x|y}(x)$ is the conditional probability of x given y.

It then follows from Eq. (6.7) that

$$P_y(y) = \int da\, db\, \delta\left(\frac{b-ab}{1-ab} - y\right) P_{a|b}(a) P_b(b) = (1-x_0) P_b(y + x_0(1-y)), \tag{6.27}$$

which leads to

$$P_b(b) = \frac{1}{1-x_0} P_y\left(\frac{b-x_0}{1-x_0}\right). \tag{6.28}$$

and analogously

$$P_a(a) = \frac{x_0}{a^2(1-x_0)} P_y\left(\frac{x_0(1-a)}{a(1-x_0)}\right). \tag{6.29}$$

This differs significantly from the previous approach, wherein $P_y(y)$, $P_a(a)$ and $P_b(b)$ are necessarily delta functions (c.f. Eq. (6.13) and Eq. (6.14)).

6.3.2.1 Estimating $P_z(z)$

As the integral for $P_z(z)$ depends on the distributions of all three model parameters a, b and c, it must be that two of the parameter distributions are conditioned on the third. For now, let us assume that b is independent of c and $P_{b|c}(b) = P_b(b)$ as given in Eq. (6.28).

Therefore, the expression for $P_z(z)$ is

$$P_z(z) = \int da\, db\, dc\, \delta(f - z)\, P_{a|b}(a) P_b(b) P_c(c), \tag{6.30}$$

where f is given in Eq. (6.12). Integrating over a, we find that

$$P_z(z) = \int db\, \frac{b(1 - x_0)}{2\sqrt{(1 - b)(b - x_0)(1 - z_0)x_0 z_0}}\, P_b(b) P_c(c_0(b, z)), \tag{6.31}$$

where

$$c_0(b, z) = \frac{b(x_0 - 1)(z - z_0) + x_0(1 - b)(1 - 2z_0)}{2\sqrt{x_0 z_0(1 - b)(b - x_0)(-z_0 + 1)}}. \tag{6.32}$$

As before, we do not know the form of $P_c(c)$, and as such must consider various *ansatzes* for its functional behavior.

What we shall do is to assume that $P_c(c)$ takes the form of either a normal or modified Gaussian distribution. These various distributions are introduced and discussed in Appendix B. Specifically, we consider $P_c(c)$ as either a normal, skew normal, or Gram-Charlier distribution. Since these distributions have respectively two, three or four free parameters, we must determine a way to fix them.

This will be done as follows: for each type of distribution in Appendix B, we shall evaluate the integral in Eq. (6.31) for the central value of z, the $\pm 1\sigma$ values, the $\pm 3\sigma$ values and the points halfway between $\pm 1\sigma$ and $\pm 3\sigma$. Then we optimize the distribution parameters by minimizing the difference between the actual and estimated $P_z(z)$, weighted by global fit values of P_z.

The optimized parameters for each neutrino mixing pattern for each density function given in Eqs. (B.1)-(B.3) are listed in Table 6.4.

	P_{Gauss} (μ, σ)	P_{skew} (μ, σ, s)	P_{CG} (μ, σ, s, k)
TBM	$(0.233,\ 0.0981)$	$(0.233,\ 0.0982,\ 0.0106)$	$(0.228,\ 0.0974,\ -0.0894,\ -0.0885)$
GR1	$(-0.213,\ 0.101)$	$(-0.214,\ 0.101,\ 0.0142)$	$(-0.214,\ 0.10,\ -0.0235,\ -0.0792)$
GR2	$(0.324,\ 0.0966)$	$(0.323,\ 0.0966,\ 0.0102)$	$(0.317,\ 0.0956,\ -0.106,\ -0.121)$
HEX	$(-0.440,\ 0.10)$	$(-0.441,\ 0.10,\ 0.0145)$	$(-0.439,\ 0.0982,\ 0.0290,\ -0.199)$

Table 6.4: Best parameter values for each probability density function to work as $P_c(c_0(b,z))$ in the integral of Eq. (6.31) by neutrino mixing pattern.

We find that using a skew normal distribution is redundant in estimating $P_z(z)$ since $s \approx 10^{-2}$, and as such its use offers minimal improvement over the use of a Gaussian. Conversely, the Gram-Charlier distribution requires nontrivial values for the skewness, s, for tribimaximal and GR2, and for the kurtosis, k, in GR2 and hexagonal mixing scenarios. Once the distribution parameters are determined, we compare the calculated $P_z(z)$ for each mixing pattern and distribution type to the globally fit $P_z(z)$.

We find that the Gram-Charlier distribution is most accurate, and as such will use it to calculate $P_c(c)$ for non-bimaximal mixing in the next subsection.

6.3.3 Estimating $P_{\cos\delta}(\cos\delta)$

With this *ansatz* for $P_c(c)$, we now calculate $P_{\cos\delta}(\cos\delta)$:

$$P_{\cos\delta}(\cos\delta) = \int da\, db\, dc\, \delta(\tilde{g} - \cos\delta) P_{a|b}(a) P_b(b) P_c(c), \tag{6.33}$$

where similarly to $P_z(z)$, it was assumed that $P_{b|c}(b) = P_b(b)$, $P_b(b)$ is given by Eq. (6.28) and $\tilde{g}$ is

$$\tilde{g} = \frac{(b - x_0)z + x_0(1-z)(1-b) - z_0 b(1-x_0)}{2\sqrt{z x_0 (1-z)(1-b)(b-x_0)}}, \tag{6.34}$$

where it is important to recall that z is still a function of b and c.

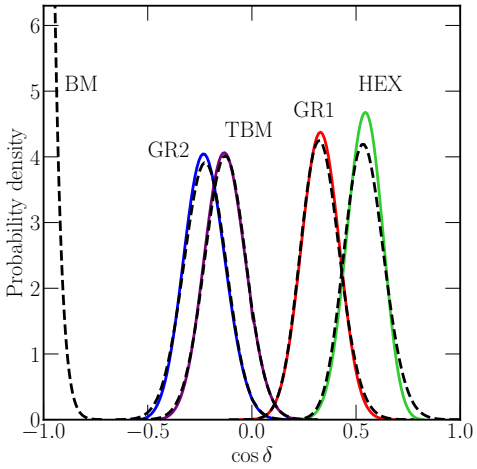

Figure 6.3: Probability densities for $\cos\delta$ from the integral in Eq. (6.35) are shown in color. The dashed black lines were obtained from the integral in Eq. (6.42).

Upon performing the integrations over a and b using Eq. (6.26), we obtain

$$P_{\cos\delta}(\cos\delta) = \int_{\mathcal{C}} dc \left(\frac{\partial\tilde{g}}{\partial b}\right)^{-1} P_b(b) P_c(c). \tag{6.35}$$

Note that this is an integral over the level curve $\mathcal{C}$ given by $\mathcal{C} = \{(b,c) : \tilde{g}(b,c) = \cos\delta\}$. That is to say we evaluate the integral in Eq. (6.35) in such a way that b along the curve $\mathcal{C}$ assumes values such that $\tilde{g}$ is constant and equal to $\cos\delta$.

The probability density functions for $\cos\delta$ obtained via this integration procedure are given by the colored lines in Figure 6.3.

6.3.4 Extending to Bimaximal Mixing

Up until now, we have omitted the application of this procedure to bimaximal mixing. The reason for this is that, as bimaximal mixing is highly disfavored by experiment. Nevertheless, we generalize our procedure in such a way that bimaximal mixing can be accommodated demonstrate that this procedure is valid for even edge cases.

As demonstrated on the left of Figure 6.4, it is impossible to consistently set y and z to their experimental central values simultaneously within the range of valid model parameters.

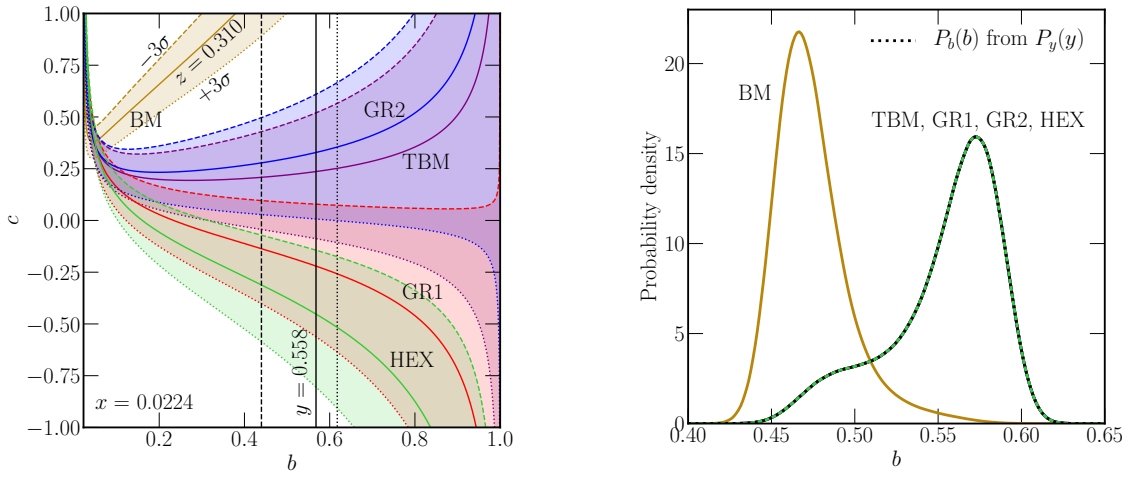

Figure 6.4: Left: Lines for the central (solid), -3σ (dashed) and $+3\sigma$ (dotted) values of z are shown in color for different patterns and in black for y. Right: In color, probability distributions obtained from marginalizing c out of $P_{b,c}(b,c)$ for all the patterns. The dotted black line is the distribution $P_b(b)$ of Eq. (6.28).

What we see, however, is that values of b along a z contour are not independent of c. Previously, we had assumed that $P_{b|c}(b) = P_b(b)$, but let us now relax that constraint consider the two-dimensional joint probability $P_{b,c}(b,c)$, which can be obtained from the two dimensional χ^2 projection for s^2_{12} and s^2_{23} as given in the July 2019 NuFIT global fits[253, 254]. A probability density may be obtained from this χ^2 by normalizing the likelihood function $e^{-\chi^2(y,z)/2}$.

This $P_{y,z}(y,z)$ distribution may be related to $P_{b,c}(b,c)$:

$$\begin{aligned} P_{y,z}(y,z) &= \int db\, dc\, \delta\big(y(b) - y\big)\, \delta\big(z(b,c) - z\big)\, \bar{P}_{b,c}(b,c) \\ &= \frac{(1-x_0)^{3/2}\left[1 + x_0 + y(1-x_0)\right]}{2\sqrt{x_0 y z_0 (1-z_0)\left[1 - x_0 - y(1-x_0)\right]}} \bar{P}_{b,c}\left(x_0 + y(1-x_0), \frac{d_2 + z_0 - z}{d_1}\right), \end{aligned} \tag{6.36}$$

	factor ($\mathcal{N}$)
TBM	$1.0 + \mathcal{O}(10^{-10})$
GR1	$1.0 + \mathcal{O}(10^{-9})$
GR2	$1.0 + \mathcal{O}(10^{-10})$
HEX	$1.0 + 9.67 \times 10^{-6}$
BM	1271.95

Table 6.5: Normalization factors for $\bar{P}_{b,c}(b,c)$, as defined in Eq. (6.40).

where $y(b)$ and $z(b,c)$ are are explicitly written functions of the model parameters. This can be rearranged to give an explicit form for $\bar{P}_{b,c}(b,c)$,

$$\bar{P}_{b,c}(b,c) = \frac{2\sqrt{x_0 z_0 (1-b)(b-x_0)(1-z_0)}}{b\,(1-x_0)^2} P_{y,z}(y(b), z(b,c)), \tag{6.37}$$

where

$$d_1 = 2\frac{\sqrt{(1-b)(b-ab)(1-z_0)abz_0}}{b(1-ab)} \tag{6.38}$$

$$d_2 = \frac{ab(1-b)(1-2z_0)}{b(1-ab)}. \tag{6.39}$$

have been defined for notational convenience.

However, we must be cognizant of the fact that $\bar{P}_{b,c}(b,c)$ cannot be considered a full probability distribution, since vast swathes of the (b,c) parameter space is unobtainable in the case of bimaximal mixing, as shown in Figure 6.4. It is for this reason that we have explicitly written the object in Eq. (6.37) with a bar, as it will not, generally, integrate to unity.

We therefore must normalize this object, which will clearly depend on the specific mixing pattern assumed. As we see in Figure 6.4, it is possible in non-bimaximal mixing patters for the parameters b and c to take on any value in the domain, albeit independently, so we might expect the quantity $\bar{P}_{b,c}(b,c)$ to integrate to 1 in those scenarios. In contradistinction, that will obviously not be possible for bimaximal mixing.

This normalization can be interpreted as a measure of how feasibly certain mixing patterns can match the global fit values of y and z. Denoting the required normalization factor by $\mathcal{N}[\text{pattern}]$ which is defined by the requirement that the object $P_{b,c}(b,c)$,

$$P_{b,c}(b,c) = \mathcal{N}[\text{pattern}] \times \bar{P}_{b,c}(b,c), \tag{6.40}$$

integrates to unity over the (b,c) domain of validity for each mixing pattern. These factors are shown in Table 6.5. Note that for the bimaximal pattern, this factor is larger than 10^3 – indicating that, as expected, bimaximal mixing is largely precluded by the global fits.

The formula for $P_z(z)$ then carries over *mutatis mutandis* from Eq. (6.30) with the replacement $P_{b|c}(b)P_c(c) \to P_{b,c}(b,c)$ as defined above. Upon doing so, we find

$$P_z(z) = \int db \, \frac{b(1-x_0)}{2\sqrt{(1-b)(b-x_0)(1-z_0)x_0 z_0}} \, P_{b,c}(b, c_0(b,z)), \tag{6.41}$$

where $c_0(b,z)$ is given by Eq. (6.32). Similarly, the integration for $\cos\delta$ can be rederived (c.f. Eq (6.35))

$$P_{\cos\delta}(\cos\delta) = \int_{\mathcal{C}} dc \left(\frac{\partial \tilde{g}}{\partial b}\right)^{-1} P_{b,c}(b,c), \tag{6.42}$$

where, as before, the level curve $\mathcal{C}$ is $\mathcal{C} = \{(b,c) : \tilde{g}(b,c) = \cos\delta\}$. The resulting $P_{\cos\delta}(\cos\delta)$ for each mixing patterns is shown in Figure 6.3 using dashed lines.

In Figure 6.3, if we compare the two forms of $P_{\cos\delta}$ as calculated in Eq. (6.35) and Eq. (6.42), we see that the distributions do not change noticeably for the cases of tribimaximal and GR2 mixing, whereas the hexagonal pattern shows a larger spread when using Eq. (6.42).

On the left of Figure 6.5, we note the discrepancy between the estimation of $P_c(c)$ as completed in Section 6.3.2.1 (solid colored lines) and the estimation of $P_c(c)$ obtained by marginalizing b out of $P_{b,c}(b,c)$ (dashed black lines). Recall that in Section 6.3.2.1, we made the assumption that $P_{b|c}(b) = P_b(b)$, so it is not surprising that the inaccuracy of this assumption should affect the resulting estimation of $P_c(c)$.

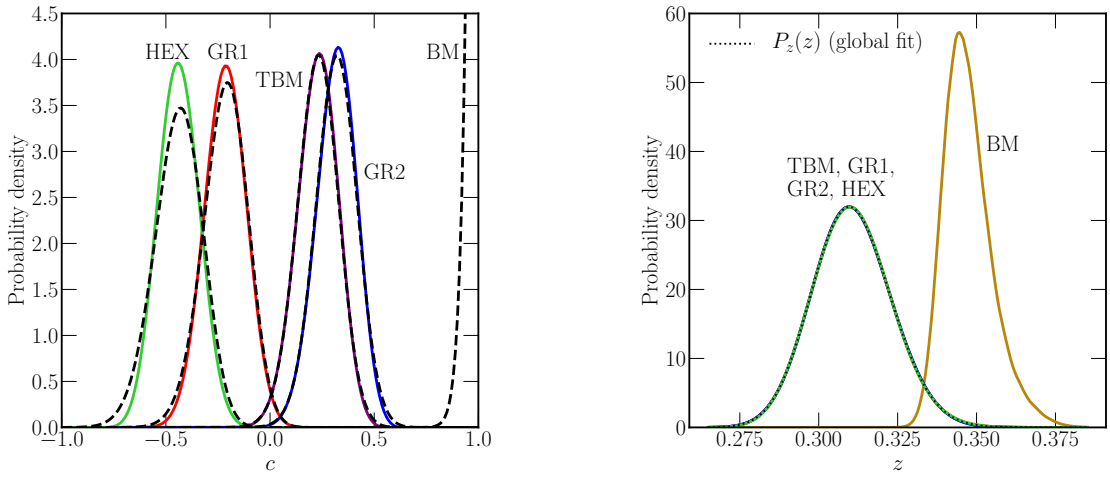

Figure 6.5: Left: colored solid lines for $P_c(c)$ as estimated in Section 6.3.2.1, while dashed black lines are for the distribution obtained by marginalizing c from $P_{b,c}(b, c)$. Right: $P_z(z)$ as obtained from $P_c(c)$. The dotted black line is $P_z(z)$ based on the global fit.

We now reiterate why this procedure was necessary. As is well known, the viable parameter space for bimaximal mixing is significantly smaller than it is for the other mixing patterns considered here, as bimaximal mixing generically predicts values for the solar mixing angle that are quite large, falling on the end of the experimentally allowed region. For instance, inside the domain of allowed values of b and c, the allowed combinations of y and z are far more limited in the bimaximal pattern than for the other patterns, disallowing large swathes of parameter space. This lack of parameter space freedom results in the fact that the step of approximating $P_{b|c}(b)$ by $P_b(b)$, as given by Eq. (6.28), is far more inaccurate for bimaximal mixing than for the other mixing scenarios. Similarly, we see that $P_b(b)$ for bimaximal mixing does not correspond to Eq. (6.28) as well as it does for the other patterns, as can be seen on the right side of Figure 6.4. Lastly, we see that the scenario of bimaximal mixing is completely unable to reproduce the global fit of $P_z(z)$, (Figure 6.5, right side) which indicates the unsuitability of using the process detailed in Section 6.3.2.1, in which $P_c(c)$ is determined by optimizing $P_z(z)$ to match the global fit.

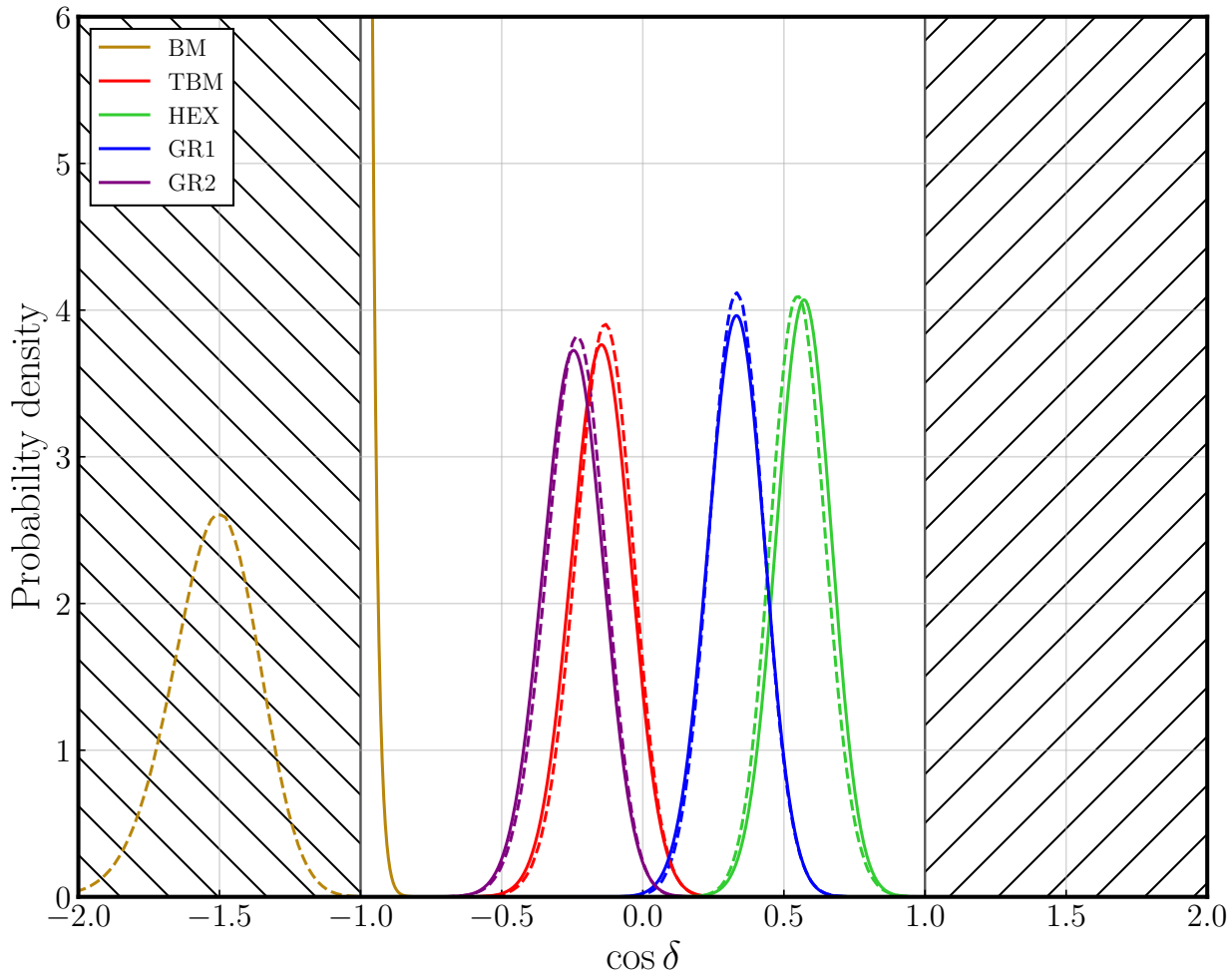

Figure 6.6: The distribution $P_{\cos\delta}(\cos\delta)$ as given in Figure 6.2, overlaid with $P_{\cos\delta}$ as obtained from treating the experimental distributions as uncorrelated (depicted with dashed lines). Note that the difference between the two approaches is slight for mixing patterns other than bimaximal, for which the peak shifts drastically in the two approaches, and resides in an unphysical regime for the case in which the restrictions of the model are not taken into account.

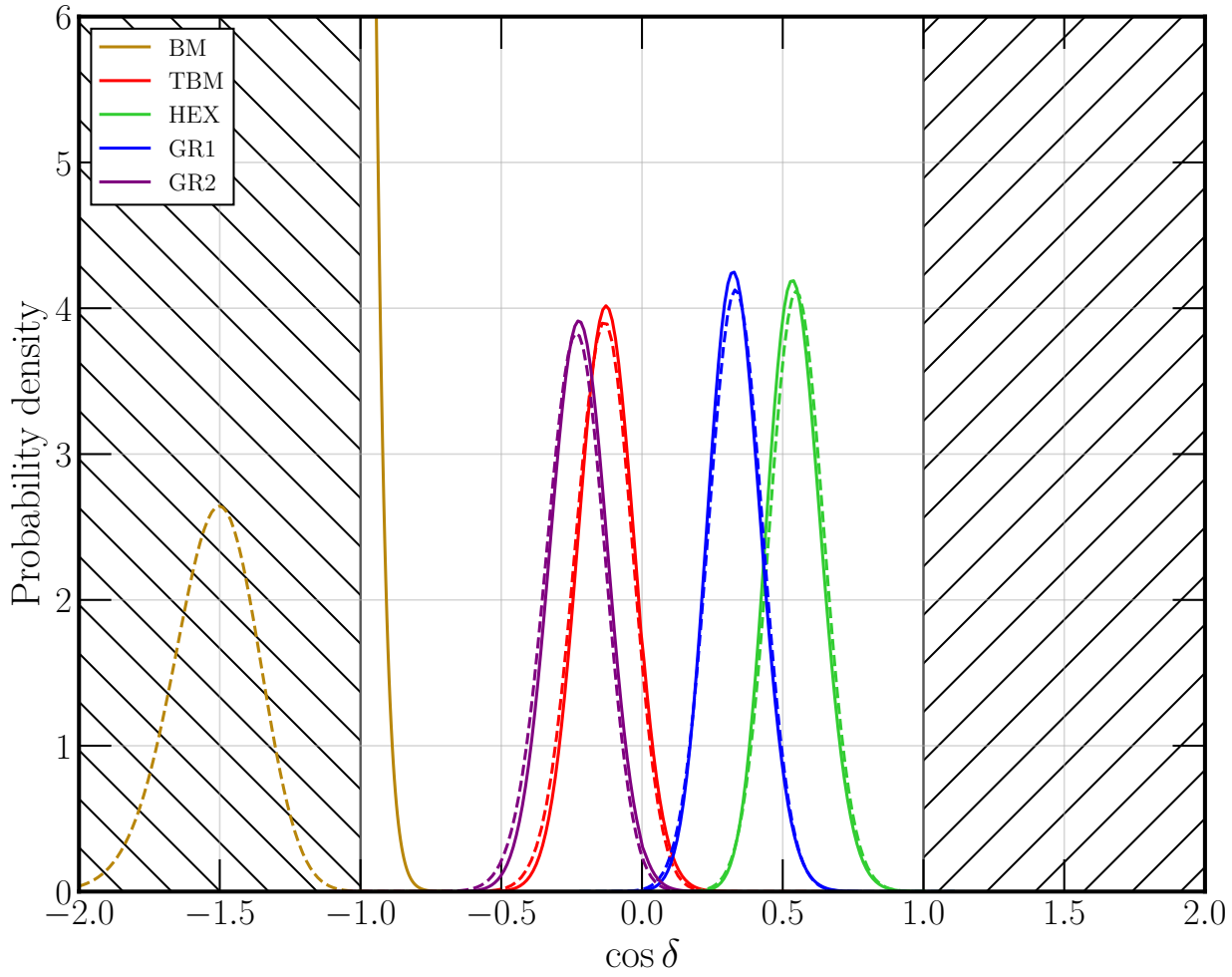

Figure 6.7: The distribution for $P_{\cos\delta}(\cos\delta)$ as given in Figure 6.3, overlaid with $P_{\cos\delta}$ as obtained from treating the experimental distributions as uncorrelated (depicted with dashed lines). This result is to be compared with the analogous result for the independent model parameter approach, as given in Figure 6.6.

Furthermore, we can also see this when comparing the approaches used in this chapter for determing $P_{\cos\delta}$ as compared to approaches taken in previous literature. As previously stated, an assumption that is often made in the literature is that the model can always accommodate all values of the experimentally measured parameters. However, we have seen that in this particular (quite simple) model scenario, the range of z is limited, as is the range of y in the approach of the previous section. As a result, it is instructive to compare these methods for the two approaches discussed in this work.

To this end, in Figure 6.6, we show a comparison of $P_{\cos\delta}$ as calculated in Section 6.3.1, where the model parameters are taken to have independent distributions, to the $P_{\cos\delta}$ as calculated using Eq. (6.1), where each experimental distribution is assumed to be uncorrelated with the others. For purposes of comparison, in both cases the parameter $y = (s^{\nu}_{23})^2$ is taken to be $1/2$, *i.e.*, $|\theta^{\nu}_{23}| = \pi/4$. Clearly, the bimaximal case shows the significant difference in these methods. The shift of the peak to unphysical regions for the case in which the experimental observables are taken to be uncorrelated reflects the well-known fact that the bimaximal pattern has difficulty reproducing the best fit values of the experimental data. Here we also note that the remaining patterns show a very slight shift in the peaks in the distributions for $P_{\cos\delta}$ as well. This is as expected, since the theoretically allowed values for the observable parameters are also restricted, albeit not as drastically as in the bimaximal pattern.

In Figure 6.7, we show an identical comparison to that of Figure 6.6, but using the method of this subsection in which the model parameters are taken to have conditional probability distributions. As expected, we see slight improvements in the agreement between this approach and that of previous literature. For example, here again we see similar features for the bimaximal distribution in our two methods, but with a slightly broader distribution for the conditional probability distribution approach. We also see that a slightly better overlap between the solid and dashed lines for the tribimaximal, hexagonal, GR1, and GR2 patterns than what was obtained in the approach in which the model parameters are assumed to have independent distributions. This reflects the expectation that

conditional probability distributions for the model parameters allows for us to optimize, within the theoretical constraints that are intrinsic to these models, the predictions for the observable mixing parameters so as to best reproduce the global fit data.

Part 3 Conclusion

In Part 3, we introduced neutrino mixing and the Maki-Nakagawa-Sakata-Pontecorvo mixing matrix, U_{MNSP}. We addressed the generation of neutrino masses and their mixings by considering an extension of the Standard Model with a type-I seesaw mechanism. As a way of understanding the parameters of the neutrino sector, we discussed the application of finite non-Abelian discrete symmetries to neutrino mixing.

As a further step, we investigated the predictions based on the sum rule of Eq. (6.1) for the leptonic Dirac CP-violating phase within a set of theoretical models that only include a leading order $1-2$ charged lepton correction that provides a single source of CP-violation. This correction acted on the neutrino mixing matrix for tribimaximal, bimaximal, GR1, GR2, or hexagonal mixing patterns.

Here we made the nontrivial assumption that such models can provide a correct description of lepton mixing, with no non-standard interactions or additional exotic fields as might be expected in a more complete theoretical description of lepton mass matrices. We then considered specific assumptions regarding the probability distributions of the three continuous, bounded model parameters of this set of theories, focusing on two cases: (i) independent distributions, such that the probability distribution for each continuous model parameter depended only on that parameter, and (ii) conditional probability distributions among the model parameters. We further assumed that the reactor mixing angle distribution could be approximated as a delta-function distribution, due to its precise measurement at reactor experiments.

As such, we then explored the predicted distributions for the observable mixing parameters in these theories, focusing on the distribution for $\cos\delta$, where δ is the Dirac lepton mixing phase. In both cases – paramerers correlated and conditional – a careful consideration of the theoretical constraints on the observable distributions due to the set of bounded model parameters was detailed, guaranteeing an appropriately bounded, phenomenologically viable value for $\cos\delta$, indicating that this analysis reflects the unitarity of U_{MNSP}.

Final Conclusions

In this thesis, we have investigated two beyond the Standard Model scenarios, each involving discrete non-Abelian symmetries.

In the first scenario, explored in Part 2, we detailed the construction of a model of flavored gauge mediated supersymmetry breaking wherein the Higgs-messenger mixing is governed by the discrete non-Abelian group $\mathcal{S}_3$. In this model, we also embeded the Standard Model matter fields in representations of the same non-Abelian discrete group as a first step in combining supersymmetry and flavor symmetry breaking. For a specific implementation of the superpotential couplings, achievable at a point of enhanced symmetry, we found that sizable stop mixing is achieved, ensuring that for much of the parameter space, the superpartner masses are at most $5 - 6$ TeV. By introducing a higher-dimensional operator perturbation of the superpotential, we were then able to generate smaller second generation fermion masses, and were also able to obtain appropriately sized Cabbibo mixing.

In the second scenario, investigated in Part 3, we explored the ramifications of using discrete non-Abelian symmetries in the development of models of neutrino masses and mixings. In particular, we focused on classes of models in which the neutrino mass matrix has an underlying non-Abelian symmetry which is then corrected by a $1-2$ charged lepton rotation with a single source of CP-violation.

Our specific aim was to develop a self-consistent framework of predicting the leptonic Dirac CP-violating phase in these models using sum rules. In contrast with existing analysis, we showed that it is possible to predict the most likely value of the CP-violating phase even in mixing scenarios at the far edge of parametric likelihood. We showed this two ways, one in which the model parameters are *a priori* uncorrelated and one in which the probability distributions of their values are conditioned on each other. In both cases we found that a careful analysis guaranteed the unitarity of U_{MNSP}, and that $\cos\delta$ is always bounded between 1 and -1.

The models and analyses in this thesis demonstrate the primacy of symmetry in BSM model building. More specifically, we have shown the feasibility of using finite non-Abelian discrete symmetries to develop a simultaneous implementation of supersymmetry and family symmetry breaking, as well as their uses in models of neutrino masses and mixings. Symmetry has been a fundamental tool in the historical development of high-energy physics, and it will continue to play an outsize role in the future of particle theory.

Appendix A:
Summary of $\mathcal{S}_3$

The group $\mathcal{S}_3$ is the group of permutations of three elements, called the *symmetric group* on three elements. It is isomorphic to the dihedral group D_6, the isometries of an equilateral triangle. The standard presentation of the group D_{2n} is (for our case of $n = 3$)

$$\langle a,\, b\, : a^3 = b^2 = abab = 1 \rangle. \tag{A.1}$$

This group has three irreducible representations. They are (up to a change in basis):

$$\mathbf{1}: \qquad a = b = 1 \tag{A.2}$$

$$\mathbf{1}': \qquad a = 1, \quad b = -1 \tag{A.3}$$

$$\mathbf{2}: \qquad a = \begin{pmatrix} \omega & 0 \\ 0 & \omega^2 \end{pmatrix}, \quad b = \begin{pmatrix} 0 & 1 \\ 1 & 0 \end{pmatrix}, \tag{A.4}$$

where $\omega = e^{i2\pi/3}$. The nontrivial tensor products are

$$\mathbf{1}' \otimes \mathbf{1}' = \mathbf{1} \tag{A.5}$$

$$\mathbf{1}' \otimes \mathbf{2} = \mathbf{2} \tag{A.6}$$

$$\mathbf{2} \otimes \mathbf{2} = \mathbf{1} \oplus \mathbf{1}' \oplus \mathbf{2}. \tag{A.7}$$

In the bases defined by the representations above, the explicit tensor product expressions are

$$(\mathbf{1}' \otimes \mathbf{2})_{\mathbf{2}} = \left[a \otimes \begin{pmatrix} b_1 \\ b_2 \end{pmatrix} \right]_{\mathbf{2}} = \begin{pmatrix} -ab_1 \\ ab_2 \end{pmatrix} \tag{A.8}$$

$$(\mathbf{2} \otimes \mathbf{2})_{\mathbf{1}} = \left[\begin{pmatrix} a_1 \\ a_2 \end{pmatrix} \otimes \begin{pmatrix} b_1 \\ b_2 \end{pmatrix} \right]_{\mathbf{1}} = a_1 b_2 + a_2 b_1 \tag{A.9}$$

$$(\mathbf{2} \otimes \mathbf{2})_{\mathbf{1}'} = \left[\begin{pmatrix} a_1 \\ a_2 \end{pmatrix} \otimes \begin{pmatrix} b_1 \\ b_2 \end{pmatrix} \right]_{\mathbf{1}'} = a_1 b_2 - a_2 b_1 \tag{A.10}$$

$$(\mathbf{2} \otimes \mathbf{2})_{\mathbf{2}} = \left[\begin{pmatrix} a_1 \\ a_2 \end{pmatrix} \otimes \begin{pmatrix} b_1 \\ b_2 \end{pmatrix} \right]_{\mathbf{2}} = \begin{pmatrix} a_2 b_2 \\ a_1 b_1 \end{pmatrix}. \tag{A.11}$$

Appendix B: Gaussian Density Functions[1]

We define the Gaussian distributions used in Chapter 6. As is standard, we denote the standard Gaussian distribution as

$$P_{\text{Gauss}}(\alpha;\mu,\sigma) = \frac{1}{\sqrt{2\pi}\sigma}\exp\left[-\frac{1}{2}\left(\frac{\alpha-\mu}{\sigma}\right)^2,\right] \tag{B.1}$$

where μ represents the mean and σ the standard deviation.

We also use two distributions obtained by modifying Eq. (B.1) by imposing applying a multiplicative modifier with additional parameters. Two well-known examples of such distributions are the skew normal and Gram-Charlier distribution, given by

$$P_{\text{skew}}(\alpha;\mu,\sigma,s) = P_{\text{Gauss}}(\alpha;\mu,\sigma)\left[1+\text{erf}\left(\frac{\text{s}}{\sqrt{2}}\cdot\frac{\alpha-\mu}{\sigma}\right)\right], \tag{B.2}$$

$$P_{\text{GC}}(\alpha;\mu,\sigma,s,k) = P_{\text{Gauss}}(\alpha;\mu,\sigma)\left[1+\frac{s}{6\sqrt{2}}H_3\left(\frac{\alpha-\mu}{\sqrt{2}\sigma}\right)+\frac{k}{96}H_4\left(\frac{\alpha-\mu}{\sqrt{2}\sigma}\right)\right], \tag{B.3}$$

where $\text{erf}(\beta)$ is the error function, and $H_{3,4}(\beta)$ are (physicists') Hermite polynomials, i.e, $H_3(\beta) = 8\beta^3 - 12\beta$ and $H_4(\beta) = 16\beta^4 - 48\beta^2 + 12$. Note that the additional parameters introduced are the skewness, s, and kurtosis, k, of the distributions.

[1] Appendix adapted from [250].

References

[1] S. L. Glashow, Nucl. Phys. **22**, 579 (1961).

[2] S. Weinberg, Phys. Rev. Lett. **19**, 1264 (1967).

[3] A. Salam, Conf. Proc. C **680519**, 367 (1968).

[4] P. A. M. Dirac, Proc. Roy. Soc. Lond. A **117**, 610 (1928).

[5] C. D. Anderson, Phys. Rev. **43**, 491 (1933).

[6] J. Chadwick, Nature **129**, 312 (1932).

[7] W. Heisenberg, Z. Phys. **77**, 1 (1932).

[8] E. Wigner, Phys. Rev. **51**, 106 (1937).

[9] E. Fermi, Z. Phys. **88**, 161 (1934).

[10] L. M. Brown, Physics Today **31**, 23 (1978).

[11] C. L. Cowan, F. Reines, F. B. Harrison, H. W. Kruse, and A. D. McGuire, Science **124**, 103 (1956).

[12] H. Yukawa, Proc. Phys. Math. Soc. Jap. **17**, 48 (1935).

[13] S. H. Neddermeyer and C. D. Anderson, Phys. Rev. **51**, 884 (1937).

[14] J. C. Street and E. C. Stevenson, Phys. Rev. **52**, 1003 (1937).

[15] C. M. G. Lattes, H. Muirhead, G. P. S. Occhialini, and C. F. Powell, Nature **159**, 694 (1947).

[16] S. Tomonaga, Prog. Theor. Phys. **1**, 27 (1946).

[17] R. P. Feynman, Rev. Mod. Phys. **20**, 367 (1948).

[18] T. D. Lee and C. N. Yang, Phys. Rev. **104**, 254 (1956).

[19] C. S. Wu, E. Ambler, R. W. Hayward, D. D. Hoppes, and R. P. Hudson, Phys. Rev. **105**, 1413 (1957).

[20] A. Salam and J. C. Ward, Phys. Lett. **13**, 168 (1964).

[21] G. Arnison *et al.* (UA1), Phys. Lett. B **126**, 398 (1983).

[22] G. Arnison *et al.* (UA1), Phys. Lett. B **122**, 103 (1983).

[23] P. Bagnaia *et al.* (UA2), Phys. Lett. B **129**, 130 (1983).

[24] M. Gell-Mann, (1961), 10.2172/4008239.

[25] Y. Ne'eman, Nucl. Phys. **26**, 222 (1961).

[26] M. Gell-Mann, Phys. Lett. **8**, 214 (1964).

[27] G. Zweig, (1964).

[28] O. W. Greenberg, Phys. Rev. Lett. **13**, 598 (1964).

[29] M. Y. Han and Y. Nambu, Phys. Rev. **139**, B1006 (1965).

[30] H. Fritzsch, M. Gell-Mann, and H. Leutwyler, Phys. Lett. B **47**, 365 (1973).

[31] N. Cabibbo, Phys. Rev. Lett. **10**, 531 (1963).

[32] S. L. Glashow, J. Iliopoulos, and L. Maiani, Phys. Rev. D **2**, 1285 (1970).

[33] J. E. Augustin *et al.* (SLAC-SP-017), Phys. Rev. Lett. **33**, 1406 (1974).

[34] J. J. Aubert *et al.* (E598), Phys. Rev. Lett. **33**, 1404 (1974).

[35] M. Kobayashi and T. Maskawa, Prog. Theor. Phys. **49**, 652 (1973).

[36] J. H. Christenson, J. W. Cronin, V. L. Fitch, and R. Turlay, Phys. Rev. Lett. **13**, 138 (1964).

[37] S. W. Herb *et al.*, Phys. Rev. Lett. **39**, 252 (1977).

[38] F. Abe *et al.* (CDF), Phys. Rev. Lett. **74**, 2626 (1995), arXiv:hep-ex/9503002 .

[39] S. Abachi *et al.* (D0), Phys. Rev. Lett. **74**, 2632 (1995), arXiv:hep-ex/9503003 .

[40] F. Englert and R. Brout, Phys. Rev. Lett. **13**, 321 (1964).

[41] P. W. Higgs, Phys. Lett. **12**, 132 (1964).

[42] P. W. Higgs, Phys. Rev. Lett. **13**, 508 (1964).

[43] G. S. Guralnik, C. R. Hagen, and T. W. B. Kibble, Phys. Rev. Lett. **13**, 585 (1964).

[44] G. Aad *et al.* (ATLAS), Phys. Lett. B **716**, 1 (2012), arXiv:1207.7214 [hep-ex] .

[45] S. Chatrchyan *et al.* (CMS), Phys. Lett. B **716**, 30 (2012), arXiv:1207.7235 [hep-ex] .

[46] M. Aaboud *et al.* (ATLAS), Phys. Lett. B **784**, 345 (2018), arXiv:1806.00242 [hep-ex] .

[47] *Standard Model Summary Plots March 2021*, Tech. Rep. (CERN, Geneva, 2021) all figures including auxiliary figures are available at https://atlas.web.cern.ch/Atlas/GROUPS/PHYSICS/PUBNOTES/ATL-PHYS-PUB-2021-005.

[48] V. Bargmann and E. P. Wigner, Proceedings of the National Academy of Sciences **34**, 211 (1948).

[49] M. H. Poincaré, Rendiconti del Circolo Matematico di Palermo (1884-1940) **21**, 129 (1906).

[50] S. Weinberg, *The Quantum theory of fields. Vol. 1: Foundations* (Cambridge University Press, 2005).

[51] E. Noether, Gott. Nachr. **1918**, 235 (1918), arXiv:physics/0503066 .

[52] C. N. Yang and R. L. Mills, Phys. Rev. **96**, 191 (1954).

[53] P. A. Zyla *et al.* (Particle Data Group), PTEP **2020**, 083C01 (2020).

[54] R. Davis, Jr., D. S. Harmer, and K. C. Hoffman, Phys. Rev. Lett. **20**, 1205 (1968).

[55] Y. Fukuda *et al.* (Super-Kamiokande), Phys. Rev. Lett. **81**, 1562 (1998), arXiv:hep-ex/9807003 .

[56] Q. R. Ahmad *et al.* (SNO), Phys. Rev. Lett. **89**, 011301 (2002), arXiv:nucl-ex/0204008 .

[57] K. Eguchi *et al.* (KamLAND), Phys. Rev. Lett. **90**, 021802 (2003), arXiv:hep-ex/0212021 .

[58] F. P. An *et al.* (Daya Bay), Phys. Rev. Lett. **108**, 171803 (2012), arXiv:1203.1669 [hep-ex] .

[59] J. K. Ahn *et al.* (RENO), Phys. Rev. Lett. **108**, 191802 (2012), arXiv:1204.0626 [hep-ex] .

[60] Y. Abe *et al.* (Double Chooz), JHEP **10**, 086 (2014), [Erratum: JHEP 02, 074 (2015)], arXiv:1406.7763 [hep-ex] .

[61] L. Wolfenstein, Phys. Rev. Lett. **51**, 1945 (1983).

[62] C. D. Froggatt and H. B. Nielsen, Nucl. Phys. B **147**, 277 (1979).

[63] H. Georgi and S. L. Glashow, Phys. Rev. Lett. **32**, 438 (1974).

[64] H. Fritzsch and P. Minkowski, Annals Phys. **93**, 193 (1975).

[65] M. Reig, J. W. F. Valle, C. A. Vaquera-Araujo, and F. Wilczek, Phys. Lett. B **774**, 667 (2017), arXiv:1706.03116 [hep-ph] .

[66] M. McCullough, in *6th Tri-Institute Summer School on Elementary Particles* (2018).

[67] C. Csáki and P. Tanedo, in *2013 European School of High-Energy Physics* (2015) arXiv:1602.04228 [hep-ph] .

[68] G. Steigman, Ann. Rev. Astron. Astrophys. **14**, 339 (1976).

[69] A. A. Penzias and R. W. Wilson, Astrophys. J. **142**, 419 (1965).

[70] C. L. Bennett *et al.* (WMAP), Astrophys. J. Suppl. **208**, 20 (2013), arXiv:1212.5225 [astro-ph.CO] .

[71] N. Aghanim *et al.* (Planck), Astron. Astrophys. **641**, A6 (2020), arXiv:1807.06209 [astro-ph.CO] .

[72] A. D. Sakharov, Pisma Zh. Eksp. Teor. Fiz. **5**, 32 (1967).

[73] M. Fukugita and T. Yanagida, Phys. Lett. B **174**, 45 (1986).

[74] M. Trodden, Rev. Mod. Phys. **71**, 1463 (1999), arXiv:hep-ph/9803479 .

[75] E. Hubble, Proc. Nat. Acad. Sci. **15**, 168 (1929).

[76] A. G. Riess *et al.* (Supernova Search Team), Astron. J. **116**, 1009 (1998), arXiv:astro-ph/9805201 .

[77] S. Perlmutter *et al.* (Supernova Cosmology Project), Astrophys. J. **517**, 565 (1999), arXiv:astro-ph/9812133 .

[78] E. J. Copeland, M. Sami, and S. Tsujikawa, Int. J. Mod. Phys. D **15**, 1753 (2006), arXiv:hep-th/0603057 .

[79] P. J. E. Peebles and B. Ratra, Rev. Mod. Phys. **75**, 559 (2003), arXiv:astro-ph/0207347 .

[80] C. F. Kolda and D. H. Lyth, Phys. Lett. B **458**, 197 (1999), arXiv:hep-ph/9811375 .

[81] P. Brax and J. Martin, Phys. Rev. D **61**, 103502 (2000), arXiv:astro-ph/9912046 .

[82] D. J. H. Chung, L. L. Everett, and A. Riotto, Phys. Lett. B **556**, 61 (2003), arXiv:hep-ph/0210427 .

[83] R. R. Caldwell, R. Dave, and P. J. Steinhardt, Phys. Rev. Lett. **80**, 1582 (1998), arXiv:astro-ph/9708069 .

[84] V. C. Rubin, W. K. Ford, Jr., and N. Thonnard, Astrophys. J. Lett. **225**, L107 (1978).

[85] F. Zwicky, Helv. Phys. Acta **6**, 110 (1933).

[86] G. Jungman, M. Kamionkowski, and K. Griest, Phys. Rept. **267**, 195 (1996), arXiv:hep-ph/9506380 .

[87] S. Dimopoulos, G. F. Giudice, and A. Pomarol, Phys. Lett. B **389**, 37 (1996), arXiv:hep-ph/9607225 .

[88] G. Bertone, D. Hooper, and J. Silk, Phys. Rept. **405**, 279 (2005), arXiv:hep-ph/0404175 .

[89] *SUSY March 2021 Summary Plot Update*, Tech. Rep. (CERN, Geneva, 2021) all figures including auxiliary figures are available at https://atlas.web.cern.ch/Atlas/GROUPS/PHYSICS/PUBNOTES/ATL-PHYS-PUB-2021-007.

[90] S. R. Coleman and J. Mandula, Phys. Rev. **159**, 1251 (1967).

[91] R. Haag, J. T. Lopuszanski, and M. Sohnius, Nucl. Phys. B **88**, 257 (1975).

[92] M. T. Grisaru, W. Siegel, and M. Rocek, Nucl. Phys. B **159**, 429 (1979).

[93] M. A. Shifman and A. I. Vainshtein, Nucl. Phys. B **277**, 456 (1986).

[94] D. Amati, K. Konishi, Y. Meurice, G. C. Rossi, and G. Veneziano, Phys. Rept. **162**, 169 (1988).

[95] M. A. Shifman and A. I. Vainshtein, Nucl. Phys. B **359**, 571 (1991).

[96] N. Seiberg, Phys. Lett. B **318**, 469 (1993), arXiv:hep-ph/9309335 .

[97] N. Seiberg, in *Particles, Strings, and Cosmology* (*PASCOS 94*) (1994) arXiv:hep-th/9408013 .

[98] L. Girardello and M. T. Grisaru, Nucl. Phys. B **194**, 65 (1982).

[99] K. Inoue, A. Kakuto, H. Komatsu, and S. Takeshita, Prog. Theor. Phys. **67**, 1889 (1982).

[100] K. Inoue, A. Kakuto, H. Komatsu, and S. Takeshita, Prog. Theor. Phys. **68**, 927 (1982), [Erratum: Prog.Theor.Phys. 70, 330 (1983)].

[101] K. Inoue, A. Kakuto, H. Komatsu, and S. Takeshita, Prog. Theor. Phys. **71**, 413 (1984).

[102] H. E. Haber, Nucl. Phys. B Proc. Suppl. **62**, 469 (1998), arXiv:hep-ph/9709450 .

[103] J. E. Kim and H. P. Nilles, Phys. Lett. B **138**, 150 (1984).

[104] M. Carena and H. E. Haber, Prog. Part. Nucl. Phys. **50**, 63 (2003), arXiv:hep-ph/0208209 .

[105] S. Heinemeyer, O. Stal, and G. Weiglein, Phys. Lett. B **710**, 201 (2012), arXiv:1112.3026 [hep-ph] .

[106] L. J. Hall, D. Pinner, and J. T. Ruderman, JHEP **04**, 131 (2012), arXiv:1112.2703 [hep-ph] .

[107] P. Draper, P. Meade, M. Reece, and D. Shih, Phys. Rev. D **85**, 095007 (2012), arXiv:1112.3068 [hep-ph] .

[108] M. A. Ajaib, I. Gogoladze, F. Nasir, and Q. Shafi, Phys. Lett. B **713**, 462 (2012), arXiv:1204.2856 [hep-ph] .

[109] S. Ferrara, L. Girardello, and F. Palumbo, Phys. Rev. D **20**, 403 (1979).

[110] S. Dimopoulos and S. Raby, Nucl. Phys. B **219**, 479 (1983).

[111] J. Polonyi, (1977).

[112] H. P. Nilles, Phys. Lett. B **115**, 193 (1982).

[113] H. P. Nilles, Nucl. Phys. B **217**, 366 (1983).

[114] H. P. Nilles, M. Srednicki, and D. Wyler, Phys. Lett. B **120**, 346 (1983).

[115] D. J. H. Chung, L. L. Everett, G. L. Kane, S. F. King, J. D. Lykken, and L.-T. Wang, Phys. Rept. **407**, 1 (2005), arXiv:hep-ph/0312378 .

[116] M. Dine, W. Fischler, and M. Srednicki, Nucl. Phys. B **189**, 575 (1981).

[117] S. Dimopoulos and S. Raby, Nucl. Phys. B **192**, 353 (1981).

[118] M. Dine and W. Fischler, Phys. Lett. B **110**, 227 (1982).

[119] C. R. Nappi and B. A. Ovrut, Phys. Lett. B **113**, 175 (1982).

[120] L. Alvarez-Gaume, M. Claudson, and M. B. Wise, Nucl. Phys. B **207**, 96 (1982).

[121] M. Dine and A. E. Nelson, Phys. Rev. D **48**, 1277 (1993), arXiv:hep-ph/9303230 .

[122] M. Dine, A. E. Nelson, and Y. Shirman, Phys. Rev. D **51**, 1362 (1995), arXiv:hep-ph/9408384 .

[123] M. Dine, A. E. Nelson, Y. Nir, and Y. Shirman, Phys. Rev. D **53**, 2658 (1996), arXiv:hep-ph/9507378 .

[124] M. Dine, Y. Nir, and Y. Shirman, Phys. Rev. D **55**, 1501 (1997), arXiv:hep-ph/9607397 .

[125] G. F. Giudice and R. Rattazzi, Phys. Rept. **322**, 419 (1999), arXiv:hep-ph/9801271 .

[126] C. F. Kolda, Nucl. Phys. B Proc. Suppl. **62**, 266 (1998), arXiv:hep-ph/9707450 .

[127] G. R. Dvali, G. F. Giudice, and A. Pomarol, Nucl. Phys. B **478**, 31 (1996), arXiv:hep-ph/9603238 .

[128] G. F. Giudice, H. D. Kim, and R. Rattazzi, Phys. Lett. B **660**, 545 (2008), arXiv:0711.4448 [hep-ph] .

[129] N. Polonsky, in *International Symposium on Supersymmetry, Supergravity and Superstring* (1999) arXiv:hep-ph/9911329 .

[130] J. A. Evans and D. Shih, JHEP **08**, 093 (2013), arXiv:1303.0228 [hep-ph] .

[131] Z. Chacko and E. Ponton, Phys. Rev. D **66**, 095004 (2002), arXiv:hep-ph/0112190 .

[132] Y. Shadmi and P. Z. Szabo, JHEP **06**, 124 (2012), arXiv:1103.0292 [hep-ph] .

[133] J. L. Evans, M. Ibe, and T. T. Yanagida, Phys. Lett. B **705**, 342 (2011), arXiv:1107.3006 [hep-ph] .

[134] J. L. Evans, M. Ibe, and T. T. Yanagida, (2011), arXiv:1108.3437 [hep-ph] .

[135] J. L. Evans, M. Ibe, S. Shirai, and T. T. Yanagida, Phys. Rev. D **85**, 095004 (2012), arXiv:1201.2611 [hep-ph] .

[136] Z. Kang, T. Li, T. Liu, C. Tong, and J. M. Yang, Phys. Rev. D **86**, 095020 (2012), arXiv:1203.2336 [hep-ph] .

[137] N. Craig, S. Knapen, D. Shih, and Y. Zhao, JHEP **03**, 154 (2013), arXiv:1206.4086 [hep-ph] .

[138] A. Albaid and K. S. Babu, Phys. Rev. D **88**, 055007 (2013), arXiv:1207.1014 [hep-ph] .

[139] M. Abdullah, I. Galon, Y. Shadmi, and Y. Shirman, JHEP **06**, 057 (2013), arXiv:1209.4904 [hep-ph] .

[140] M. J. Pérez, P. Ramond, and J. Zhang, Phys. Rev. D **87**, 035021 (2013), arXiv:1209.6071 [hep-ph] .

[141] P. Byakti and T. S. Ray, JHEP **05**, 055 (2013), arXiv:1301.7605 [hep-ph] .

[142] L. Calibbi, P. Paradisi, and R. Ziegler, JHEP **06**, 052 (2013), arXiv:1304.1453 [hep-ph] .

[143] J. A. Evans, D. Shih, and A. Thalapillil, JHEP **07**, 040 (2015), arXiv:1504.00930 [hep-ph] .

[144] I. Galon, G. Perez, and Y. Shadmi, JHEP **09**, 117 (2013), arXiv:1306.6631 [hep-ph] .

[145] W. Fischler and W. Tangarife, JHEP **05**, 151 (2014), arXiv:1310.6369 [hep-ph] .

[146] L. Calibbi, P. Paradisi, and R. Ziegler, Eur. Phys. J. C **74**, 3211 (2014), arXiv:1408.0754 [hep-ph] .

[147] N. Ierushalmi, S. Iwamoto, G. Lee, V. Nepomnyashy, and Y. Shadmi, JHEP **07**, 058 (2016), arXiv:1603.02637 [hep-ph] .

[148] T. Jelinski and J. Gluza, Phys. Lett. B **751**, 541 (2015), arXiv:1505.07443 [hep-ph] .

[149] L. L. Everett and T. S. Garon, Phys. Rev. D **97**, 095028 (2018), arXiv:1610.09024 [hep-ph] .

[150] W. Ahmed, L. Calibbi, T. Li, A. Mustafayev, and S. Raza, Phys. Rev. D **95**, 095031 (2017), arXiv:1612.07125 [hep-ph] .

[151] L. L. Everett, T. S. Garon, and A. B. Rock, Phys. Rev. D **100**, 015039 (2019), arXiv:1812.10811 [hep-ph] .

[152] L. L. Everett, T. S. Garon, and A. B. Rock, Phys. Rev. D **101**, 115003 (2020), arXiv:1912.12938 [hep-ph] .

[153] S. P. Martin, Adv. Ser. Direct. High Energy Phys. **18**, 1 (1998), arXiv:hep-ph/9709356 .

[154] A. Arbey, M. Battaglia, A. Djouadi, F. Mahmoudi, and J. Quevillon, Phys. Lett. B **708**, 162 (2012), arXiv:1112.3028 [hep-ph] .

[155] B. C. Allanach, Comput. Phys. Commun. **143**, 305 (2002), arXiv:hep-ph/0104145 .

[156] S. Pakvasa and H. Sugawara, Phys. Lett. B **73**, 61 (1978).

[157] E. Ma, Phys. Rev. D **43**, 2761 (1991).

[158] F. González Canales, A. Mondragón, M. Mondragón, U. J. Saldaña Salazar, and L. Velasco-Sevilla, Phys. Rev. D **88**, 096004 (2013), arXiv:1304.6644 [hep-ph] .

[159] H. Harari, H. Haut, and J. Weyers, Phys. Lett. B **78**, 459 (1978).

[160] Y. Koide, Z. Phys. C **45**, 39 (1989).

[161] M. Tanimoto, Phys. Rev. D **41**, 1586 (1990).

[162] H. Fritzsch and J. Plankl, Phys. Lett. B **237**, 451 (1990).

[163] G. Cvetic and C. S. Kim, Phys. Rev. D **51**, 201 (1995), arXiv:hep-ph/9405416 .

[164] H. Fritzsch and Z.-Z. Xing, Phys. Lett. B **372**, 265 (1996), arXiv:hep-ph/9509389 .

[165] Z.-z. Xing, J. Phys. G **23**, 1563 (1997), arXiv:hep-ph/9609204 .

[166] S. A. Abel and S. F. King, Phys. Lett. B **435**, 73 (1998), arXiv:hep-ph/9804446 .

[167] A. Mondragon and E. Rodriguez-Jauregui, Phys. Rev. D **59**, 093009 (1999), arXiv:hep-ph/9807214 .

[168] H. Fritzsch and Z.-z. Xing, Phys. Lett. B **440**, 313 (1998), arXiv:hep-ph/9808272 .

[169] H. Fritzsch and Z.-z. Xing, Prog. Part. Nucl. Phys. **45**, 1 (2000), arXiv:hep-ph/9912358 .

[170] G. C. Branco and J. I. Silva-Marcos, Phys. Lett. B **526**, 104 (2002), arXiv:hep-ph/0106125 .

[171] W. Rodejohann and Z.-z. Xing, Phys. Lett. B **601**, 176 (2004), arXiv:hep-ph/0408195 .

[172] J.-M. Gerard and Z.-z. Xing, Phys. Lett. B **713**, 29 (2012), arXiv:1203.0496 [hep-ph] .

[173] H. Fritzsch, Z.-z. Xing, and D. Zhang, Chin. Phys. C **41**, 093104 (2017), arXiv:1705.01391 [hep-ph] .

[174] U. Kaya and S. Sultansoy, (2018), arXiv:1801.03927 [hep-ph] .

[175] T. Ghosh, J. Liao, D. Marfatia, and T. T. Yanagida, Phys. Lett. B **785**, 268 (2018), arXiv:1805.05030 [hep-ph] .

[176] Z. Maki, M. Nakagawa, and S. Sakata, Prog. Theor. Phys. **28**, 870 (1962).

[177] B. Pontecorvo, Sov. Phys. JETP **6**, 429 (1957).

[178] N. Collaboration, "Nufit 5.0," (2020).

[179] I. Esteban, M. C. Gonzalez-Garcia, M. Maltoni, T. Schwetz, and A. Zhou, JHEP **09**, 178 (2020), arXiv:2007.14792 [hep-ph] .

[180] E. Majorana, Nuovo Cim. **14**, 171 (1937).

[181] S. Weinberg, Phys. Rev. Lett. **43**, 1566 (1979).

[182] P. Minkowski, Phys. Lett. B **67**, 421 (1977).

[183] M. Gell-Mann, P. Ramond, and R. Slansky, Conf. Proc. C **790927**, 315 (1979), arXiv:1306.4669 [hep-th] .

[184] E. Ma, Phys. Rev. Lett. **81**, 1171 (1998), arXiv:hep-ph/9805219 .

[185] A. Bandyopadhyay (ISS Physics Working Group), Rept. Prog. Phys. **72**, 106201 (2009), arXiv:0710.4947 [hep-ph] .

[186] F. Feruglio, "Are neutrino masses modular forms?" in *From My Vast Repertoire ...: Guido Altarelli's Legacy*, edited by A. Levy, S. Forte, and G. Ridolfi (2019) arXiv:1706.08749 [hep-ph] .

[187] P. F. Harrison, D. H. Perkins, and W. G. Scott, Phys. Lett. B **530**, 167 (2002), arXiv:hep-ph/0202074 .

[188] P. F. Harrison and W. G. Scott, Phys. Lett. B **535**, 163 (2002), arXiv:hep-ph/0203209 .

[189] Z.-z. Xing, H. Zhang, and S. Zhou, Phys. Lett. B **641**, 189 (2006), arXiv:hep-ph/0607091 .

[190] X. G. He and A. Zee, Phys. Lett. B **560**, 87 (2003), arXiv:hep-ph/0301092 .

[191] L. Wolfenstein, Phys. Rev. D **18**, 958 (1978).

[192] F. Vissani, (1997), arXiv:hep-ph/9708483 .

[193] V. D. Barger, S. Pakvasa, T. J. Weiler, and K. Whisnant, Phys. Lett. B **437**, 107 (1998), arXiv:hep-ph/9806387 .

[194] A. J. Baltz, A. S. Goldhaber, and M. Goldhaber, Phys. Rev. Lett. **81**, 5730 (1998), arXiv:hep-ph/9806540 .

[195] H. Georgi and S. L. Glashow, Phys. Rev. D **61**, 097301 (2000), arXiv:hep-ph/9808293 .

[196] I. Stancu and D. V. Ahluwalia, Phys. Lett. B **460**, 431 (1999), arXiv:hep-ph/9903408 .

[197] A. Datta, F.-S. Ling, and P. Ramond, Nucl. Phys. B **671**, 383 (2003), arXiv:hep-ph/0306002 .

[198] L. L. Everett and A. J. Stuart, Phys. Rev. D **79**, 085005 (2009), arXiv:0812.1057 [hep-ph] .

[199] F. Feruglio and A. Paris, JHEP **03**, 101 (2011), arXiv:1101.0393 [hep-ph] .

[200] G.-J. Ding, L. L. Everett, and A. J. Stuart, Nucl. Phys. B **857**, 219 (2012), arXiv:1110.1688 [hep-ph] .

[201] W. Rodejohann, Phys. Lett. B **671**, 267 (2009), arXiv:0810.5239 [hep-ph] .

[202] A. Adulpravitchai, A. Blum, and W. Rodejohann, New J. Phys. **11**, 063026 (2009), arXiv:0903.0531 [hep-ph] .

[203] C. H. Albright, A. Dueck, and W. Rodejohann, Eur. Phys. J. C **70**, 1099 (2010), arXiv:1004.2798 [hep-ph] .

[204] S. F. King and C. Luhn, Rept. Prog. Phys. **76**, 056201 (2013), arXiv:1301.1340 [hep-ph] .

[205] E. Ma, Phys. Rev. D **70**, 031901 (2004), arXiv:hep-ph/0404199 .

[206] E. Ma and U. Sarkar, Phys. Rev. Lett. **80**, 5716 (1998), arXiv:hep-ph/9802445 .

[207] E. Ma and G. Rajasekaran, Phys. Rev. D **64**, 113012 (2001), arXiv:hep-ph/0106291 .

[208] S. F. King, Phys. Lett. B **659**, 244 (2008), arXiv:0710.0530 [hep-ph] .

[209] D. Hernandez and A. Y. Smirnov, Phys. Rev. D **86**, 053014 (2012), arXiv:1204.0445 [hep-ph] .

[210] D. Hernandez and A. Y. Smirnov, Phys. Rev. D **87**, 053005 (2013), arXiv:1212.2149 [hep-ph] .

[211] P. Ballett, S. F. King, C. Luhn, S. Pascoli, and M. A. Schmidt, Phys. Rev. D **89**, 016016 (2014), arXiv:1308.4314 [hep-ph] .

[212] Y. Shimizu, M. Tanimoto, and A. Watanabe, Prog. Theor. Phys. **126**, 81 (2011), arXiv:1105.2929 [hep-ph] .

[213] S. F. King and C. Luhn, JHEP **09**, 042 (2011), arXiv:1107.5332 [hep-ph] .

[214] S. Antusch, S. F. King, C. Luhn, and M. Spinrath, Nucl. Phys. B **856**, 328 (2012), arXiv:1108.4278 [hep-ph] .

[215] S. F. King, JHEP **07**, 137 (2013), arXiv:1304.6264 [hep-ph] .

[216] S. F. King, Phys. Lett. B **724**, 92 (2013), arXiv:1305.4846 [hep-ph] .

[217] S. F. King, JHEP **08**, 105 (2005), arXiv:hep-ph/0506297 .

[218] S. F. King, A. Merle, S. Morisi, Y. Shimizu, and M. Tanimoto, New J. Phys. **16**, 045018 (2014), arXiv:1402.4271 [hep-ph] .

[219] I. Masina, Phys. Lett. B **633**, 134 (2006), arXiv:hep-ph/0508031 .

[220] S. Antusch and S. F. King, Phys. Lett. B **631**, 42 (2005), arXiv:hep-ph/0508044 .

[221] S. Antusch, P. Huber, S. F. King, and T. Schwetz, JHEP **04**, 060 (2007), arXiv:hep-ph/0702286 .

[222] D. Marzocca, S. T. Petcov, A. Romanino, and M. Spinrath, JHEP **11**, 009 (2011), arXiv:1108.0614 [hep-ph] .

[223] A. Meroni, S. T. Petcov, and M. Spinrath, Phys. Rev. D **86**, 113003 (2012), arXiv:1205.5241 [hep-ph] .

[224] D. Marzocca, S. T. Petcov, A. Romanino, and M. C. Sevilla, JHEP **05**, 073 (2013), arXiv:1302.0423 [hep-ph] .

[225] I. Girardi, A. Meroni, S. T. Petcov, and M. Spinrath, JHEP **02**, 050 (2014), arXiv:1312.1966 [hep-ph] .

[226] S. T. Petcov, Nucl. Phys. B **892**, 400 (2015), arXiv:1405.6006 [hep-ph] .

[227] J. Gehrlein, S. T. Petcov, M. Spinrath, and X. Zhang, Nucl. Phys. B **896**, 311 (2015), arXiv:1502.00110 [hep-ph] .

[228] J. Gehrlein, S. T. Petcov, M. Spinrath, and X. Zhang, (2015), 10.1016/j.nuclphysb.2015.08.019, [Addendum: Nucl.Phys.B 899, 617–630 (2015)], arXiv:1508.07930 [hep-ph] .

[229] P. Ballett, S. F. King, C. Luhn, S. Pascoli, and M. A. Schmidt, JHEP **12**, 122 (2014), arXiv:1410.7573 [hep-ph] .

[230] I. Girardi, S. T. Petcov, and A. V. Titov, Nucl. Phys. B **894**, 733 (2015), arXiv:1410.8056 [hep-ph] .

[231] I. Girardi, S. T. Petcov, and A. V. Titov, Eur. Phys. J. C **75**, 345 (2015), arXiv:1504.00658 [hep-ph] .

[232] I. Girardi, S. T. Petcov, A. J. Stuart, and A. V. Titov, Nucl. Phys. B **902**, 1 (2016), arXiv:1509.02502 [hep-ph] .

[233] I. Girardi, S. T. Petcov, and A. V. Titov, Nucl. Phys. B **911**, 754 (2016), arXiv:1605.04172 [hep-ph] .

[234] S. K. Agarwalla, S. S. Chatterjee, S. T. Petcov, and A. V. Titov, Eur. Phys. J. C **78**, 286 (2018), arXiv:1711.02107 [hep-ph] .

[235] J. Gehrlein, S. T. Petcov, M. Spinrath, and A. V. Titov, JHEP **11**, 146 (2016), arXiv:1608.08409 [hep-ph] .

[236] F. Buccella, M. Chianese, G. Mangano, G. Miele, S. Morisi, and P. Santorelli, JHEP **04**, 004 (2017), arXiv:1701.00491 [hep-ph] .

[237] J. T. Penedo, S. T. Petcov, and A. V. Titov, JHEP **12**, 022 (2017), arXiv:1705.00309 [hep-ph] .

[238] S. T. Petcov, Eur. Phys. J. C **78**, 709 (2018), arXiv:1711.10806 [hep-ph] .

[239] D. A. Dicus, S.-F. Ge, and W. W. Repko, Phys. Rev. D **83**, 093007 (2011), arXiv:1012.2571 [hep-ph] .

[240] S.-F. Ge, D. A. Dicus, and W. W. Repko, Phys. Lett. B **702**, 220 (2011), arXiv:1104.0602 [hep-ph] .

[241] S.-F. Ge, D. A. Dicus, and W. W. Repko, Phys. Rev. Lett. **108**, 041801 (2012), arXiv:1108.0964 [hep-ph] .

[242] A. D. Hanlon, S.-F. Ge, and W. W. Repko, Phys. Lett. B **729**, 185 (2014), arXiv:1308.6522 [hep-ph] .

[243] S.-F. Ge, (2014), arXiv:1406.1985 [hep-ph] .

[244] L. A. Delgadillo, L. L. Everett, R. Ramos, and A. J. Stuart, Phys. Rev. D **97**, 095001 (2018), arXiv:1801.06377 [hep-ph] .

[245] S. T. Petcov and A. V. Titov, Phys. Rev. D **97**, 115045 (2018), arXiv:1804.00182 [hep-ph] .

[246] S. K. Garg, (2018), arXiv:1806.08239 [hep-ph] .

[247] M. H. Rahat, P. Ramond, and B. Xu, Phys. Rev. D **98**, 055030 (2018), arXiv:1805.10684 [hep-ph] .

[248] M. J. Pérez, M. H. Rahat, P. Ramond, A. J. Stuart, and B. Xu, Phys. Rev. D **100**, 075008 (2019), arXiv:1907.10698 [hep-ph] .

[249] M. J. Pérez, M. H. Rahat, P. Ramond, A. J. Stuart, and B. Xu, Phys. Rev. D **101**, 075018 (2020), arXiv:2001.04019 [hep-ph] .

[250] L. L. Everett, R. Ramos, A. B. Rock, and A. J. Stuart, (2019), arXiv:1912.10139 [hep-ph] .

[251] K. Abe *et al.* (T2K), Phys. Rev. Lett. **112**, 061802 (2014), arXiv:1311.4750 [hep-ex] .

[252] P. Adamson *et al.* (NOvA), Phys. Rev. Lett. **118**, 231801 (2017), arXiv:1703.03328 [hep-ex] .

[253] I. Esteban, M. C. Gonzalez-Garcia, A. Hernandez-Cabezudo, M. Maltoni, and T. Schwetz, JHEP **01**, 106 (2019), arXiv:1811.05487 [hep-ph] .

[254] N. Collaboration, "Nufit 4.1," (2019).

[255] P. F. de Salas, D. V. Forero, C. A. Ternes, M. Tortola, and J. W. F. Valle, Phys. Lett. B **782**, 633 (2018), arXiv:1708.01186 [hep-ph] .

[256] F. Capozzi, E. Lisi, A. Marrone, and A. Palazzo, Prog. Part. Nucl. Phys. **102**, 48 (2018), arXiv:1804.09678 [hep-ph] .